UNIVERSIDADE DE LISBOA

FACULDADE DE CIÊNCIAS

DEPARTAMENTO DE FÍSICA

Exploring Sexual Dimorphism in Dendritic Morphology and Connectivity: Implications for Neuronal Optimality

Natália Russo Marques

Mestrado Integrado em Engenharia Biomédica e Biofísica

Perfil em Sinais e Imagens Médicas

Dissertação orientada por:

Alexandre Andrade, PhD

Mara Dierssen, MD, PhD

Dedicatória e Agradecimentos

I would like to start by thanking Mara Dierssen, for making this Master Dissertation possible by giving me the opportunity to work at CRG in her lab. Thank you for your continuing guidance, your interest and excitement in all of my results, all your patience with my learning curve (especially with the written part!) and for shaping me into the better scientist and researcher I am today. To my other advisor, Alexandre Andrade, thank you for your support and help with all the bureaucracy involved, and for all your input. To Linus Manubens-Gil, who acted as an unofficial dissertation advisor, thank you for always supporting and helping me with my coding issues, and for answering to endless emails with all my questions. And thank you for sharing your passion of neuronal modulation with me, and teaching me so much in this time. To the remaining lab members of the Dierssen lab, a huge thank you for all your contributions at lab meetings, and all your help on a day-to-day basis: María Martínez, Eduardo Dominguez, Ilario de Toma, Álvaro Fernandez, Cèsar-lluís Sierra, Juanlu Musoles, Santiago Acosta and Karla Ivankovic. A special thank you to Ilario, for helping me with my issues on the statistical analysis.

This experience would have been nothing without the people I met and that made me feel at home. Even though all my lab mates are included in this list, I must highlight Álvaro, Juanlu and Karla. Thank you for your friendship, for always making me laugh and for all the coffees in the terrace, and for still keeping in touch. Most importantly, to the best two friends I could ever hope to make: Cristina Rodríguez and Federica Mantica. Thank you for all the talks, coffees, beers, hugs, advices, laughs, nights in Cris's balcony, adventures and trips. I hope we can travel together soon again, and share so many new moments. You guys are the best.

Mais importante que as novas experiências, são as amizades de sempre e o apoio constante que continuei a sentir, mesmo estando longe. Um muito obrigada a todos os meus amigos, entre eles Beatriz, Catarina, Liliana, Joana e Nuno, seja por manterem o contacto e contarem sempre as novidades, partilhar piadas, ou simplesmente por perceberem quando estava farta de falar sobre a dissertação e trocarem de assunto. À Catarina Pereira e à Joana Leitão, muito muito obrigada por sempre fazerem questão de estar comigo quando ia a Lisboa; que venham muitos mais *brunches* juntas. Um especial destaque à Joana, por me ter visitado alguns dias a Barcelona, mesmo que na minha última semana lá. Obrigada por trazeres tanta felicidade ao meu coração nesses dias. À Marta Silva, obrigada por passeares comigo sempre que ias a Barcelona, e por me mostrares tantos cantos fantásticos e restaurantes deliciosos.

Não podia deixar de agradecer especialmente ao Nuno Gonçalves. Desde o primeiro dia sempre me apoiaste e motivaste a ser uma pessoa melhor. Obrigada por todas as videochamadas e conversas diárias, e pelo carinho especial que tiveste com os meus pais de os visitar quando eu estava longe. Obrigada por me lembrares dos meus objetivos e prioridades sempre que necessário, por todas as "*pep talks*" e por festejares todas as etapas desta dissertação comigo. Obrigada também pelo teu contributo e por me ajudares a perceber quando eu precisava de explicar algo melhor. Espero um dia conseguir retribuir toda a tua ajuda e apoio, e que sejamos sempre o "fã número 1" um do outro.

À minha família, os meus eternos líderes de claque, obrigada por todo o vosso apoio constante e amor: aos meus pais, Lourenço e Rosana, aos meus irmãos Fábio, Fernando, Flávio e Lygia, e restante família mais próxima, Letícia, Marcelle e Nuno. Um obrigada especial à minha irmã, por todo o interesse que mostrou pela minha dissertação, sempre tentando me ajudar/motivar, apesar de eu saber que ela não percebia quase nada – obrigada pelo esforço e carinho; não poderia querer uma irmã melhor.

Esta dissertação dedico aos meus pais, Lourenço e Rosana, por me ensinarem a seguir os meus sonhos e a trabalhar para atingi-los, e por me poderem proporcionar toda esta experiência. Obrigada por me terem feito na pessoa que sou hoje, por toda a vossa preocupação, amor e carinho. As minhas vitórias são também as vossas. Obrigada obrigada obrigada – adoro-vos.

Summary

A remarkable feature of the human brain is its sexual dimorphism. While it is well-documented that the sexual dimorphism in brain structure and function exists, there is a sex bias in neuroscience research. Either single-sex male studies are favoured, or the works do not provide a sex-based analysis when both sexes are included. Experimental results obtained from research using only one sex are sometimes extrapolated to both sexes without thorough justification, which might cause conceptual errors and unintended biased practices.

It has been suggested that the hippocampus is sexually dimorphic, although not at the macroscopic anatomical level, as sex difference was eliminated in meta-analyses of studies that correct for overall brain volume. Instead, at the cellular level, differences between male and female rats have been detected with respect to the number of dentate granule cells and branching patterns of dentate granule and hippocampal pyramidal cell dendrites. However, most studies focus on CA3 and dentate gyrus neuronal morphology, and few have studied sex-dependent differences in CA1 neurons.

We explored sex-dependent differences in the dendritic morphology, functional capabilities and optimality of CA1 pyramidal neurons using digitally reconstructed neurons from the Neuromorpho.Org database. We analysed a total of 66 basal dendritic trees (33 of each sex) from control mice. Using cluster analysis, we identified two clusters, separated by size: neurons with larger (cluster 1) and smaller (cluster 2) average size.

To assess sex differences in the morphology we chose 9 metrics describing the main features of a neuron. In cluster 1, male neurons present significantly larger total length, maximum path length, tree radius, volume and number of branch points. Sholl analysis also revealed increased complexity in male cluster 1 neurons. Instead, no sex-dependent differences in morphology nor Sholl analysis were identified in cluster 2. Fractal analysis assessed how much the dendrites filled their space, and there were no differences between sexes in either clusters. The same was true for centripetal bias, but it revealed that neurons favour faster conduction time over a smaller cable length.

To assess neuronal optimality, we took two different approaches. We first applied known power laws and compared the exponents to their optimal value, but they proved to be unreliable to determine optimality. The second approach was a multi-objective optimization. We calculated 3 measures of functional capabilities which depend on neuromorphological properties: connectivity repertoire, signal integration efficiency and cable cost. An optimal neuron will maximize the first two, while minimizing the cost. Male neurons of cluster 1 had significantly higher connectivity repertoire and signal integration efficiency, but at a higher cost than females. After normalizing by cost, signal integration was significantly more efficient in female neurons of cluster 1. In cluster 2, no significant differences were found. To determine optimality, we defined a Pareto front using synthetic neurons and calculated the euclidean distance between this surface and each of the neurons from the dataset. In both clusters there were no significant differences, but neurons of cluster 2 were significantly more optimal than those of cluster 1.

In conclusion, we found novel sex-dependent differences in the morphology of CA1 basal pyramidal neurons. Results on optimality varied according to the chosen Pareto front, and so no clear conclusions can be drawn. Nevertheless, our multi-objective approach is a first step in understanding sex differences.

Key words: sex-dependent differences, neuromorphology, functional capabilities, neuronal optimality.

Resumo

O cérebro é um órgão diferenciado sexualmente desde o período perinatal, caracterizado pelo seu dimorfismo sexual. Apesar de existir uma extensa documentação deste dimorfismo tanto a nível estrutural como a nível funcional, existe um certo enviesamento em investigação na área da neurociência. Estudos com apenas o sexo masculino são favorecidos, sendo que os resultados são depois extrapolados sem grande justificação, quando estes podem não se verificar para o sexo feminino. Esta prática é cada vez menos comum, sendo que a percentagem de estudos que incluem ambos os sexos subiu de 29% em 2009 para 63% em 2019. No entanto, apenas 20% destes realizaram uma análise com o sexo em consideração, e portanto diferenças sexuais são negligenciadas. Isto pode causar erros conceptuais e enviesamento não intencional em prática clínica.

O hipocampo é uma área do cérebro considerada como sexualmente dimórfica, e está associado à consolidação de memórias de longo e curto prazo, e memória espacial. Tanto em humanos como em modelos animais, o sexo masculino supera o feminino no que toca à navegação espacial, enquanto que o contrário acontece com informação semântica. No entanto, a nível macroscópico, não se encontram diferenças sexuais na sua anatomia, visto que estas são eliminadas quando corrigidas pelo volume cerebral. Já a nível celular, foram encontradas diferenças entre ratos machos e fêmeas no que toca ao número de células na circunvolução dentada, assim como nos padrões de ramificação das dendrites, tanto das células da circunvolução dentada como das células piramidais. Porém, a maior parte dos estudos são focados na morfologia neuronal das células do CA3 e da circunvolução dentada, enquanto que poucos estudaram diferenças sexuais nos neurónios do CA1.

Na primeira parte desta dissertação explorámos diferenças sexuais na morfologia dos neurónios piramidais do CA1. Para tal, utilizámos reconstruções neuronais disponíveis na base de dados NeuroMorpho.Org, analisando um total de 66 dendrites basais (33 de cada sexo) de ratos C57BL/6J (controlo). Realizámos uma análise de aglomeração de dados (clustering), onde encontrámos dois *clusters*, que separavam os neurónios de acordo com a sua dimensão. O *cluster* 1 contém os neurónios de maiores dimensões, enquanto que o *cluster* 2 contém os de menores. Para averiguar a existência de diferenças na morfologia escolhemos 9 variáveis que descrevem as propriedades principais de um neurónio: comprimento total das dendrites, comprimento máximo das dendrites, comprimento médio dos ramos dendríticos, raio do soma, raio da arborização dendrítica, volume da arborização dendrítica, número de pontos de ramificação dendrítica (bifurcação), ordem média dos ramos dendríticos, e retidão das dendrites. Os neurónios do sexo masculino do *cluster* 1 tinham significativamente maior comprimento total e comprimento máximo, maior volume e raio da arborização, e mais bifurcações que os neurónios do sexo feminino. Já no *cluster* 2, não foram encontradas diferenças significativas entre sexos.

Já na segunda parte desta dissertação, quisemos fazer a ponte entre as diferenças neuromorfológicas que identificámos, e possíveis diferenças sexuais nas capacidades funcionais dos neurónios e na sua otimalidade. Desde a década de 1970 que existe o consenso de que as propriedades morfológicas do neurónio determinam a sua função, assim como influenciam a forma como este integra os sinais que recebe. Pequenas alterações são suficientes para perturbar os circuitos neuronais, como é o caso nas doenças neurológicas. No entanto, ainda não se sabe como a morfologia de cada célula afeta a rede neuronal. No fim do século XIX, Ramón y Cajal fez a primeira proposta sobre otimalidade neuronal, dizendo que as dendrites vão otimizar a sua conectividade ao minimizar o tempo de condução num compromisso com o custo material associado ao seu comprimento. Atualmente este conceito evoluiu, sendo proposto que a arborização dendrítica cresce de forma a preencher um espaço alvo, enquanto minimiza o tempo de condução e o custo. É portanto possível classificar um neurónio como ótimo ou subótimo, em que o ótimo é aquele que consegue chegar a todos os axónios que passam pelo seu espaço

alvo, com o mínimo comprimento total. Utilizando este conceito de otimalidade, é possível fazer o salto entre morfologia e implicações na rede neuronal.

Para aferir a otimalidade neuronal, utilizámos duas abordagens diferentes. Primeiramente, calculei duas leis de potência que relacionam propriedades morfológicas, e cujo expoente tem um valor otimal. Se um neurónio seguir a lei de potência, então é considerado como ótimo, caso contrário é subótimo. No entanto, com estas leis obtivemos resultados contraditórios, e elas mostraram-se como um método não confiável de aferir a otimalidade dos neurónios. A outra abordagem passou por definirmos uma otimização com múltiplos objetivos. Para tal calculámos três medidas de capacidades funcionais de um neurónio: o repertório de possíveis conexões, a eficiência na integração dos sinais, e o custo material. Estas três medidas comportam-se como uma configuração de Pareto, ou seja, é necessário atingir um balanço entre as três. Um neurónio ótimo é aquele que maximiza as primeiras duas medidas, enquanto minimiza o custo (multiobjetivos). Começámos por comparar cada uma destas capacidades funcionais individualmente, e no *cluster* 1 encontrámos diferenças significativas entre os sexos: os neurónios do sexo masculino tinham maior eficiência e repertório de conexões, mas também tinham um maior custo. Devido a terem um custo superior ao dos neurónios femininos, não é possível dizer diretamente que estes são mais ótimos ou não. Também comparámos o repertório e a eficiência após normalizá-los pelo custo, sendo que os neurónios do sexo feminino passaram a ser significativamente mais eficientes que os do masculino. Isto indica que os neurónios femininos são na verdade mais ótimos que os masculinos. Já nos neurónios do *cluster* 2, não encontrámos quaisquer diferenças significativas. Para poder determinar efetivamente a otimalidade de cada neurónio com esta abordagem, é preciso ter em consideração o balanço entre as três capacidades funcionais. Para tal, é necessário resolver este problema de otimização com múltiplos objetivos, e assim obter a fronteira de Pareto. A distância euclidiana entre cada neurónio e esta fronteira determina o quão próximo eles estão de ser ótimos. Uma vez que a eficiência na integração dos sinais foi obtida através modelos computacionais, foi necessário encontrar uma alternativa para obter a fronteira de Pareto. Neste caso, não obtivemos a verdadeira fronteira, mas sim escolhemos uma superfície que se adaptava aos dados. De acordo com a superfície que escolhemos como fronteira de Pareto, em ambos os *clusters* não encontrámos diferenças significativas entre os sexos. Comparando cada *cluster*, os neurónios do *cluster* 2 são significativamente mais ótimos que os do *cluster* 1. É de referir que se escolhêssemos outra superfície, os resultados seriam diferentes ao comparar os sexos no *cluster* 1, com os neurónios do sexo feminino significativamente mais ótimos, como era de esperar pelos resultados anteriores. Portanto, os resultados de otimalidade com esta abordagem também não são confiáveis, sendo que é necessário obter a verdadeira fronteira de Pareto.

Para além destas análises, também realizámos análise de Sholl e calculámos a dimensão fractal e o enviesamento centrípeto. A análise de Sholl revelou uma maior complexidade nos neurónios do sexo masculino do *cluster* 1, mas não no *cluster* 2. A dimensão fractal, que é uma medida de quanto as dendrites ocupam o espaço, não revelou diferenças em nenhum dos *clusters*. O mesmo sucedeu para o enviesamento centrípeto, no entanto este revelou que existe um certo enviesamento. Isto significa que os neurónios favorecem uma diminuição no tempo de condução sobre um menor comprimento total.

Em conclusão, encontrámos diferenças sexuais na neuromorfologia das dendrites basais do hipocampo CA1 de ratos C57BL/6J. Estas diferenças só se verificam nos neurónios de maiores dimensões, e influenciam as capacidades funcionais dos mesmos. Já os resultados sobre a otimalidade não eram confiáveis em nenhuma das abordagens, e portanto ainda não é possível fazer conclusões sobre a influência do sexo. No entanto, a nossa proposta de otimização de multiobjetivos é um primeiro passo na direção correta, e pode ainda ser melhorada.

Palavras-chave: diferenças sexuais, neuromorfologia, capacidades funcionais, otimalidade neuronal.

Contents

List of figures

List of tables

List of abbreviations

AIC – Akaike information criteria.
ANOVA – Analysis of variance.
AUC – Area under the curve.
C-I – Class I.
C-IV – Class IV.
CA*N* – *Cornu Ammonis N*.
CV – Coefficient of variation.
GLMM – Generalized Linear Mixed Model.
LMM – Linear Mixed Model.
MST – Minimum spanning tree.
NS – Non-significant.
PC – Principal Component.
PCA – Principal Component Analysis.
P*N* – Postnatal day *N*.
Q-Q – Quantile-quantile.
R^2 – Coefficient of determination.
RMSE – Root mean square error.
SC – Silhouette coefficient.
SIP – Sholl intersection profile.
WT – Wild-type.

General introduction

It is known that the brain is sexually differentiated during a perinatally sensitive period *(Lenz et al., 2012; Phoenix et al., 1959).* In 2009 Beery and Zucker did a literature search and found that single-sex studies in the field of neuroscience would favour male animals over females at a ratio of 5.5:1 *(Beery & Zucker, 2011)*. In 2019, they reported that 63% of neuroscience studies included both sexes, versus 29% in 2009. However, less than 20% of them have conducted sex-based analysis *(Woitowich et al., 2020)*.

There is a consensus that the morphological properties of a neuron will determine its function and impact how the signals are integrated. Therefore, differences in hippocampal function between males and females in spatial tasks, working memory and semantic information *(Wang et al., 2018; Yagi & Galea, 2019)* could be associated with differences in morphology. However, few studies have assessed sex-dependent differences in CA1 pyramidal neurons *(Keil et al., 2017; Koss & Frick, 2017)*, and there is a gap between single-cell architecture and the implications in the network they form. Studies assessing differences in wiring optimality between sexes are also lacking. It is clear that a sex bias still exists, and needs to be addressed.

Hypothesis and objectives

We hypothesize that differences between males and females in dendritic morphology of CA1 pyramidal neurons may affect their computational capabilities and wiring optimality.

To investigate this hypothesis, we have divided this dissertation into two objectives:

1. Investigate the existence of sex-dependent differences in different neuromorphological metrics.
2. Assess if any found differences in morphology imply significant differences in computational capabilities and wiring optimality.

This dissertation is divided in two chapters, one for each objective: **Chapter 1** explores the first, while **Chapter 2** explores the second. They are followed by the **General conclusions** of the dissertation, as well as some **Supplementary Information**.

Chapter 1: Exploring sexual dimorphism in the morphology of CA1 basal trees from mice

1.1. Introduction

During normal neurodevelopment, gonadal hormones influence the brain and sex-specific behaviour. Shortly, according to the Organizational/Activational hypothesis, the hormones act on a perinatally sensitive period to organize a male or female phenotype, leading to brain sexual differentiation; across the lifespan, these hormones also act on the brain to activate sex-specific behaviour *(Lenz et al., 2012; Phoenix et al., 1959)*. Areas of the brain associated with sexual behaviour such as the preoptic area are more affected by these hormones *(Lenz et al., 2012)*, but others such as the cortex and hippocampus are also influenced *(Keil et al., 2017)*.

The hippocampus is an important area of the brain, associated with short- and long-term memory, as well as spatial memory. Studies have shown a sexual difference in learning strategies during spatial tasks, both in humans and rodents. Males outperform females in spatial navigation and working memory *(Yagi & Galea, 2019)*, whereas the reverse happens for semantic information *(Wang et al., 2018)*. Furthermore, the hippocampus contains sex hormones receptors, and their density varies in a region-specific way according to sex *(Yagi & Galea, 2019)*. These hormones have been implicated in single cell differences, for example interacting with histone modifying enzymes, and histone modifications were associated with neural sexual differentiation in the mouse hippocampus *(Tsai et al., 2009)*. There have been a number of studies demonstrating differential effects of gonadal steroids on the various subfields of the hippocampus *(Duarte-Guterman et al., 2015; Hajszan et al., 2007; Woolley, 2007)*, and numerous sex differences in hippocampus have been described *(Duarte-Guterman et al., 2015; McEwen, 2010; McLaughlin et al., 2009)*.

Neurons are the main components of the nervous tissue and typically consist of a soma (cell body), dendrites (afferent) and an axon (efferent) **(Figure 1.1)**. The last two represent the communication interfaces of a neuron, receiving and transmitting information, respectively. The dendrites usually have many subdivisions (branches), which form a dense arborization surrounding the soma, called dendritic tree. These branches have membrane protrusions called dendritic spines which are responsible for receiving information in the form of an electrochemical impulse from other cells through synapses. This information is then conducted to the soma, where it will be integrated, and the resulting action potential sent through the axon. This cable-like structure is thinner than a dendrite and connects the soma in one end to the terminal bulbs in the other. Once the electrochemical impulse reaches the terminal bulbs, it will be synapsed onto the next cell.

It has been shown that neurons with different morphological or anatomical features exhibit differences in stimulus-specific temporal encoding and firing reliability. These findings support the idea that in addition to biophysical membrane properties, the dendritic morphology and the synaptic topology of a neuron can play a significant role in neuronal information processing and may directly contribute to various brain functions. Even though the importance of single cell analysis is revealing as highly relevant, there is a lack of studies assessing if hippocampal dendritic morphology varies with sex, especially in the CA1 layer *(Keil et al., 2017)*.

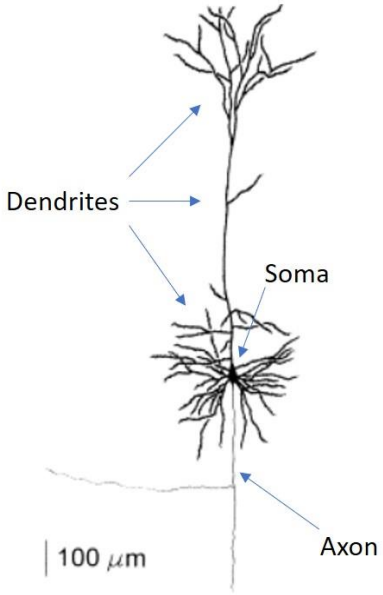

Figure 1.1 - Camera lucida drawing of a layer V neuron from the rat. The three main compartments of the cell are highlighted. Adapted from Franceschetti *et al* 1998.

In the field of neuroscience, single-sex studies favour male animals over females at a ratio of 5.5:1 in 2009, and even when both sexes were included, the results would not always be analysed by sex *(Beery & Zucker, 2011)*. Ten years later these values have improved, with 63% of neuroscience studies reporting the inclusion of both sexes, versus 29% in 2009. However, less than 20% of them have conducted sex-based analysis *(Woitowich et al., 2020)*, showing how sex differences are still overlooked. In relation to this work, only few studies have assessed sex-dependent differences in CA1 pyramidal neurons in animal models *(Keil et al., 2017; Koss & Frick, 2017)*. Studies can be found comparing the total number of cells and number per unit of volume, which were significantly larger in male rats *(Madeira et al., 1992)*, and some simple morphological properties such as cell body area, branch points and length of longest dendrite, which have no significant sex differences in rats *(Gould et al., 1990)*. Dendritic complexity was also studied by Sholl analysis, where male mice had significantly more intersections, indicating a higher dendritic complexity *(Keil et al., 2017)*. It is clear that an in-depth comparison of neuronal morphology between sexes is missing.

1.2. Methods

1.2.1. Dataset and morphological metrics

In this dissertation we used data from NeuroMorpho.Org *(Ascoli, 2006; Ascoli et al., 2007)*. This is an online repository of curated digitally reconstructed neurons associated with peer-reviewed publications. Alongside each neuron is the respective published article and available metadata. A summary of the process and criteria used to select the dataset to work with can be found in **Supplementary Information I**.

We selected a dataset in which all neurons were from the same study, and hence no technical constraints. This allowed us to compare sex-dependent differences in pyramidal cells. The selected sample was composed of 66 neurons, 33 of each sex (variable of interest) reconstructed from the CA1 hippocampal region of 10 C57BL/6J mice. The neurons come only from 5 male and 5 female mice, meaning we have multiple neurons from the same animal *(Wilson et al., 2017)*.

NeuroMorpho.Org provides the digital reconstructions of the neurons in *.swc files. This format represents a neuron by nodes, containing 7 fields of information: indexed number of the node, type of neuronal compartment (basal/apical dendrites, axon, soma, etc.), x, y and z coordinates, radius and indexed number of the parent node. We can export these files to MATLAB using the TREES Toolbox (version 1.15), which will use the different fields to generate the neuronal tree. This toolbox is a software with a myriad of functions for editing, visualizing and analysing neurons, and many other applications *(Cuntz et al., 2010)*. All functions used in the subsequent analysis of this section, unless stated otherwise, are from the TREES Toolbox.

After exporting the files, the neurons were pre-processed, removing any existing multifurcations, which are not biologically possible (function *elimt_tree*). We also added a structure representing the soma of the tree (functions *quaddiameter_tree* and *soma_tree*), which made it easier to find possible correlations between the size of the soma and, for example, the size of the tree. The *.swc files contained the soma as the first node, and so in this case the radius field of the first node is the radius of the soma. After exporting the data to the toolbox, the software saves the diameter of the soma in *tree.D(1)*.

The function *stats_tree* was used to calculate total length, maximum path length, mean branch length, number of branch points, mean branch order and straightness (**Figure 1.2** and **Table 1.1**). We also calculated 3 other metrics: soma radius, dendritic tree radius and volume. We chose these 9 metrics since they describe the main morphological properties of neuronal trees relevant for their functional impact on network connectivity.

The value for the soma radius, as explained previously, is in the *.swc file provided in the NeuroMorpho.Org datasets. The volume was obtained with the *boundary* function from MATLAB (version 2016a) with a shrink factor of 0.7. It determines the span of the tree and the respective volume.

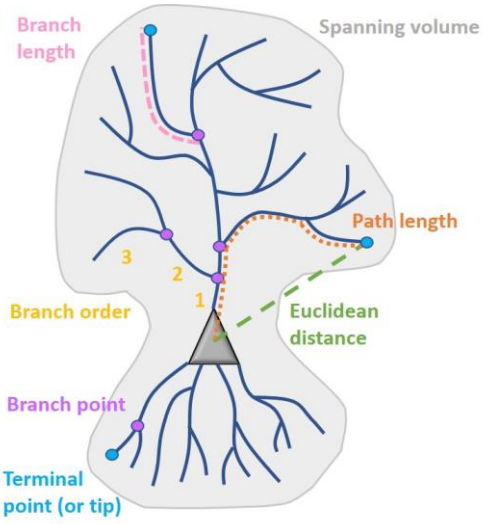

Figure 1.2 - Schematic representation of the neuromorphological metrics of a pyramidal neuron.

Table 1.1 - Description of the selected neuromorphological metrics. Each metric has one value for the whole tree.

Name	**Description**
Total length [µm]	Sum of the length of all the segments of the dendritic tree
Maximum path length [µm]	Distance along the dendritic tree (path) from the soma to the tip of the longest dendrite
Mean branch length [µm]	Mean of the length of all the branches in a tree, calculated between every consecutive branching points (bifurcation) or terminal point to its respective branching point
Soma radius [µm]	Radius of the soma of the neuron
Tree radius [µm]	Radius of the spanning volume of a dendritic tree, as defined by Wen *et al* 2009
Volume [μm^3]	Spanning volume of a dendritic tree
Number of branch points	Number of bifurcations in a tree
Mean branch order	The branch order is defined for every branch. It is 0 at the soma and with each branching point, the order increases by 1
Straightness	Mean of the ratios between the euclidean distance and the respective path length. The ratio is obtained for every branch point and tip of the tree

To calculate the radius of a neuronal tree, the maximum euclidean distance from a tip to the soma is normally used. This would result in a sphere enclosing the whole tree, centered at the soma, whose radius would be assumed as the radius of the neuron **(Figure 1.3)**. However, this approach is only valid when the neuron has a regular distribution of dendrites in a circle **(Figure 1.3A)**. Since the dendritic trees of our dataset do not spread circularly, but are mostly spread in one direction, we cannot use this approach **(Figure 1.3B)**. For this reason, to calculate their radius, we implemented on MATLAB the definition given by Wen, where the tree radius *R* is defined as the root mean square distance between any 2 dendritic segments *(Wen et al., 2009)*:

$$R^2 = \frac{1}{L^2}\sum_{i=1}^{k}\sum_{j=1,j\neq i}^{k}\delta l_i \delta l_j \left(r_i - r_j\right)^2 \qquad (\mathbf{1.1})$$

Being L the total length, k the total number of segments, δl_i the length of the segment i and r_i the position vector of the segment i.

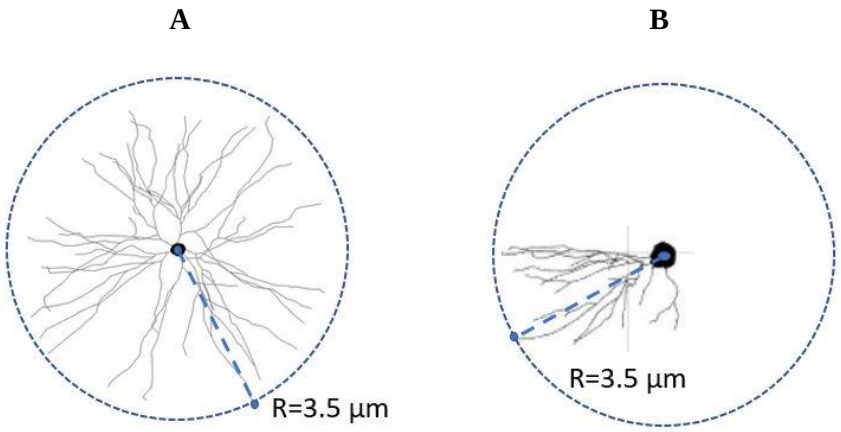

Figure 1.3 - Examples of the bias in dendritic arbor radius (R) calculation. A: Taking the maximum euclidean distance from a tip to the soma is the same as having a circle centered at the soma to the furthest tip, and extracting its radius. This approach is used for circular trees. **B**: Example of when using a centered circle does not make sense. The neuron in this case has the dendrites all to one side, so this value would be incorrect.

After obtaining the 9 metrics of interest, we calculated their coefficient of variation (CV), a dimensionless number that accounts for the data variability. It is defined as the ratio between the standard deviation and the sample mean, so the larger the CV, the more dispersed the data is. Besides calculating the global CV of each metric and of each sex separately, we also calculated the CV for each animal individually, to make sure it did not influence data dispersion. The metrics were exported to R (version 3.5.0) to perform cluster and statistical analysis.

1.2.2. Cluster analysis

To identify if there is an underlying structure to our data, we performed a hierarchical cluster analysis *(Kaufman & Rousseeuw, 1990)* in R (version 3.5.0). To this aim we used function *heatmap.2* (*cluster*, version 2.0.9). The cluster analysis was applied to (a) the whole dataset and (b) separately to the data from each sex. In (b), we obtained 2 clusters for each sex, making a total of 4 clusters. We took 1 cluster from each sex with similar metrics and merged them together, resulting in 2 subsets of the data (2 clusters).

The type of hierarchical cluster analysis performed was divisive, which means it consecutively divided the data into the two most distinct clusters. The separation between data points was measured by the euclidean distance, and given that each point had very different ranges of values, the metrics needed to be scaled because euclidean distance does not make sense without scaling.

One of the possible ways to visualize the result of a hierarchical cluster analysis is by combining heatmaps and dendrograms. Heatmaps represent the scaled data with intensity colours, aiding in visualizing the generated clusters; dendrograms show the hierarchy of cluster separation. Considering we have a total of 66 neurons and 9 metrics, the dendrogram could either interpret the metrics as being characterized by the neurons (meaning we had 66 measurements of each metric) or vice-versa (9 measurements for each neuron). When the dendrogram was applied to the neurons, it compared the 9 values of the neurons with each other, showing the underlying structure of the data. If the dendrogram was applied to the metrics, it compared the 66 values of the metrics with each other, obtaining relationships between them.

To classify the obtained clusters, we computed the silhouette coefficient (SC) for $k=2$, with k the number of clusters *(Rousseeuw, 1987)*. The SC calculated the ratio between the intra and inter cluster distances. The first is how close the point is to its cluster, and the second how distant it is to its neighbour cluster. If the SC was between 0 and 0.25, the clustering was not necessarily due to some structure of the data; between 0.25 and 0.5 there was some structure; between 0.5 and 1 it was a good cluster. The results and graphical representations of the SC are provided in **Supplementary Information III.**

1.2.3. Statistical Analysis

As mentioned before **(Section 1.2.1)**, in our dataset we have 5 mice per sex, with 5 to 8 neurons from each animal. It was previously shown that having multiple neurons from the same animal introduces some variability in the data that needs to be accounted for *(Wilson et al., 2017)*. We categorized this as a random effect, for which we applied Generalized Linear Mixed Models (GLMMs) with the *glmer* function (*lme4*, version 1.1.19). With GLMMs besides defining the random effect, the response variable does not need to be normally distributed. This is why the model is called generalized linear, where one of the inputs is the distribution.

The first step was to check for the normality of each metric, for which we applied Shapiro-Wilk tests *(Shapiro & Wilk, 1965)*. If p-value$\leq$0.05 (alpha value), we rejected the null hypothesis and concluded the metric was not normally distributed; if p-value>0.05 we could not discard that the metric could follow a normal distribution. However, not being able to discard this possibility does not mean that a normal distribution is the best fit for the metric. For this reason, when the p-value was above the alpha value but still quite small (0.05>p-value<0.15), we also checked the skewness of the metric. If the skewness is below 0.5, then we can approximate the metric to a normal distribution; otherwise, we cannot assume the metric is normal *(Webster & Oliver, 2007, Chapter 2)*.

For variables which are not normally distributed, we visually inspected the histograms to assess which distributions could fit **(Figure 1.4)** *(Damodaran, 2008, Chapter 6)*. The *descdist* function (*fitdistrplus*, version 1.0.14) plots a Cullen and Frey graph, which shows how close the metric's behaviour ("observation") is to different theoretical distributions **(Figure 1.5)**. With this information, we fitted only the closest distributions with the *fitdist* function (also from *fitdistrplus* package), which estimates parameters and provides goodness-of-fit graphs for a given distribution. For selecting the best-fit model, we compared graphical criteria by using quantile-quantile (Q-Q) plots **(Figure 1.6)** *(Gibbons & Chakraborti, 2003, Chapter 4)*, and numerical criteria with the Akaike information criterion (AIC) *(Akaike, 1974; Bozdogan, 1987)*. The distribution with a better fit in the Q-Q plot and/or with the smallest AIC would be selected.

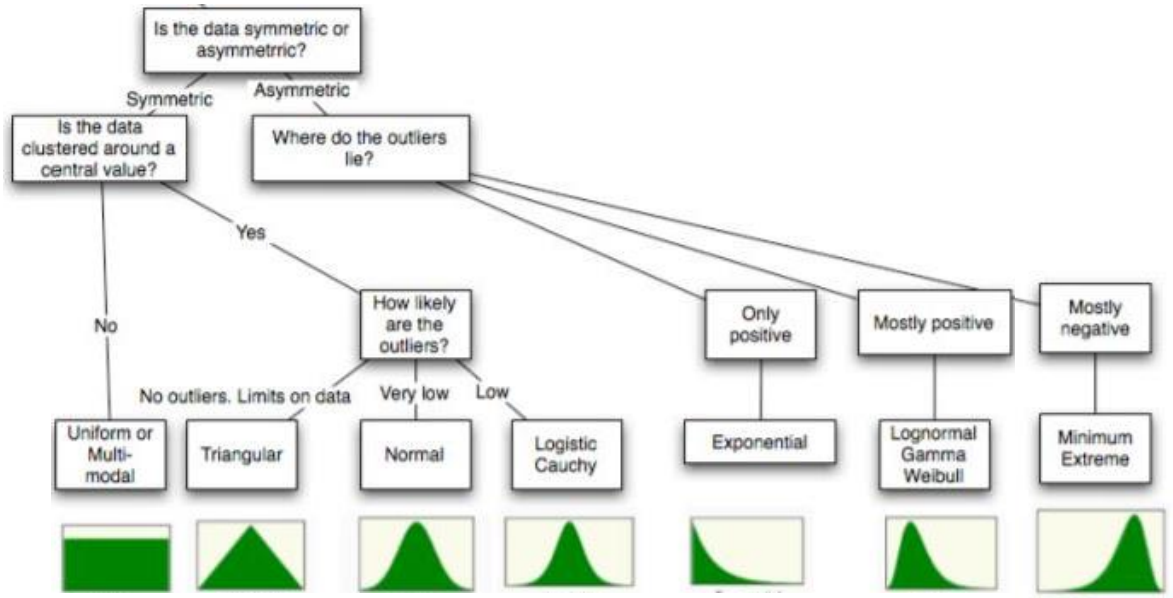

Figure 1.4 - Decision tree for what distribution should fit best a continuous data. Adapted from Damodaran 2008.

In the case of the number of branch points, since it is a discrete variable, we did not check for normality. Given it is a count metric, it usually takes either a poisson or a negative binomial distribution. We fitted both and completed the same Q-Q plots and AIC analysis to choose the best one.

It is also important to note that for variables with very high values, it is not possible to fit gamma distributions, as it gives an error. This was the case of volume, so in order to do the fit, the metric was scaled by dividing it by 100. For comparison purposes, we also used this scaling for the other distribution fits of volume.

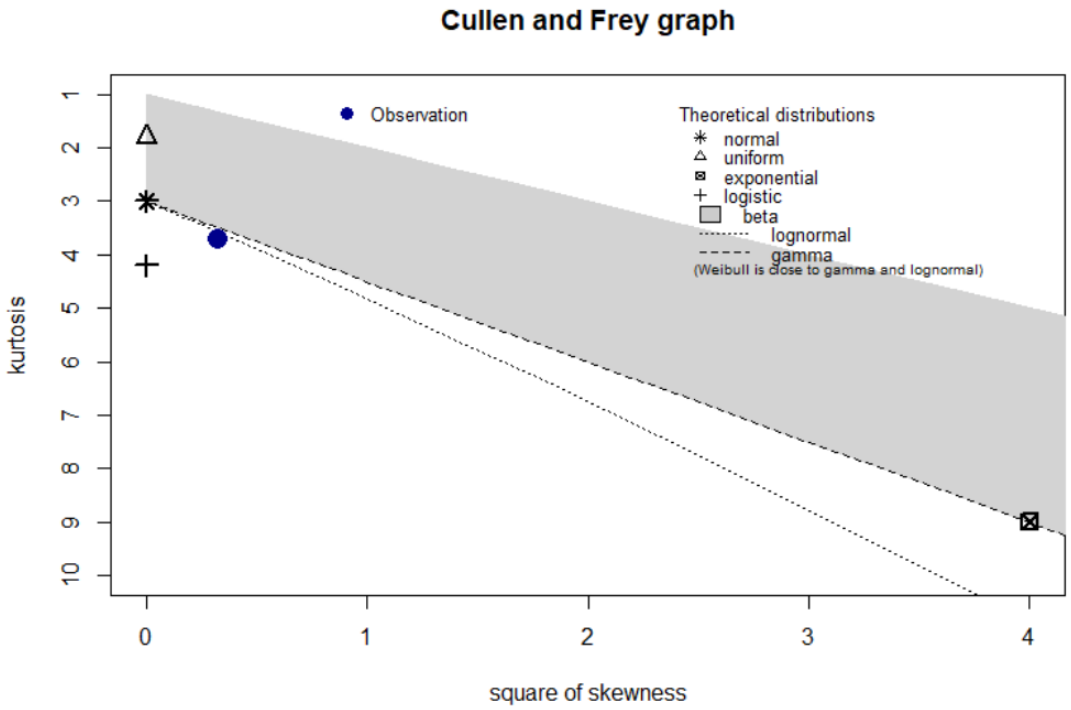

Figure 1.5 - Example of a Cullen and Frey graph. It locates the observed metric in a kurtosis-skewness space, where common distributions (continuous or discrete) are also represented. This visually aids in choosing which distributions to fit the data. In this case, the observed metric (blue point) could fit either a lognormal or a gamma distribution. Generated in R with the *descdist* function.

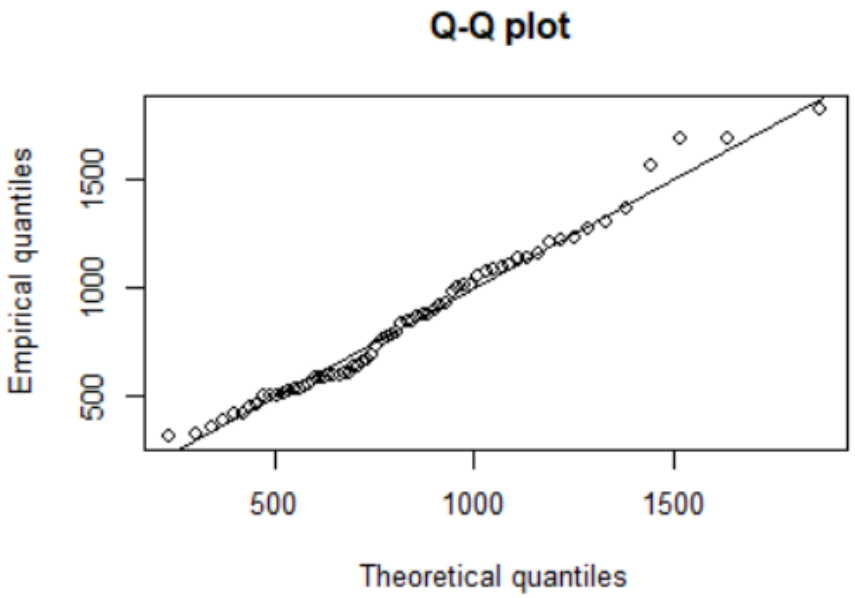

Figure 1.6 - Example of a Q-Q plot. The line is the relationship we should see between the quantiles, and the points represent how the data actually behaves. Generated in R with the *fitdist* function.

One constraint to GLMMs is the lack of available distributions. When all the available distributions in the *glmer* function did not describe a metric, we performed a permutation test, using the *aovp* function (*lmPerm*, version 2.1.0). This is a non-parametric test where there is no need to define the distribution, so we were still able to assess if there was a difference due to sex while accounting for random effects. After defining the distribution of the metric, we fitted the GLMM model m_i as:

$$m_i = glmer(y_i \sim sex + (1|animal\ ID), distribution) \qquad (\mathbf{2.2})$$

Being y_i the variable of interest and *animal ID* the random effect.

There is no straightforward way to extract the p-values of the models, since the developers of the *lme4* R package deliberately did not include it. Their choice was due to the many issues revolving around the calculation of p-values with Linear Mixed Models (LMM) and GLMMs. These have been described in length elsewhere *(Bolker & others)*. The scientific community in general cannot come to a consensus on what approach to use, and so we decided to use a contrast matrix. To do so, we built a design matrix with the values of sex and transformed it into a contrast matrix (*limma*, version 3.36.5). Given all the coefficients of a model fit, this matrix specifies which comparisons should be extracted. Using function *glht* (*multcomp*, version 1.4.10), it applies a general linear hypothesis comparing the contrast matrix with the model. As a result, we are provided the p-value of the difference between sexes.

The model m_i was applied for the whole dataset (see **Supplementary Information II**), and for each of the obtained clusters. We show the results for each metric by a combination of three graphical outputs: (a) violin plots, to have the probability density *(Hintze & Nelson, 1998)*; (b) boxplots, to see the quartiles and outliers; (c) data points, to see the data distribution. It also contains the significance of the model: NS is non-significant, * is p-value<0.05, ** is p-value<0.005 and *** is p-value<0.001. The metrics are identified by a label that contains its name, units, and chosen distribution. When the distribution was determined as log-normal, we represent the variable with its log values. The same applies when the distribution fits were done with the metric scaled, as was the case of volume, which is represented divided by 100.

1.3. Results

1.3.1. Dataset and morphological metrics

We explored the neuromorphological differences between sexes in basal dendrites from the CA1 layer of the hippocampus of young male and female mice **(Table 1.2)**. The selected 3D neurons are depicted in **Figure 1.7** as 2D projections, separated by sex. It is visually clear they are extremely variable, as both males and females have neurons with smaller and larger dimensions. We wondered if this variability was because we had multiple neurons from the same animal **(Table 1.2)**. For this reason we calculated the CV of each of the 9 selected metrics, not only the global CV and for each sex separately, but also the CV for each animal **(Table 1.3)**. The global CV confirms the existence of data dispersion, especially regarding volume and total length (0.73 and 0.42, respectively). Straightness is an exception, with a CV of only 0.06, which might be due to the metric's values being extremely specific for a given type of neuron, especially given we are focused on basal dendrites. As for the CV of each sex, the values are close to the global CV, as expected. Mean branch order is the only metric where females have a higher CV than males. Total length (females 0.32, males 0.47) and volume (females 0.65, males 0.77) are the ones with the strongest sex-difference, while the other metrics have more similar CV. When considering the CV of each animal, the values fluctuate around their global CV, usually implying data variability. Once again straightness is an exception, as well as soma radius, which has some mice with low CV. Another interesting thing to note is how the CV of the volume of two male mice is above 1 (male-147 and male-183, with a CV of 1.00 and 1.02, respectively), which means the variation of volume between all selected neurons is greater than the mean of the animals **(Table 1.3)**.

Table 1.2 - Summary of the study sample.

Category	**Data specification**
Species (strain)	Mouse (C57BL/6J)
Age	28 days
Brain region	Hippocampus CA1
Cell type	Pyramidal cell (only basal dendrites)
Number of subjects	5 per sex
Number of neurons	5 to 8 from each subject
Total sample size	66: 33 females and 33 males

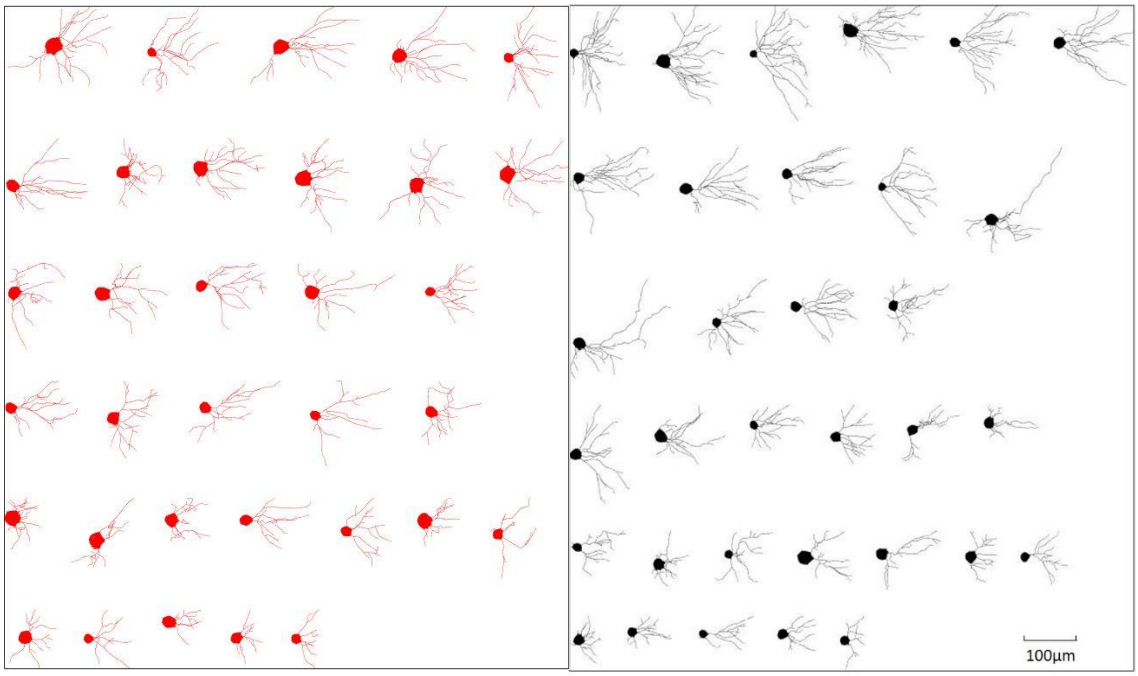

Figure 1.7 - 2D projections of the neuronal trees. They are arranged from the largest to the smallest total length, and aligned along the x-axis. Females are represented in red and males in black.

Table 1.3 - Coefficient of variation (CV) of each metric shows data variability. When considering the global CV, straightness is the most uniform metric, while the others have more variability, especially volume and total length. Overall males have higher CV than females, except for mean branch order. As for the CV of each animal, no animal seems to introduce bias in the data, as generally all CV point towards the existence of data dispersion, except for straightness.

	Total Length	Max. Path Length	Mean Branch Length	Number of Branch Points	Mean Branch Order	Vol-ume	Straight-ness	Tree Radius	Soma Radius
Global CV	0.42	0.30	0.23	0.30	0.18	0.73	0.06	0.24	0.16
CV Females	0.32	0.28	0.20	0.26	0.19	0.65	0.05	0.21	0.15
CV Males	0.47	0.30	0.26	0.32	0.16	0.77	0.06	0.25	0.16
Fem-122	0.27	0.32	0.27	0.29	0.21	0.57	0.04	0.23	0.18
Fem-146	0.18	0.09	0.12	0.19	0.12	0.63	0.07	0.16	0.07
Fem-152	0.45	0.34	0.20	0.28	0.19	0.76	0.04	0.26	0.15
Fem-181	0.39	0.26	0.23	0.31	0.26	0.65	0.04	0.23	0.14
Fem-96	0.22	0.27	0.11	0.21	0.17	0.39	0.07	0.14	0.07
Male-105	0.37	0.28	0.26	0.30	0.18	0.49	0.04	0.20	0.18
Male-124	0.31	0.19	0.17	0.36	0.13	0.40	0.07	0.13	0.11
Male-147	0.46	0.31	0.22	0.26	0.21	1.00	0.04	0.26	0.09
Male-153	0.48	0.24	0.22	0.30	0.16	0.72	0.06	0.23	0.07
Male-183	0.32	0.33	0.30	0.16	0.15	1.02	0.05	0.27	0.17

1.3.2. Cluster analysis

To determine if the neurons of our dataset could be classified into a number of different groups on the basis of a set of measured variables, we performed a divisive hierarchical cluster analysis.

When clustering the whole dataset, we found a clear separation of the neurons in two clusters that did not separate the data by sex. One of the clusters contained many more trees (40 of 66) than the other (remaining 26), the latter having a proportion of 10 females to 16 males. This separation mostly depends on metrics related to the size of the trees. Overall, the cluster with only 26 trees has a larger radius, maximum path length, volume and total length **(Figure 1.8)**.

Looking at the dendrograms of the metrics, which shows possible relations between them, we found three different clusters. As expected, metrics relating to the dimension of the tree clustered together (total length, tree radius, mean branch length, volume and maximum path length). The same happens to the ones associated with branching (mean branch order and number of branch points, with soma radius). However, straightness is separated from the others. This means it is not directly related to the remaining variables **(Figure 1.8)**.

To assess the quality of the clusters we obtained the SC of each data point, cluster and total analysis. The average SC of the analysis with just 2 clusters is 0.29. This indicates the data has some structure **(Figure SIII.1)**.

Because clustering on the whole dataset did not find a sex-related clustering, we decided to apply the clustering algorithm to males and females separately (**Figure 1.9** and **Figure 1.10**, respectively). This time the aim was to find clusters in each sex that could be explained by the same metrics. In both sexes two clusters were obtained that depend mainly on the metrics related to the size of the neuronal trees (total length, volume, maximum path length and radius). This is especially clear in the males **(Figure 1.9)**, which shows a clear separation of the high and low intensity values of each cluster. Since both the male and female clusters are classified by the same metrics, it makes sense to combine their results, to represent the whole dataset as two subgroups.

Looking at the dendrograms of the metrics, in the females we found three relations: metrics associated to the dimension of the tree clustered together, and so did the metrics related to branching; straightness is a cluster on its own, meaning it is not related to the remaining metrics **(Figure 1.10)**. This is as we have previously seen when we clustered on the whole dataset **(Figure 1.8)**. Looking at the dendrograms of the metrics in the males, besides these 3 relations, soma radius is also a cluster on its own **(Figure 1.9)**.

For the males the average SC is 0.37, with all values over the threshold of 0.25 **(Figure SIII.2)**. For the females the average SC is 0.22, not passing the threshold of 0.25 due to the misclassification of 3 neurons **(Figure SIII.3)**. After reclassifying these 3 neurons from cluster 1 to cluster 2, the final average SC is 0.28 **(Figure SIII.4)**.

Given that the classification of the 2 clusters of each sex was mainly driven by metrics of size (**Figure 1.9** and **Figure 1.10**), we can combine the results to have two subsets of the data: of large- and of small-sized neurons **(Figure 1.11)**. The clusters of neurons of larger size from each sex make up cluster 1, containing 29 neurons. Cluster 2, with the remaining 37 trees, has the neurons of the clusters of smaller size from each sex.

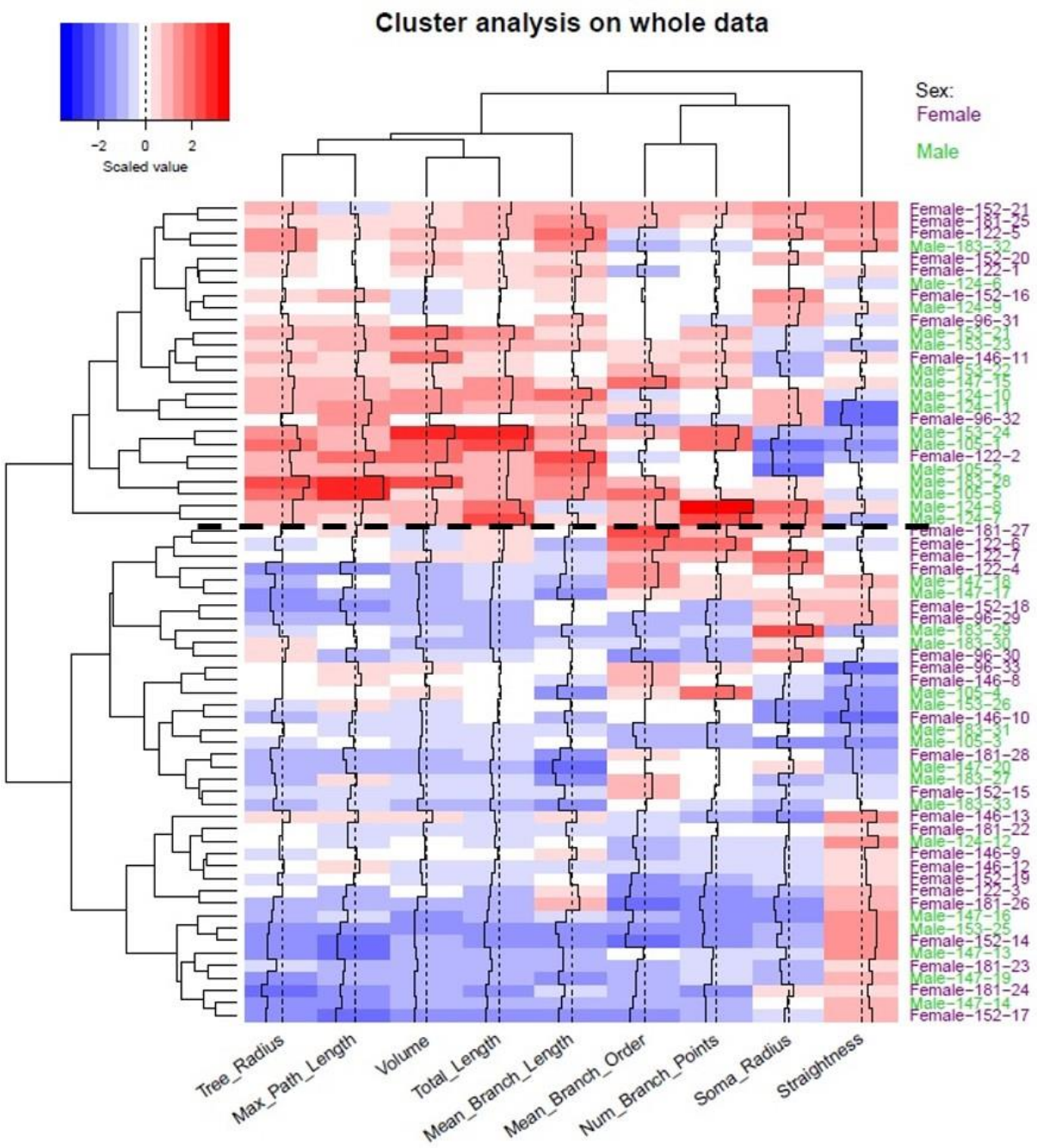

Figure 1.8 - Dendrograms and heatmap of the divisive hierarchical cluster analysis on the whole dataset. Each column of the heatmap is one of the metrics, labelled at the bottom and with its dendrogram on the top. Each row is a neuron, labelled on the right as sex-animal ID-number (coloured by sex), with the dendrogram on the left. The heatmap uses the scaled values of the observations and attributes a colour according to it. It ranges from blue, through white (zero), to red, as it is shown on the upper left corner. The black line in each column (metric) aids in understanding the value of the intensity, as it shifts from left (blue) to right (red) with a height according to the magnitude of the scaled value. The black horizontal dashed line was added manually where the algorithm separated the data between two clusters, to help the visualization. The top cluster contains 26 neurons (10 females and 16 males), whereas the bottom one contains the remaining 40 (23 females and 17 males). This separation is due to metrics related to the size of the trees: radius, maximum path length, volume and total length. The clustering of the variables (top dendrogram) shows metrics of size cluster together and so do the ones related to branches; straightness is a cluster by itself, meaning it is not very related to the other metrics.

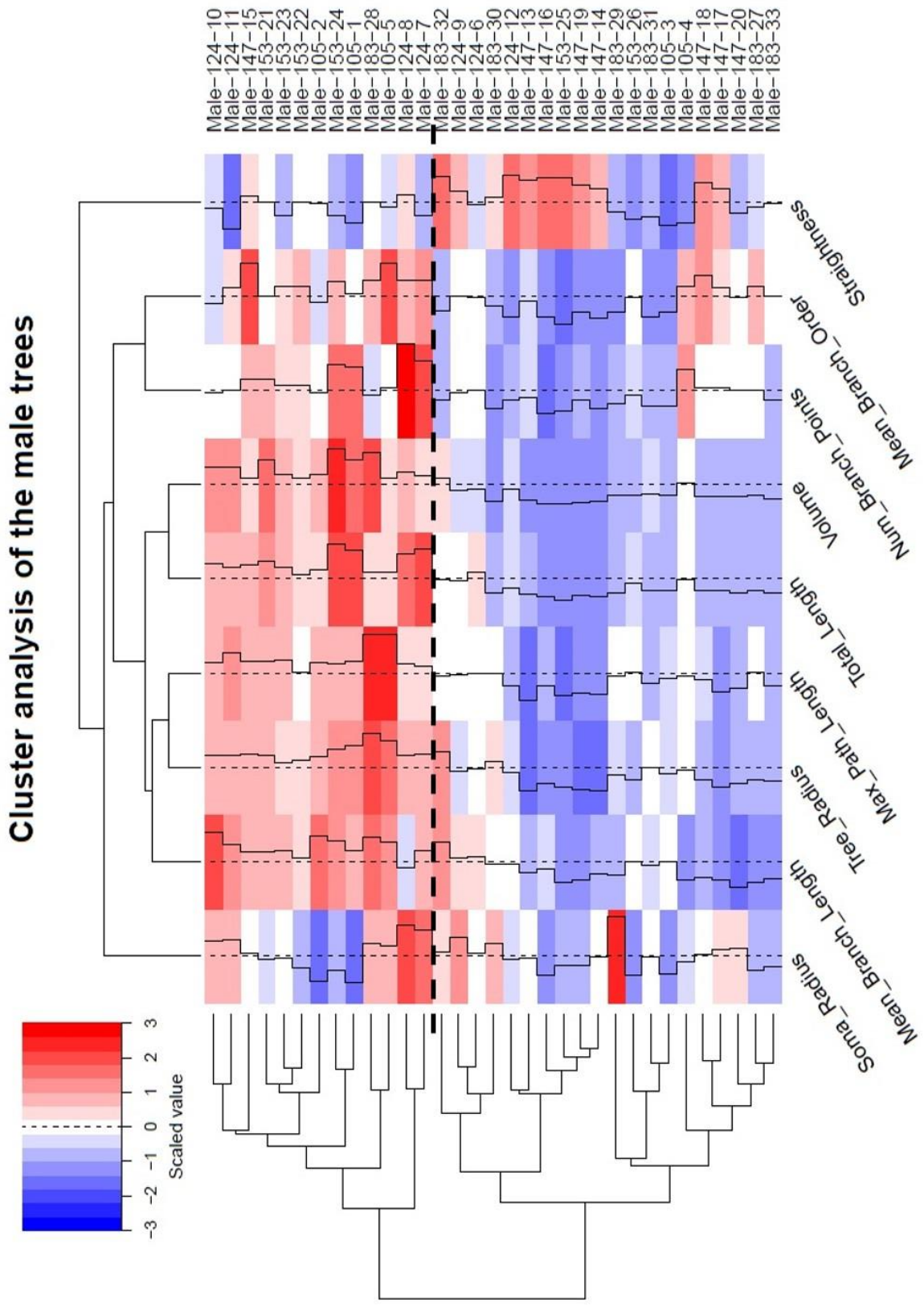

Figure 1.9 - Dendrograms and heatmap of the divisive hierarchical cluster analysis on the male neurons. The top cluster contains 13 neurons and the bottom one contains the remaining 20. This is due to metrics related to the size of the trees: radius, maximum path length, volume and total length, as well as from number of branch points and mean branch length. Clustering of the variables shows both straightness and soma radius cluster by themselves, metrics of size cluster together and so do the ones related to branches. Labels are explained in **Figure 1.8**.

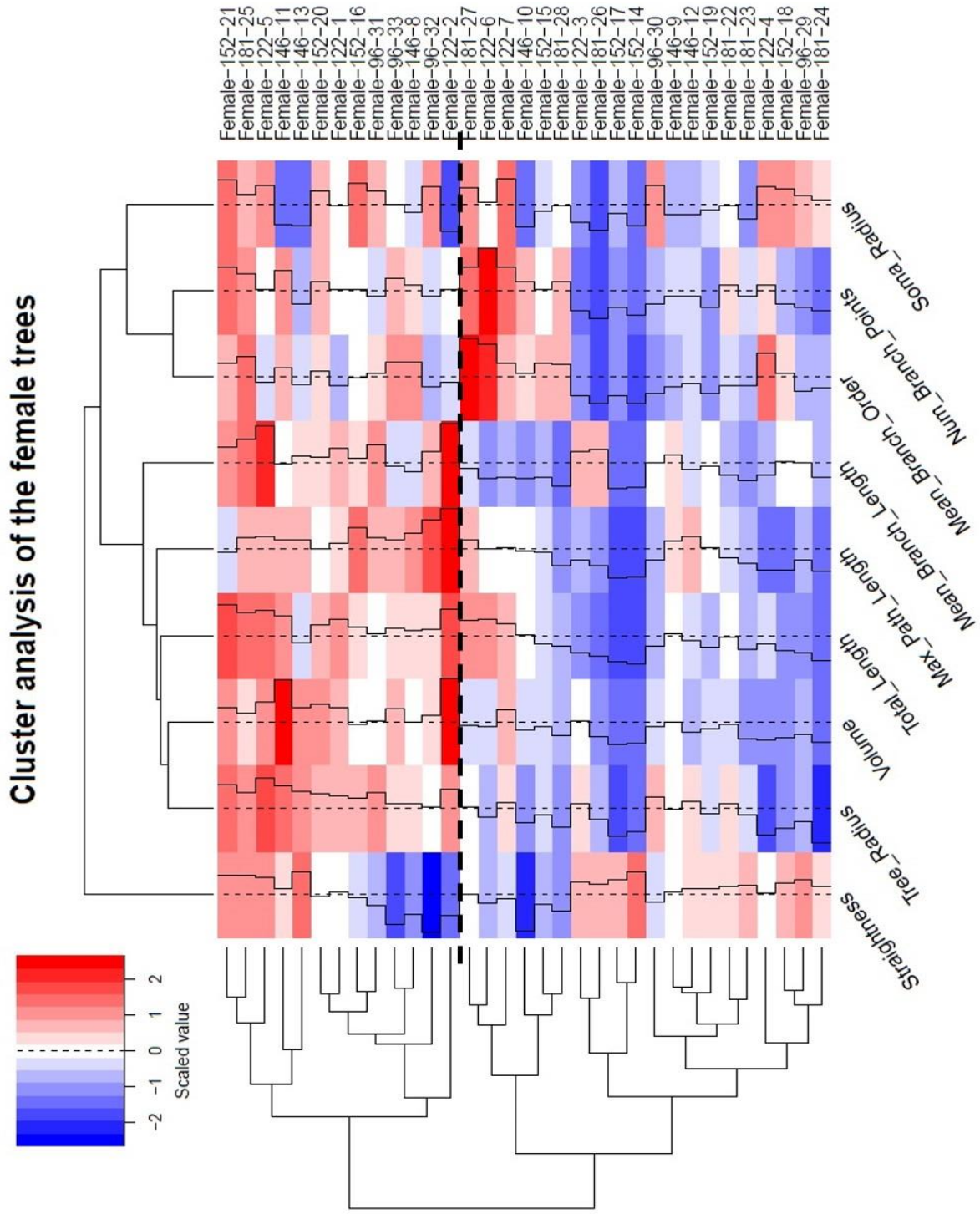

Figure 1.10 - Dendrograms and heatmap of the divisive hierarchical cluster analysis on the female neurons. The top cluster contains 13 neurons and the bottom one contains the remaining 20. This is due to metrics related to the size of the trees: radius, maximum path length, volume and total length. Clustering of the variables revealed straightness forms a cluster, metrics of size cluster together and so do the ones related to branches. Labels are explained in **Figure 1.8**.

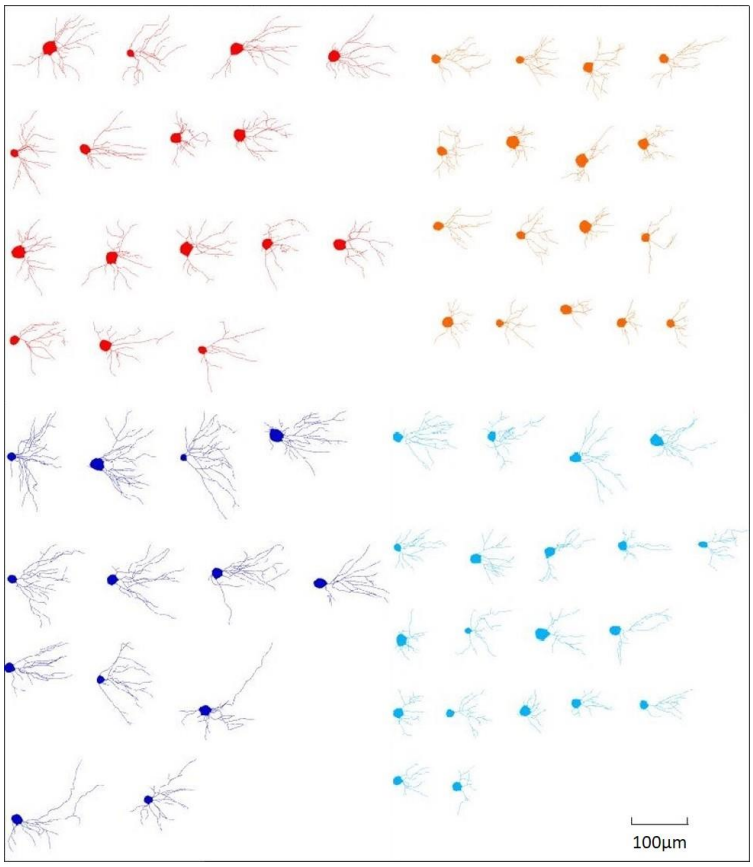

Figure 1.11 - 2D projections of the neuronal trees, coloured by sex and cluster. Neurons of cluster 1 are on the left: females are represented in red and males in dark blue. Neurons of cluster 2 are on the right: females are represented in orange and males in light blue. Each group is arranged from largest to smallest total length, and aligned along the x-axis.

1.3.3. Statistical analysis

When assessing the normality of the metrics in the clusters, Shapiro-Wilk tests revealed only one metric was not normal in each subset **(Table 1.4)**. In cluster 1 it was maximum path length (p-value 0.007), assuming a log-normal distribution. In cluster 2 it was straightness (p-value 0.034), where the distribution that could fit the shape of the metric would be a minimum extreme. This is not available in the *glmer* function, so we performed a permutation test instead of applying a GLMM. Soma radius and volume passed the Shapiro-Wilk test in both subsamples with very small p-values (soma radius: 0.081 and 0.115; volume: 0.069 and 0.068, respectively for each cluster). For this reason, we calculated the skewness of both cases. For the volume we used volume/100 to be able to fit a Gamma distribution, which turned out to be the best fit for both clusters. As for the soma radius, in the cluster 1 it is considered as normally distributed (-0.405), but not in cluster 2 (0.772), fitting a log-normal. Other metrics for which we calculated the skewness were total length in cluster 1 (p-value 0.071, skewness 0.83) and mean branch order in cluster 2 (p-value 0.109, skewness 0.42). The latter could be approximated as normal, as opposed to total length, which fits a log-normal distribution **(Table 1.4)**.

Table 1.4 - Statistical comparisons between sexes of each cluster. Overview of the mean and standard deviation for each sex (F for females and M for males) of each cluster and summary of the results obtained in each step of the GLMM. If there is a dash, it means the test was not performed. P-values in bold are statistically significant.

	Cluster	Mean	Standard deviation	Shapiro-Wilk (p-value)	Skewness	Assumed distribution	GLMM p-value
Total length [µm]	1	F: 962.91 M: 1346.19	F: 150.48 M: 265.18	0.071	0.83	Log-normal	**1.2×10^{-6}**
	2	F: 568.44 M: 618.55	F: 137.03 M: 189.13	0.169	-	Normal	0.414
Maximum path length [µm]	1	F: 146.83 M: 177.56	F: 23.90 M: 30.76	0.007	-	Log-normal	**0.0011**
	2	F: 98.31 M: 111.95	F: 24.87 M: 23.58	0.178	-	Normal	0.208
Mean branch length [µm]	1	F: 30.42 M: 33.06	F: 5.67 M: 4.24	0.823	-	Normal	0.163
	2	F: 24.93 M: 22.73	F: 4.22 M: 4.98	0.436	-	Normal	0.211
Soma radius [µm]	1	F: 9.98 M: 9.37	F: 1.55 M: 1.69	0.081	-0.40	Normal	0.472
	2	F: 9.07 M: 9.05	F: 1.27 M: 1.29	0.115	0.77	Log-normal	0.960
Tree radius [µm]	1	F: 58.54 M: 69.09	F: 6.54 M: 7.35	0.618	-	Normal	**4.4×10^{-5}**
	2	F: 43.87 M: 46.65	F: 8.73 M: 9.21	0.709	-	Normal	0.505
Volume [µm^3]	1	F: 174436.4 M: 256670.4	F: 66568.4 M: 69044.2	0.069	0.58	Gamma (Volume/100)	**2.7×10^{-5}**
	2	F: 63541.4 M: 67609.9	F: 34813.5 M: 46122.9	0.068	0.80	Gamma (Volume/100)	0.861
Number of branch points	1	F: 19.25 M: 23.38	F: 3.89 M: 5.94	-	-	Poisson	**0.016**
	2	F: 14.06 M: 16.00	F: 3.23 M: 4.00	-	-	Poisson	0.130
Mean branch order	1	F: 6.12 M: 6.52	F: 0.96 M: 0.75	0.260	-	Normal	0.215
	2	F: 5.09 M: 5.42	F: 0.97 M: 0.80	0.109	0.42	Normal	0.254
Straightness	1	F: 0.85 M: 0.83	F: 0.05 M: 0.03	0.579	-	Normal	0.240
	2	F: 0.87 M: 0.86	F: 0.04 M: 0.05	0.034	-	Permutation test	0.646

After defining the distribution of each metric, we applied the GLMMs. Looking at the results from cluster 1, more than half of the metrics reach significance. Total length is the metric with the smaller p-value (1.2×10^{-6}). All metrics that depend or are related to total length are also significantly different, which was expected. This is what we see for maximum path length, tree radius and volume (p-values 0.0011, 4.4×10^{-5}, 2.7×10^{-5}, respectively). One would also expect to see this trend with mean branch length, as it is related to total length. However, since we are dealing with the mean values, this influences the result, making the metric non-significant (p-value 0.163). Number of branch points also reaches significance, but less as compared to the other metrics (p-value 0.016). All these significant differences are with males having higher values than females, both in means and in the maximum value (**Table 1.4** and **Figure 1.12**).

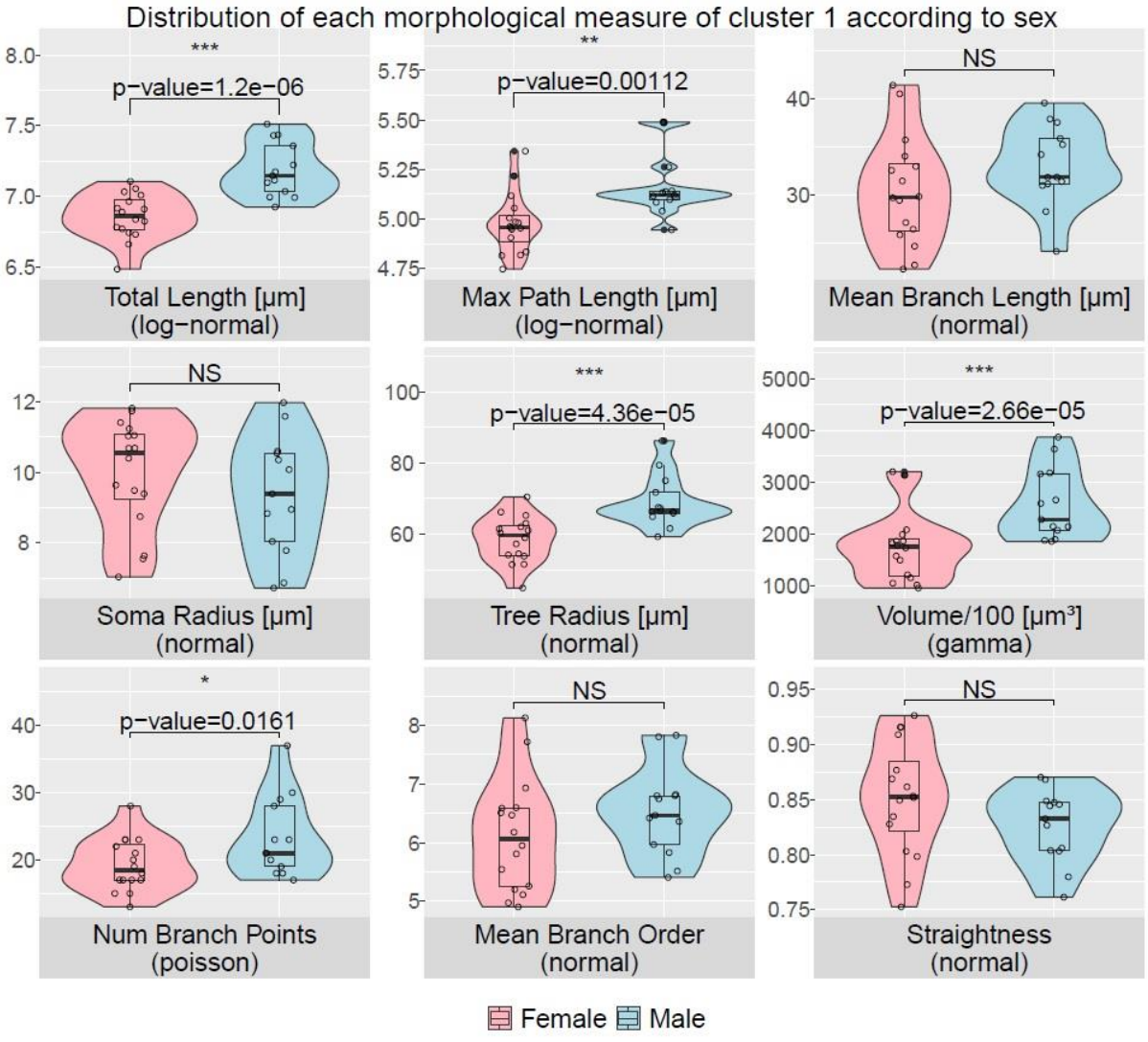

Figure 1.12 - Sex-dependent neuromorphological differences for Cluster 1. Each panel has violin, boxplot and data points of each variable, the latter representing each neuron of the dataset. The label of the panels has the name, unit and distribution used in the GLMM of the corresponding metric. The significance level of the test is shown on top of each panel: NS is not significant, * is p-value<0.05, ** is p-value<0.05 and *** is p-value<0.001. If it passes the threshold of significance, the p-value is also shown. Females are represented in pink and males in blue. Total length, maximum path length, radius, volume and number of branch points reach significance.

In cluster 2, we see similar results as obtained with the whole dataset **(Figure SII.1)**, where none of the metrics reach significance (**Table 1.4** and **Figure 1.13**). The variable closest to reach significance was the number of branch points with a p-value of 0.130. The remaining metrics all have p-values>0.20. The fact that we do not see any significant differences in this cluster makes us wonder if it has a specific category of neurons, such as pruned or still developing neurons.

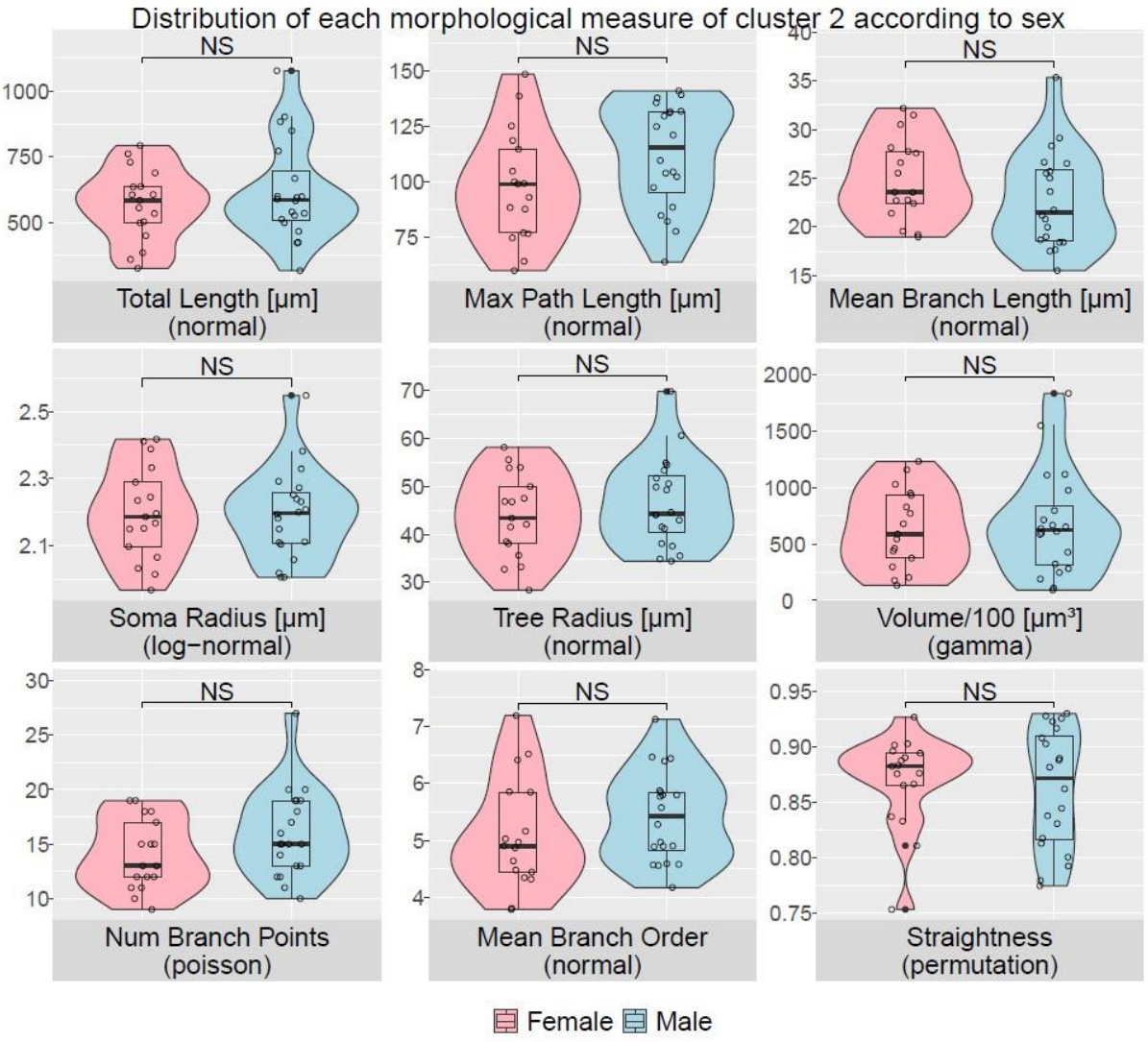

Figure 1.13 - Sex-dependent neuromorphological differences for Cluster 2. Labels are explained in **Figure 1.12**. There are no significant metrics in the small-sized neurons.

1.4. Discussion and Conclusions

In this chapter we explored morphological differences in CA1 pyramidal neurons of female and male mice. Our dataset comes from only 5 mice of each sex, meaning we have multiple neurons from each animal. It is assumed that using multiple neurons per animal does not introduce as much new information as using a neuron from a new animal *(Wilson et al., 2017)*. This is not the case of our data, as one animal can have one of the largest and also one of the smallest neurons. This variability is shown through the calculated CV for each animal, but is even more obvious when we assess the Principal Component Analysis (PCA), where each mouse is spread out in the PCA space **(Figure SIV.2)**. One limitation in our study is that we cannot account for the exact location of the neurons in the CA1 layer. In the study where the dataset was obtained, one of the inclusion criteria was that the cell body was located in the middle third of the thickness of the 100 µm sections *(Lein et al., 2007)*. However, this is not very specific, as it was previously shown that the properties of CA1 pyramidal neurons vary across the three different spatial axes of the hippocampus (proximal-distal, dorsal-ventral and superficial-deep) *(Cembrowski & Spruston, 2019)*. These include differences in function, electrophysiological properties, morphology and other characteristics *(Cembrowski & Spruston, 2019; Danielson et al., 2016; Mizuseki et al., 2011)*. The inhomogeneity of the CA1 pyramidal layer *(Cembrowski & Spruston, 2019)* could explain the variability we have seen in morphology, especially between neurons of the same animal.

Even though we had high data variability, using a cluster analysis we could identify two clusters, separating overall smaller-sized neurons from larger ones. This clustering was always driven by the metrics associated with the size of the neurons, and the average SCs also cemented the validity of this approach. We speculate that either the neurons were selected from different sublayers of CA1, or they reflect differences in pruning. The former, as it was already mentioned, is a possibility we cannot account for, since the exact location of the neurons within the sublayers of CA1 was not provided by the authors *(Wilson et al., 2017)*. The latter is a process of removal of synapses or dendritic material *(Koss et al., 2014)*. Thus, our cluster algorithm could be separating cells that are at different developmental stages, as the mice used in the sample are 28 days old *(Flurkey, Currer, & Harrison, 2007, Chapter 20)*. In fact, a recent study has shown the postnatal day 21 (P21) as the peak of synaptic pruning in CA1 neurons of wild-type (WT) C57BL/6J mice, with P28 closely following *(Jawaid et al., 2018)*. This finding supports the speculation that the identified clusters would be capturing neurons at different developmental stages.

When considering the whole dataset, without separating the clusters, we did not find sex-dependent differences **(Figure SII.1)**. However, when repeating the same analysis separating the two clusters, in cluster 1 we found significant sex-dependent differences in 5 of the 9 metrics analysed. Metrics related to size of the trees, total length, maximum path length, tree radius and volume, are all significantly larger (p-values<0.002) in male CA1 neurons. The other metric to be significantly different in the first cluster is the number of branch points. This metric is related to the dimension of the tree, as usually if there are more branch points, the neuron tends to be larger *(Brown et al., 2008)*.

Considering that our clusters separated the smaller-sized from the larger-sized neurons, our results show that the larger female dendritic trees are significantly smaller than their male counterparts. This difference does not apply to the smaller ones, which are possibly in earlier developmental stages, suggesting that probably non-cell autonomous factors drive the differences in final size.

Given the underlying differences in brain morphology, i.e., sexual dimorphism in hippocampal volume, we could also interpret those differences as a reflection of mechanical constraints. Although many studies have been made to compare hippocampal volumetric differences, the results are contradictory. One can easily find mice studies where there are no significant differences *(Koshibu et*

al., 2004, 2005), or where males have significantly larger hippocampus volume *(Meyer et al., 2017; Qiu et al., 2018)*. When separately comparing the volumes of anterior and posterior hippocampus, the former is found to be significantly larger in females, whereas the latter is significantly larger in males *(Meyer et al., 2017; Spring et al., 2007)*. When looking at human studies, the results have also been contradictory. We have found a study where the total male hippocampal volume was larger *(Egloff et al., 2018)*, and another where the posterior hippocampus was larger in females, while the anterior and the total volume showed no significant differences *(Persson et al., 2014)*. When separating by right and left side, both sides were larger in females, and more specifically there were no differences in the CA1 layer *(Sussman et al., 2016)*. A recent meta-analysis study showed how after correcting the volume by total brain volume or intracranial volume there would be no significant differences, whereas previously both total, left and right hippocampal volume were larger in males *(Tan et al., 2016)*. Therefore, we cannot make conclusions regarding the possibility of a relationship between the size of the neurons and the size of the hippocampus, and so it is left as an interesting research question. One can also consider a recent study by Qiu *et al*, where they longitudinally imaged male and female C57BL/6J mice in different postnatal days. Comparing the scans from consequent time points, they were able to assess not only the sexually dimorphic areas, but also when the dimorphism occurred. They found that areas that are relatively larger in males develop earlier in life (pre-pubertal), whereas those larger in females only occur later in life (post-pubertal) *(Qiu et al., 2018)*. One wonders if, as the areas develop at different rates, so could the neurons. This would imply that male neurons developed faster than females. Just as the case of comparison of size with the volume of the hippocampus, it is left as an interesting research question.

As for the statistical analysis of the second cluster, it revealed no significant sex-related differences. It is important to note that female and male trees of this cluster are of the same size. As we speculated above, neurons of cluster 2 could have undergone pruning. If this would be the case, then the lack of difference in male and female neuronal size in cluster 2 would reflect a more important loss of dendritic material in the male neurons. Another possibility is a difference in onset of dendritic pruning between males and females *(Keil et al., 2017; Koss et al., 2014)*. If it occurs later for females, then perhaps what we see in our dataset is two different stages of pruning: males have started sooner and females still did not reach this point, and thus have not lost the same amount of dendritic material yet. In fact, there is evidence of different rates of dendritic pruning in rats, where female neurons of the medial prefrontal cortex are pruned from P35 to P90, but not males *(Koss et al., 2014)*. Thus, dendritic pruning occurring at different times for each sex is a possibility that one should consider, and an interesting question to further investigate.

Dendritic morphology and their sex-dependent differences have been better studied in the adult brain, but a detailed analysis in younger mouse models is missing *(Keil et al., 2017)*. This is particularly true for the hippocampus layer CA1, as to our knowledge, few studies analysing the morphology of neurons have been done. Madeira *et al* analysed both P30 and P180 rats and found that the total number of cells was significantly larger in male of both ages, and the number of cells per unit of volume was also significantly larger in P30 males. As for the number of cells per unit of surface area and the mean nuclear volume, they showed no sexual dimorphism in both ages, nor did the number of cells per unit of volume for P180 rats *(Madeira et al., 1992)*. When studying P60 rats, Gould *et al* found no significant sex differences in cell body area, dendritic branch points or length of the longest dendrite for pyramidal cells of CA1 *(Gould et al., 1990)*. Keil *et al* looked at *in vivo* P28 and *in vitro* P0 mice. As the authors mentioned, *in vitro* and *in vivo* results are not directly comparable, and so we will not mention the P0 results *(Keil et al., 2017)*. The P28 neurons overlap with the neurons used in our analysis, as they refer to the same data from Wilson *et al*, but with different sample sizes for each sex *(Wilson et al., 2017)*. They found an increased number of intersections for males when

performing Sholl analysis, indicating a higher dendritic complexity, but no significant differences regarding the number of primary dendrites or area of the soma *(Keil et al., 2017)*. They do not report other morphological metrics, and so our study, which considers 9 different metrics obtained through computational methods, is a more in-depth and, to our knowledge, novel comparison for CA1 pyramidal neurons.

Even though our study has limitations regarding the unspecified location in the CA1 layer of the neurons, our results are still a step forward in understanding sex differences in neurotypical dendritic morphology. We raised interesting research questions concerning neuronal development and synaptic pruning, and the possibility of sexual dimorphism regarding their rates. These speculations were mainly motivated by the significant differences we found in total length, as well maximum path length, tree radius, volume and number of branch points, as they all relate to the dimensions of the neuronal trees. These findings are particularly important for studies of neurodevelopmental disorders, since their prevalence, manifestation and severity are sex-dependent *(Yagi & Galea, 2019)*: males tend to have diseases with early onset such as autism spectrum disorder and attention deficit disorders, while females have more prevalence of anxiety and depression, which occur later in life *(Qiu et al., 2018)*. Thus, these novel findings need to be taken into account in further analysis, both in control cases and disease models.

Chapter 2: Bridging the gap between neuronal morphology, functional capability and neuronal optimality

2.1. Introduction

Since the 1970s, there is a growing consensus among neuroscientists that the morphological properties of a neuron will determine its function and impact how the signals are integrated. Some examples are how the radius of a dendritic branch influences the temporal response of an action potential *(Ramón et al., 1976; Sasaki et al., 2012)*, and how specific architectural alterations regarding the spines disrupts neuronal circuits, leading to brain disorders *(Kulkarni & Firestein, 2012)*. These changes affect the synaptic connections, constraining the neuronal circuit, but it is still unknown how single-cell morphology can have an impact on the network level.

The first proposition regarding neuronal optimality was made by Ramón y Cajal at the end of the 19th century, saying that dendrites will optimize their connectivity by minimizing conduction time in a trade off with total cable length cost. This idea has evolved in the last decades, and it has been proposed that dendritic trees grow to fill optimally a target space while minimizing conduction time and cost. With this in mind, we can define two possible classifications for the wiring of a neuron: optimal and suboptimal *(Wen & Chklovskii, 2008)*. An optimally wired neuron is one that reaches all axons passing through its area, while minimizing its material cost, the total dendrite length **(Figure 2.1 (1))**. Moreover, a balance between total length (sum of the length of all dendrites) and path length (distance along a dendrite, from the soma to the tip) is necessary, as conduction time directly depends on the latter. Therefore, a neuron that reaches the same number of axons with the same total length, but a larger path length, is suboptimal **(Figure 2.1 (2))**. The same happens for a neuron that makes more than one potential synapse with each axon, which will have an unnecessarily longer total length **(Figure 2.1 (4))**. A neuron is also suboptimal if the dendrites are sparse, meaning the spine-reach area is not enough to connect the neuron to all the passing axons **(Figure 2.1 (3))**.

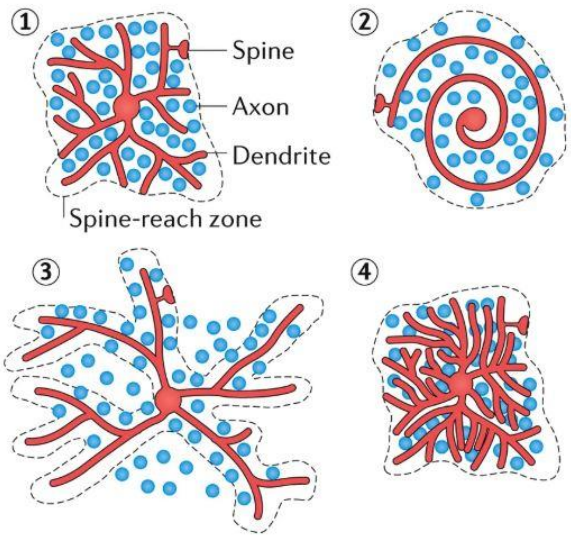

Figure 2.1 - Schematic representation of four dendritic arbor conformations and respective spine-reach zones. The only optimal neuron is case 1, where all axons are connected, and total length and path length are balanced. In case 2 the conduction time is higher because of the longer path length, making it suboptimal even though all axons are reached. In case 3 some axons make no connections with the tree, and in case 4 there is an overabundance of connections and higher material cost. From Schröter *et al.* 2017.

Using the concept of optimality, one can try to bridge the gap between single-cell architecture and the implications in the network they form. However, studies on wiring optimality usually do not take into account fine morphological details and how they might impact it, and so this gap remains to be understood *(London & Häusser, 2005; Orlandi et al., 2013; Voges et al., 2010)*. Two neuromorphological laws that imply optimal wiring have been derived from a functional reasoning of connectivity and integration efficiency maximization *(Cuntz et al., 2012; Wen et al., 2009)*. This allows one to generalize from morphology properties towards impaired function. Nevertheless, the variables which account for connectivity and integration efficiency are not explicitly considered in the proposed power laws. Hence, the ability to assess their relative contributions to dendritic architecture is constrained. This means that even when single-cell architecture is considered when assessing optimality, the association to functional capabilities is missing. Recently, Manubens-Gil defined a neuron's computational capabilities by taking into account specific neuromorphological properties, and determined its wiring optimality as the maximization and minimization of these functional aspects *(Manubens-Gil, 2018)*. By doing so, he was able to explicitly connect single-cell architecture, wiring optimality and functional capabilities. Building on this work, we applied a similar approach to our study.

In this chapter we set out to determine if the sex-dependent morphological differences we found in **Chapter 1** have implications on their computational capabilities and wiring optimality. To this end, we assessed optimality with previously derived power laws *(Cuntz et al., 2012; Wen et al., 2009)*, and calculated some measures of dendritic complexity. We also proposed a multi-objective approach to optimality, which is assessed by the balance of three measures of a neuron's functional capabilities. These measures are defined directly or indirectly in function of neuromorphological properties. We hypothesize that the sex-dependent morphological differences in neurons of cluster 1 may impact their functional capabilities and optimality. We also hypothesize such differences will not be found in neurons of cluster 2, since they also showed no significant sex-dependent differences in morphological properties **(Section 1.3.3)**.

2.2. Methods

2.2.1. Power law relations

Studies have shown that some dendritic tree morphology features are related by power laws *(Cuntz et al., 2012; Wen et al., 2009)*. Both power laws take into consideration total length, with Cuntz's power law relating it to the number of branch points, and Wen's to the arbor radius (see below). It has been proposed that these laws are associated with wiring optimality: a neuron that follows the power law is considered optimal, whereas a neuron that does not follow it is considered suboptimal. In order to explore putative functional consequences of sex dimorphism in our dataset, we assessed both Cuntz's *(Cuntz et al., 2012)* and Wen's *(Wen et al., 2009)* laws with the use of R (version 3.5.0).

To obtain the power laws, we used a nonlinear model to estimate the parameters. Using function *nls* (*stats*, version 3.5.0), we defined the models as:

$$y \sim a \times x^b \qquad (\mathbf{2.1})$$

With *x* and *y* the related neuromorphological metrics, *b* the estimated power and *a* the multiplication factor.

To see if there were significant differences due to sex in the estimated parameters, we compared two models through analysis of variance (ANOVA): the one separating by sex and one considering the data as a whole. If p-value$\leq$0.05, the null-hypothesis that the models are equal is rejected. Therefore, one can say there are sex-related differences between the power laws *(Ritz & Streibig, 2008, Chapter 8)*.

Cuntz's power law

This power law was based on Cajal's law for conservation of cytoplasm and conduction time *(Ramón y Cajal, 1995)*. When considering a minimum spanning tree (MST), Cuntz found a relationship between total length and the number of branch points of a tree. An MST algorithm connects randomly distributed points in a volume in an optimal way by minimizing the path length. This means a tree that optimizes wiring will tend to connect points to their nearest neighbours. In the case of 3D trees, the relationship found was of a ⅔ power:

$$L \sim bp^{2/3} \qquad (\mathbf{2.2})$$

With *L* the total length and *bp* the number of branch points.

Cuntz also tested this power law in real neuronal morphologies, by analysing the available reconstructed neurons in NeuroMorpho.Org *(Ascoli, 2006; Ascoli et al., 2007)*. This made up a total of 74 datasets of different neuronal types, each with at least 10 reconstructions. Considering all datasets together, he obtained a power law of 0.72 ± 0.10, thus asserting the general applicability of the law *(Cuntz et al., 2012)*.

To fit our data to this power law, we scaled the previously calculated total length and number of branch points by the spanning volume of the tree **(Section 1.3.1)**. We extracted the observed values of power for each sex, and compared them to the expected value of ⅔. The results are shown in a log-log scale, as in Cuntz's work *(Cuntz et al., 2012)*.

Wen's power law

Wen derived this power law from experimental measurements of pyramidal cells. They are from different cortical areas, with 2,161 2D neurons from primate neocortex and 10 3D neurons from cat visual cortex. Considering only the basal dendrites, a relationship of 0.44 power was found between the arbor radius and the total length of the tree:

$$R \sim L^{0.44} \qquad (\mathbf{2.3})$$

Being *R* the arbor radius, defined as the root mean square between any two dendritic segments, and *L* the total length.

We fitted our data to this power law and extracted the observed values of power for each sex, comparing them with the expected value of 0.44 *(Wen et al., 2009)*.

2.2.2. Multi-objective optimality

Assessing wiring optimality by comparing power law fits obtained with small sample sizes might be misleading. Furthermore, in these power laws there is an association of neuromorphological features with the concept of optimality, however a bridge between morphology and the neuron's functional capabilities is missing. Hence, to extend the existing work and try to overcome the issues we have faced, we defined 3 variables that accounted for computational capabilities of a neuron: the material cost of wiring a tree, the ability to identify different combinations of axons that could synapse on the tree (connectivity repertoire), and the efficiency in the signal integration towards the soma (see below). This section builds on previous work done in the lab *(Manubens-Gil, 2018)*.

The dendritic tree wiring optimality is hence given by the maximization of connectivity repertoire and signal integration efficiency, while preserving the material cost. This means we have a multi-objective optimality, where all 3 variables need to be balanced to achieve optimality. First introduced by Vilfredo Pareto in the area of economic sciences, he defined a Pareto-optimal configuration of a system as one where no change can be made to improve any aspect without deteriorating another *(Pareto, 1963)*. This means that in an optimal neuron, one cannot, for example, reduce the material cost without that change worsening one or both the other variables. In this case we are in the Pareto front, which is a boundary that implies multi-objective optimality. Subsequently, a suboptimal neuron can undergo Pareto improvement while maintaining the other Pareto measures.

The 3 Pareto measures were defined either directly (cost and connectivity repertoire) or indirectly through multi-compartmental models (signal integration efficiency) in function of 3D single-neuron architectural properties. They were computed with MATLAB, as described below, and afterwards we performed statistical analysis with GLMMs in R. To minimize any existing effect of total length, we also looked at connectivity repertoire and signal integration efficiency after normalizing by this metric. Finally, we defined a Pareto front based on an exploration of synthetic dendritic trees generated *in silico* and computed the proximity between the neurons of the dataset and this front (see below).

Cost

The material cost of wiring a dendritic tree is the same as its total length. To be optimal, a neuron will try to minimize its cost, since the longer the information has to travel, the more energy the neuron spends.

Connectivity repertoire

The concept of connectivity repertoire was introduced by Wen as a measure of arbor functionality (described in detail in Wen *et al.*, 2009). Briefly, it is defined as the natural logarithm of the total number of different combinations of axons that could synapse on a dendritic arbor of given dimensions. Maximizing the arbor functionality, in turn, means maximizing the connectivity repertoire. To compute this measure, they took into account two contributions: 1) counting all possible shapes a dendritic arbor of given dimensions could present; 2) for a given shape, the number of combinations available from defining which synapses to make, out of the existing potential connections. The supplementary information of Wen *et al*. 2009 describes deeply how these two contributions were calculated and which assumptions were made, and from equation S32 we were able to derive the following equation for connectivity repertoire, *S*:

$$S \simeq MH(W) + \frac{L}{a}\left(1 + log\left(1 - \frac{R}{l}\right)\right) - \frac{l^2}{La} - s_l s_d \frac{L^2}{R^2} \qquad (\mathbf{2.4})$$

The second and third terms of **Eq. 2.4** are, respectively, *R*- and *l*-dependent corrections to the first contribution to *S*. Maximizing the number of different arbor shapes favours tortuous branches (*R*-dependent correction), as well as branchy dendrites (*l*-dependent correction) *(Wen et al., 2009)*. The last term of **Eq. 2.4** is an *R*-dependent correction of the second contribution to *S*. Axons could establish multiple potential synapses in different locations of the dendritic arbor, and so when selecting actual synapses out of potential ones there is an overcounting of redundant connections that must be subtracted *(Wen et al., 2009)*. Lastly, the first term of **Eq. 2.4** is the independent one, which accounts for both contributions to *S*. **Table 2.1** has the definition of each variable of **Eq. 2.4**, and in the supplementary information is in detail how we obtained it **(Supplementary Information V)**.

Table 2.1 - Description of the variables used in the calculation of connectivity repertoire, Eq. 2.4.

Variable [units]	**Meaning**
L [µm]	Total length of the tree, as defined in **Table 1.1**
R [µm]	Tree radius, as defined in **Table 1.1**
l [µm]	Average distance along the path from the soma to the tip of a branch (path length)
s_d [spines/µm]	Spine density, given by the total number of spines s **(Supplementary Information V)** divided by the total length L
$s_l = 2$ µm	Spine reach length, which is the maximum distance between spines and accessible axons passing through the dendrite *(Wen et al., 2009)*. Value from Wen *et al*., 2009
$a = 4$ µm	Persistence length, which is the length below a dendrite cannot bend. Value from Wen *et al*., 2009
$\rho_a = 8.15$ µm/µm^3	The axon length per unit of volume, which is the total length of axons enclosed in a given volume, divided by the volume *(Wen et al., 2009)*. Value from Calí *et al*., 2018, figure 4D
M	A simplification of $s_l L \rho_a$, to more easily apply to the binary entropy function $H(W)$
$H(W)$	Binary entropy function: $W log\left(\frac{1}{W}\right) + (1-W) log\left(\frac{1}{1-W}\right)$, with $W = \frac{s_d L}{M}$ being a simplification to more easily apply the function

Signal integration efficiency

Signal integration efficiency is a measure of how efficiently a neuron will integrate a received input, i.e., how long it takes to generate an action potential after receiving an input. To this time interval we call time response, and the signal integration efficiency is defined as the inverse of the time response. We assume that an optimal neuron will then tend to be as efficient as possible.

To obtain this efficiency, we modelled the behaviour of the neurons using T2N *(Beining et al., 2017)* and the NEURON simulation environment (https://neuron.yale.edu/neuron/). T2N is an extension of the TREES toolbox that makes the bridge between MATLAB and NEURON, exporting a multi-compartmental model in NEURON format, where it is possible to simulate neuron dynamics upon injection of synaptic currents. These currents are injected at random nodes of the tree, which have a probability function of the inverse of the interspine distance. This uses the equation we derived which calculates interspine distance in function of the distance to the soma **(Eq. SV.1)**, which can be found in **Supplementary Information V**. Shortly, we did a polynomial fit to the measured values of interspine distance in function of the path distance to the soma *(Konur et al., 2003)*. This produced an equation that gives the interspine distance of each compartment i of a tree **(Eq. SV.1)**. By taking the inverse and normalizing the values to [0, 1], we obtain the probability function for each neuron. As a result, distance intervals with higher spine density are more likely to receive an input, which is closer to reality than all having the same probability. The percentage of activated spines, i.e., the amount of

inputs each neuron receives, is also dependent on this function, as one can use it to calculate the number of spines of a neuronal tree **(Eq. SV.1)**. The percentage was defined as the lowest necessary to generate an action potential in the smallest neuron of the dataset, which was 8% for an input frequency of 30 Hz. This means that all neurons had 8% of their number of spines being activated. To note that for a neuronal tree with nodes at each µm, the number of spines will always be larger than the number of nodes; therefore, the percentage of chosen nodes will be larger than 8%. Having the model parameters defined, NEURON simulates these dynamics for each dendritic tree individually and outputs its time response, from which we calculate the signal integration efficiency.

A more in-depth study of signal integration efficiency can be found in **Supplementary Information V**.

Pareto front

Defining the Pareto front is an optimization problem with three objectives: maximizing connectivity repertoire and signal integration efficiency, and minimizing the cost. Signal integration efficiency is determined through computational models, and so we do not have a function that determines it. Hence, we cannot simply maximize and minimize the functions of each Pareto measure to solve the optimization problem. A way around this is to determine a Pareto front from a set of points. For this, we generated synthetic dendritic trees with different conformations and calculated their Pareto measures.

The synthetic trees were obtained using the TREES Toolbox's function *clone_tree*, which connects points distributed randomly in the spanning fields of the input trees by using an MST algorithm *(Cuntz et al., 2011)*. We varied 3 parameters so we could explore the impact of neuron architecture in the Pareto measures: balancing factor, branch and terminal scaling factor, and tree radius. The balancing factor impacts how the MST algorithm will connect the points. It accounts for the trade-off between material cost and conduction time, and so the straightness of dendritic branches varies *(Cuntz et al., 2010)*. The branch and terminal scaling factor impacts the branch density, since it scales the amount of points used to generate the cloned trees *(Manubens-Gil, 2018)*. Lastly, the tree radius was used to scale the size of the input trees with the TREES Toolbox's function *scale_tree*. To be able to create a set of clones as uniform as possible for this analysis, we first generated 10 clones of each sex from our dataset without changing any of the parameters. From this initial set of clones, the clones for the exploration itself were generated. As a result, the data variability we previously saw in **Chapter 1** was minimized, and the results of the exploration were more reliable. For each set of parameters, 3 clones of each sex were generated, making a total of 300 trees (150 of each sex), and their signal integration efficiency, connectivity repertoire and cost were calculated. Because we were only interested in comparing how close each neuron was to the Pareto front, we normalized the Pareto measures to [0.1, 1.1]. Since they were all normalized, they are adimensional.

To identify the Pareto front from a set of points, we adapted MATLAB's File Exchange function *find_pareto_frontier (Ma, 2014)*, which identifies the points of the Pareto front with both x and y minimized. Our function *find_3dpareto_frontier* takes a set of (x,y,z) points, and identifies the points with x and z maximized, and y minimized. These identified points are the ones that make up the Pareto front. After determining them, one can then fit a surface using MATLAB's Curve Fitting App, where different types of curves can be fitted interactively to the data. After obtaining the surface that best described the Pareto front, we measured the minimum euclidean distance from the neurons of our dataset to the Pareto front surface. This euclidean distance is a measure of how close a neuron is to being considered optimal. To see which sex was overall closer to optimality, we performed a statistical analysis in R using GLMMs to their euclidean distances. The GLMMs were also applied to each sex, to understand which cluster was overall closer to being optimal.

2.2.3. Measures of dendritic complexity

Sholl analysis, fractal dimension and centripetal bias can also provide some information on morphology and dendritic complexity as one-dimensional values. Even though they do not directly infer optimality, one can draw parallels between them and neuronal capabilities we took into consideration in our Pareto measures. We calculated them to gain some more insight about the neurons of our dataset.

Sholl analysis

Introduced in 1953, Sholl Analysis is a widely used measure of dendritic complexity *(Sholl, 1953)*. It allows one to study how the number of branches, branch geometry and overall branching patterns vary with the distance to the soma. It is also useful to determine the location and size of the connective zone, i.e., the region where synapses are possible. It is thus related to connectivity repertoire, since it assesses the arbor shape, which is the first contribution of the Pareto measure. It is also indirectly related with its second contribution, since the branching patterns influence the sites of potential synapses **(Section 2.2.2)**.

This method counts the number of times that a dendrite intersects a sphere centered at the soma with a given radius *r* **(Figure 2.2)**. This is repeated for increasing radius, giving us a Sholl intersection profile (SIP). The 3D complexity of the dendrites is thus reduced into a one-dimension metric. This makes it possible to compare neurons of different groups, such as control cases with diseased subjects or with neurons after undergoing treatments, which nowadays are the main applications of Sholl analysis. Because the SIP depends on the distance to the soma, it is also related with cost.

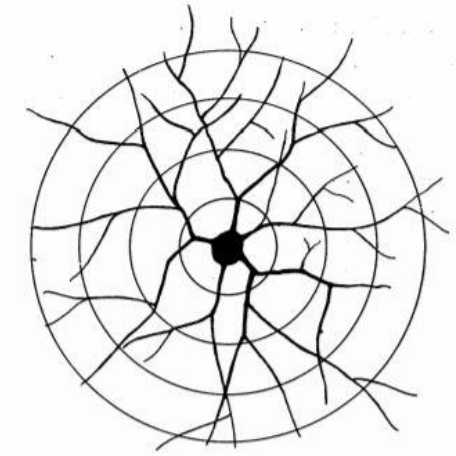

Figure 2.2 - Example of a Sholl analysis. Concentric circles are centered at the soma to estimate the number of intersections. From Sholl 1953.

We used the TREES Toolbox (function *sholl_tree*) to compare the SIPs produced for each sex as well as in each cluster. In it, concentric equispaced spheres with an *r* step of 5 µm were used. This means any branches smaller than 5 µm are not counted. The function interprets the soma (distance of 0 µm) as one intersection.

The results are graphs with the median number of intersections of each group in function of the distance to the soma. Since total length is highly variable in our dataset, from a certain distance there are few neurons with longer dendrites, which makes the median zero. It does not make sense to compare between sexes when the median of one of the sexes is zero. For this reason, the graphs contain the number of intersections of each sex up until the first distance of median zero. The remaining values are discarded.

To check for statistical differences at each *r*, the data was exported to R. Since the number of intersections is count data, we fitted either a poisson or a negative binomial distribution. This was done for each *r*, only considering the neurons of median different to zero. We then applied GLMMs and extracted the p-values, similarly to **Chapter 1**. When there is a significant difference, the graph has one or more asterisks, depending on the level of significance: * is p-value$\leq$0.05, ** is p-value$\leq$0.01 and *** is p-value$\leq$0.001.

We calculated the area under the curve (AUC), to be able to better compare each group as a total, instead of only at each *r*. For this we obtained two types of AUC: a single value for each sex, calculated from the median of all SIPs (our graphical output) and a value from the SIP of each neuronal tree. The first is shown in the graphical output to aid in visualizing the difference between the median SIP of each sex, and the second was used to determine if this difference was significant through GLMMs. We also performed a correlation test between the AUC and both connectivity repertoire and cost, with R's function *cor* (*stats*, version 3.5.0). This is because we propose the Sholl analysis is related to these two Pareto measures, and the correlation test could validate our hypothesis.

Fractal dimension

Fractal analysis can be applied to many fields, which leads to different conclusions drawn from the results. In neuroscience, the fractal dimension *D* of a neuron represents a measure of the dendritic complexity, quantifying how well a neuronal tree fills its dendritic field. It takes into account the straightness of individual dendrites, and so it is able to uncover differences in complexity patterns that Sholl analysis cannot **(Figure 2.3)** *(Jelinek et al., 2006)*. This is why we decided to assess the fractal dimension *D*.

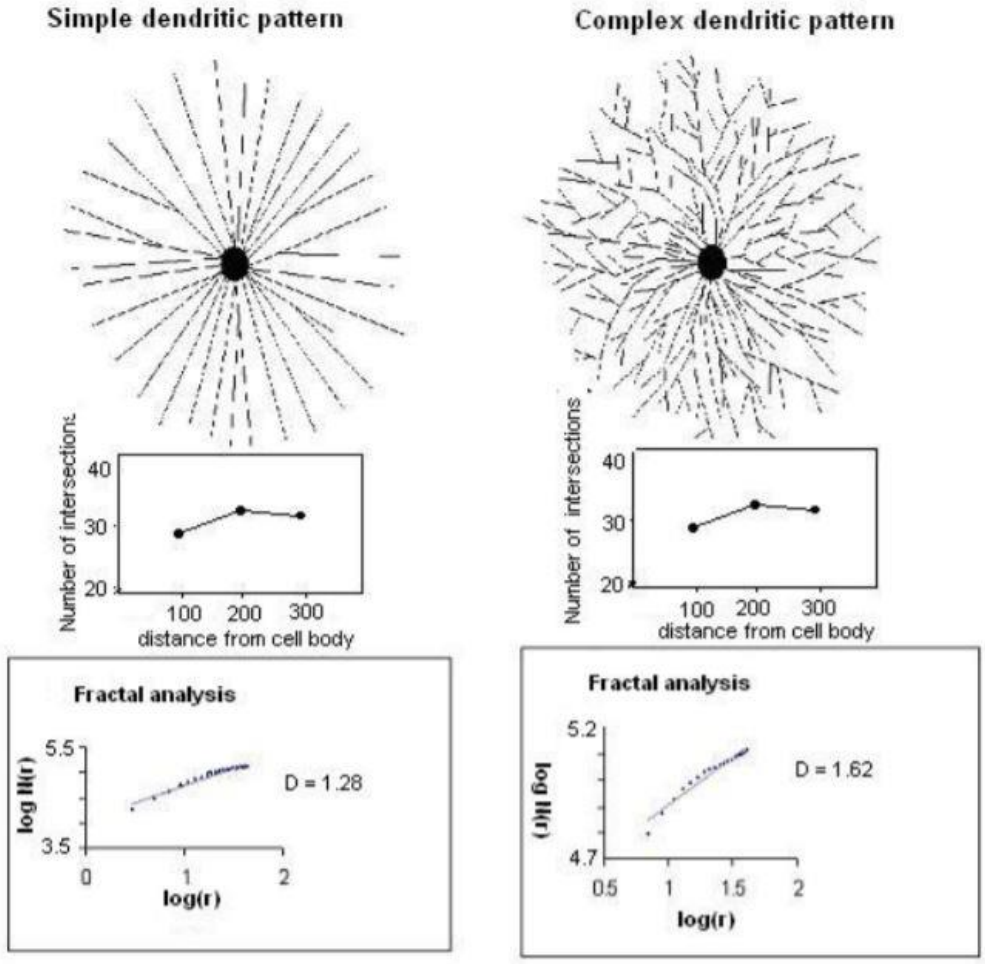

Figure 2.3 - Example of when the fractal dimension can distinguish the branching complexity of two neurons, but Sholl analysis fails to. From Jelinek *et al*., 2006.

To calculate *D*, we used L-measure *(Scorcioni et al., 2008)*, a tool that extracts quantitative morphological measurements from neuronal reconstructions. *D* is estimated for each branch, and the *D* of a neuron is the mean of all branches. First, the path length and the euclidean distance to the soma must be calculated at each branch point **(Figure 2.4)**. These value pairs are plotted as log-log, and the *D* of the branch is the slope of the regression line that fits the points **(Figure 2.4)**. When *D*=1, the branches are straight and when *D*=2, they fill the space as random walks. Using this method, a dendrite branch usually has a *D* around 1.05 *(Marks & Burke, 2007)*.

After obtaining the fractal dimensions, we checked for the normality of the measure and applied a GLMM, as completed in **Chapter 1**.

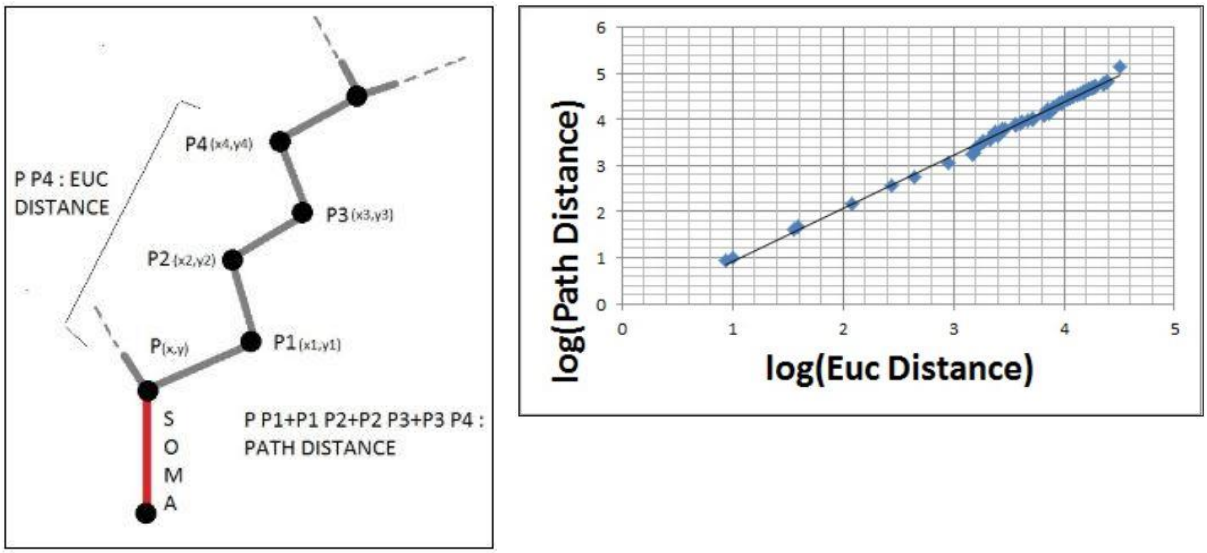

Figure 2.4 - How L-measure calculates the fractal dimension *D*. Calculation of each value pair of path length and euclidean distance plotted as log-log to estimate the fractal dimension *D* of each branch. From http://cng.gmu.edu:8080/Lm/help/index.htm.

Centripetal bias

Centripetal bias happens when a neuron has most of its dendritic branches pointing towards the soma. This is due to the balance between minimizing the cable cost and the delays in conduction time, which is related to the balancing factor *(Cuntz et al., 2010)*. Introduced by Bird and Cuntz, the root angle arises from optimal wiring and is the first direct measure of centripetal bias *(Bird & Cuntz, 2019)*. It is defined as the angle between a dendritic segment and its euclidean distance to the soma: the smaller the root angle, the larger is the centripetal bias **(Figure 2.5A)**. When the centripetal bias k is zero, the root angles are distributed uniformly. This means if we want to connect a new point to the neuronal tree, it will connect in any direction with the same probability **(Figure 2.5B)**. The larger k is, the more the neuron will favour the conduction of the synaptic currents over minimizing the cable cost. This means a new point will tend to connect to the neuron as close to the soma as possible **(Figure 2.5B)**. With $k \to \infty$, all the dendritic segments will be pointing to the soma. Hence, centripetal bias is a branching statistic that estimates the need for conduction speed, depending only on the shape of the dendrite span and properties of the branches.

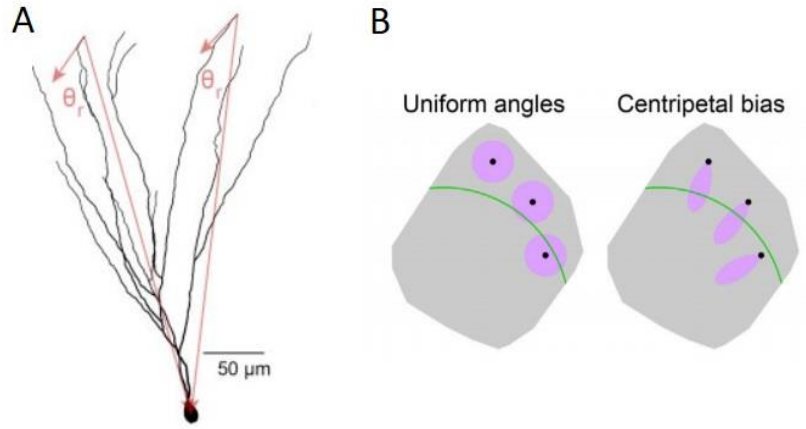

Figure 2.5 - Example of how the root angle is obtained and consequences of centripetal bias. A: The longer arrow is the euclidean distance from the soma to the dendritic segment, and the shorter arrow is the orientation of the segment. The smaller the angle between them, the larger is the centripetal bias. **B:** In a uniform root angle distribution new points (black) will tend to connect equally in all directions (purple shaded area). When there is centripetal bias, the same points tend to connect towards the soma. In green is a Sholl radius, to aid in visualizing the direction of the soma. From Bird & Cuntz, 2019.

We used the TREES Toolbox (function *vonMises_tree*) to estimate the centripetal bias, which is calculated from the root angle distribution *(Bird & Cuntz, 2019)*. After obtaining the values for my neurons, we applied a GLMM to see if there were any significant differences between sexes, just as was done previously for other metrics.

2.3. Results

2.3.1. Power law relations

To estimate Cuntz's power law, we plotted together the number of branch points and the total length of the neurons, both normalized by the volume, for each cluster and sex. We do not see a clear separation between sex in each cluster **(Figure 2.6)**. The estimated power laws have no significant differences in either cluster, since the ANOVA between the models with and without accounting for sex did not reach significance (p-value 0.403 and 0.112 for cluster 1 and 2, respectively). This implies that in terms of optimality, there are no sex-related differences.

We estimated the exponent of the observed power laws for each sex. Considering it should be around 0.67, the estimated values are what we expected in cluster 1: females are optimal (0.68±0.05) and males can still be considered as such (0.64±0.10). In cluster 2 the female trees only deviate slightly (0.77±0.08), with the males deviating strongly with an estimated power of 0.97±0.06 **(Figure 2.6)**.

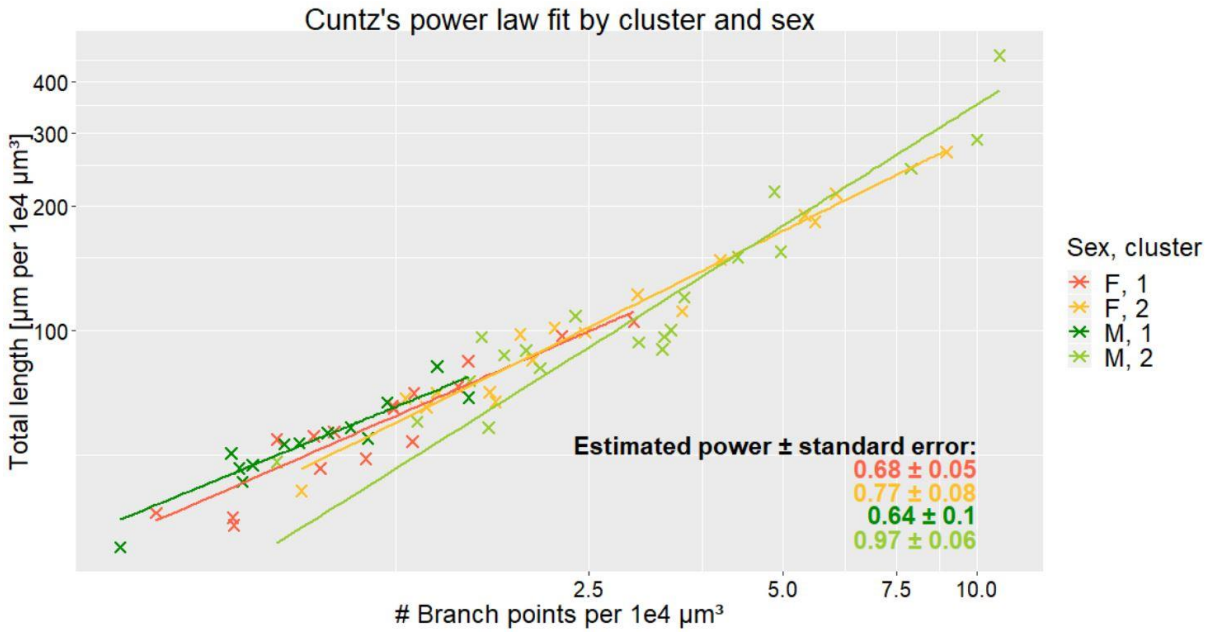

Figure 2.6 - Estimation of Cuntz's power law when considering the 2 clusters. Both the number of branch points and total length are normalized by the volume of the neuronal tree, and represented in logarithm scale. Each cross is a neuron, with the lines being the power law fit for each sex in the respective cluster. In cluster 1 both sexes follow Cuntz's law (female neurons with 0.68±0.05 and males with 0.64±0.10). In cluster 2 females deviate slightly (0.77±0.08) and males are far from the optimal value of 0.67 (0.97±0.06).

We followed the same procedure to estimate Wen's power law, this time plotting together the total length with the tree radius. Considering the optimal value for the power law is of 0.43, the results were very unexpected. Given we see a clear separation between sex in cluster 1, one would expect to see significant differences. However, the ANOVA between the models with and without accounting for sex revealed there are no differences in either cluster (p-value 0.054 and 0.877 for cluster 1 and 2, respectively). This is probably due to the data dispersion, as the observations deviate more from the estimated power law, with standard errors larger than 0.15 in cluster 1.

In the first cluster, which we assumed was optimal, the estimated values were far from it: males have the largest deviation, with a value of -0.01±0.15, which shows there is barely any change in tree radius with the variation in total length; the females also have a large deviation, but not as much as the males (0.24±0.19). In the second cluster both the female (0.44±0.17) and the male neurons (0.43±0.12) are actually optimal **(Figure 2.7)**.

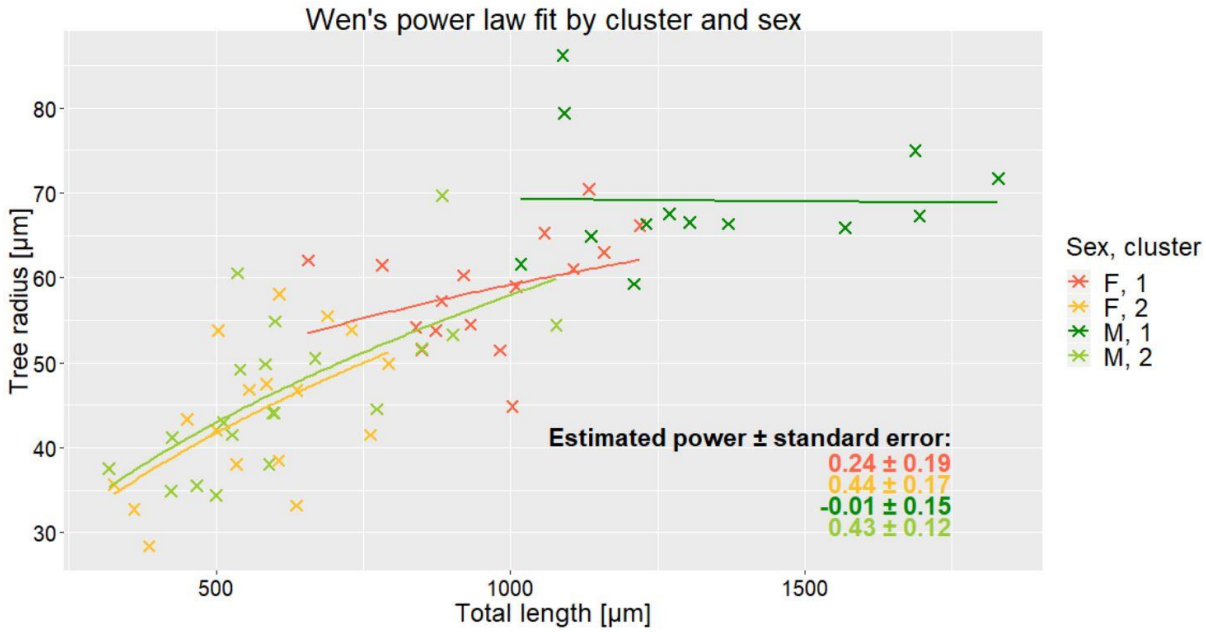

Figure 2.7 - Estimation of Wen's power law when considering the 2 clusters. Labels are explained in **Figure 2.6**. In cluster 1 both sexes deviate strongly from Wen's law: female neurons with 0.24±0.19 and males with an unexpected value of -0.01±0.15. In cluster 2 females (0.44±0.17) and males (0.43±0.12) are actually optimal.

Comparing both power laws, with Cuntz's we only see optimal values for cluster 1 **(Figure 2.6)**. However with Wen's it is the reverse, with optimal values for the trees of cluster 2, and the neurons of cluster 1 not appearing to be optimal, especially the males **(Figure 2.7)**. Both power laws should classify the neurons equally in terms of optimality, but that is not what we see. The discrepancy in these results, which should follow the same direction, point towards the fact that these laws are not the best measures of optimality.

2.3.2. Multi-objective optimality

With our multi-objective approach to optimality, not only we assess if each of the Pareto measures is minimized or maximized, but also take into consideration the balance between the three, as a Pareto configuration. When assessing their normality, Shapiro-Wilk tests revealed only connectivity repertoire was not normal in cluster 2 (p-value 0.041), which assumes a log-normal distribution **(Table 2.2)**. Both cost and connectivity repertoire in cluster 1 passed the Shapiro-Wilk test, but with very low p-values (0.071 and 0.061, respectively). For this reason we calculated their skewness, which showed they should not be approximated to a normal distribution (cost 0.83 and connectivity repertoire 0.60), both fitting a log-normal distribution **(Table 2.2)**.

Table 2.2 - Statistical comparisons of the Pareto measures between sexes of each cluster. Overview of the mean and standard deviation for each sex (F for females and M for males) of each cluster and summary of the results obtained in each step of the GLMM. If there is a dash, it means the test was not performed. p-values in bold are statistically significant.

	Cluster	**Mean**	**Standard deviation**	**Shapiro-Wilk (p-value)**	**Skewness**	**Assumed distribution**	**GLMM p-value**
Connectivity repertoire	1	F: 4446.08 M: 6675.37	F: 682.43 M: 1261.32	0.061	0.60	Log-normal	**1.09×10^{-9}**
	2	F: 2690.73 M: 2822.28	F: 816.34 M: 1083.39	0.041	-	Log-normal	0.334
Signal integration efficiency [ms^{-1}]	1	F: 0.520 M: 0.600	F: 0.071 M: 0.080	0.884	-	Normal	**0.004**
	2	F: 0.441 M: 0.438	F: 0.109 M: 0.139	0.290	-	Normal	0.317
Cost [µm]	1	F: 962.91 M: 1346.19	F: 150.48 M: 265.18	0.071	0.83	Log-normal	**1.2×10^{-6}**
	2	F: 575.66 M: 632.20	F: 148.66 M: 197.45	0.69	-	Normal	0.414
Normalized connectivity repertoire [per µm]	1	F: 4.646 M: 4.970	F: 0.489 M: 0.375	0.733	-	Normal	0.067
	2	F: 4.640 M: 4.418	F: 0.487 M: 0.505	0.471	-	Normal	0.215
Normalized signal integration efficiency [ms^{-1} per µm]	1	F: 5.53×10^{-4} M: 4.55×10^{-4}	F: 1.17×10^{-4} M: 7.04×10^{-5}	0.153	-	Normal	**0.028**
	2	F: 7.86×10^{-4} M: 7.13×10^{-4}	F: 1.66×10^{-4} M: 2.02×10^{-4}	0.807	-	Normal	0.620

After defining the distributions of the Pareto measures, we applied the GLMMs. As expected, we see significant differences for cluster 1, but not for cluster 2. Overall, males have a higher connectivity repertoire (p-value 1.09×10^{-9}) and signal integration efficiency (p-value 0.004) than females, which would point towards the males being more optimal. However, this maximization comes at a higher cost (p-value 1.2×10^{-6}). Therefore we cannot directly say which sex is more optimal than the other (**Table 2.2** and **Figure 2.8**).

As for cluster 2 we see no significant differences, which follows in line with the results from **Chapter 1**, since we saw no significant differences in any of the neuromorphological metrics as well **(Figure 1.13)**. This does not necessarily mean the neurons of this cluster are not optimal, but that sex does not play a role in the Pareto measures (**Table 2.2** and **Figure 2.8**).

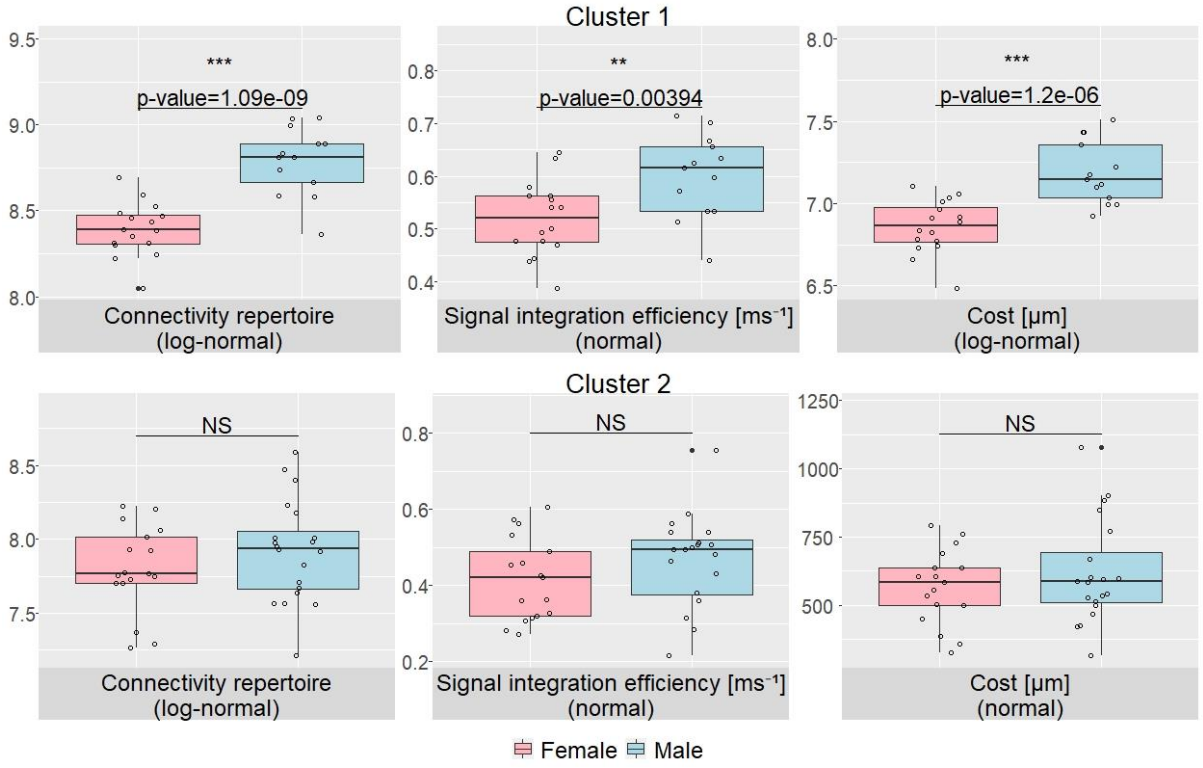

Figure 2.8 - Variance of the 3 Pareto measures in both clusters. Panels contain the boxplot and data points of each variable, the latter representing each neuron of the dataset. The label of the panels has the name, unit and distribution used in the GLMM of the corresponding Pareto measure. The significance level of the test is shown on top of each panel: NS is not significant, * is p-value<0.05, ** is p-value<0.05 and *** is p-value<0.001. If it passes the threshold of significance, the p-value is also shown. We only see significant differences in the first cluster for all three Pareto measures, where the males have higher values. In terms of optimality, males of cluster 1 are more optimal due to connectivity repertoire and signal integration efficiency, but less optimal than females due to cost.

Because in cluster 1 we had a very significant statistical difference in total length (**Table 1.4** and **Figure 1.12**) we wondered if connectivity repertoire and signal integration efficiency did not have high dependencies on this metric. If so, that could be the reason why we had the significant differences in these 2 Pareto measures, with males showing higher values (**Table 2.2** and **Figure 2.8**). For this reason, we normalized them by total length to see if it would influence the results. Since cost is defined as the total length, it would not make sense to normalize it as well.

Both Pareto measures passed the Shapiro-Wilk tests in the 2 subsets of the data, which means they are normally distributed **(Table 2.2)**. After applying the GLMMs, the results of cluster 2 remained non-significant, as was expected. However, in cluster 1 we see that connectivity repertoire is no longer significant (p-value 0.067). This means that after removing the dependency of cost, both males and females have the same connectivity repertoire (**Table 2.2** and **Figure 2.9**). What is interesting to see, is how signal integration efficiency remains to be significantly different, and this time with the females having higher values (p-value 0.028). So if we remove the influence of cost, the female neurons are actually the more efficient, and not the other way around as we observed before normalizing **(Figure 2.8)**. This result indicates that the female neurons of cluster 1 could be more optimal than their male counterparts (**Table 2.2** and **Figure 2.9**).

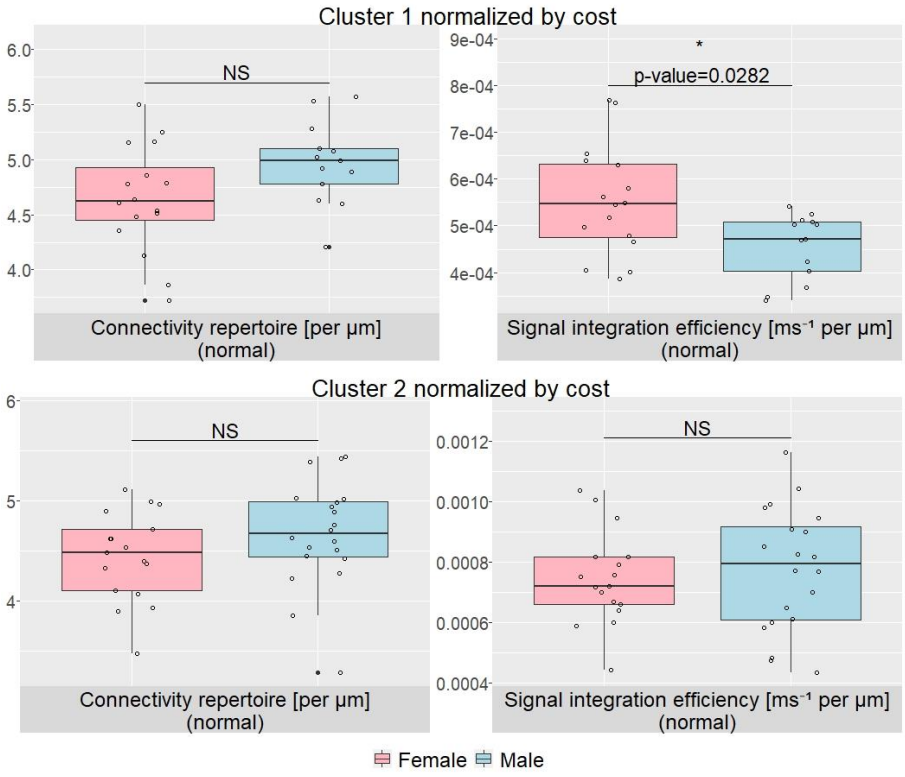

Figure 2.9 - Removing the dependency on total length of both connectivity repertoire and signal integration efficiency. Only signal integration efficiency of cluster 1 remains significant, with female neurons now displaying higher values than males. This is the reverse of what we saw before normalizing. Connectivity repertoire is no longer significant, not even in cluster 1. Labels are explained in **Figure 2.8**.

To be able to understand which neurons are more optimal, we defined the Pareto front. From the 300 synthetic trees, we discarded 17 of them, since their Pareto measures were outliers. By using the remaining 283, we were able to determine which dendrites maximized the connectivity repertoire and signal integration efficiency, while minimizing the cost. We obtained a Pareto front composed of 72 neurons, to which we fitted a surface using the Curve Fitting App. We applied polynomials of different degrees to obtain the function, f(x,y), that best defined this surface. A polynomial of degree 3 for x and degree 1 for y was the best fitted surface **(Figure 2.10)**. Neurons from the dataset that are on the surface are classified as optimal, and the ones under or over the surface are considered suboptimal. After extracting f(x,y), we computed the minimum euclidean distance between each neuron from our dataset and f(x,y), which is also represented in **Figure 2.10**.

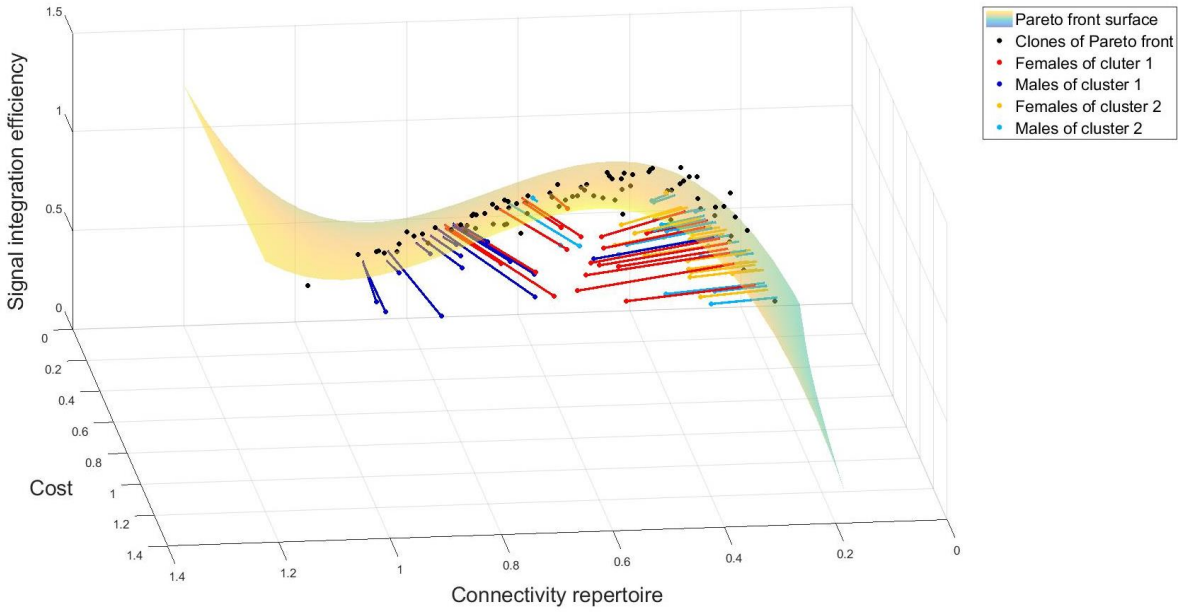

Figure 2.10 - Euclidean distance of each neuron to the Pareto front in the 3D space. The surface is determined by a polynomial function f(x,y) of degree 3 for x and degree 1 for y, obtained with the Curve Fitting App. Each black point is a clone that makes up the Pareto front. Each coloured point represents a neuron, with the respective colour classifying it by sex and cluster. The lines represent the minimum euclidean distance between them and the surface. Connectivity repertoire, cost and signal integration efficiency were normalized to [0.1, 1.1], and so are adimensional. Neurons that are under and over the surface are suboptimal, and the ones that are on the surface are optimal.

To know which neurons are closer to the surface of the Pareto front, we performed a statistical analysis between sexes in each cluster separately. We also compared between clusters in each sex separately, i.e., compared female neurons of cluster 1 versus female neurons of cluster 2, and repeated for males. Shapiro-Wilk tests revealed the euclidean distance was not normally distributed when considering all the male neurons (p-value 0.021), and it follows a gamma distribution; the remaining three comparisons are normally distributed **(Table 2.3)**. When comparing male and female neurons of each cluster, there were no significant differences in the euclidean distance (**Table 2.3** and **Figure 2.11**). This means that female and male neurons of both clusters are equally close to the Pareto front, and thus have no significant sex-dependent differences in terms of optimality. We can also see the difference between neurons of different clusters of the same sex. Interestingly, neurons of cluster 2 are significantly closer to the Pareto front than neurons of cluster 1 for both sexes (**Table 2.3** and **Figure 2.11**). This was an unexpected result, since we expected the neurons of cluster 2 to be less optimal than neurons of cluster 1.

Table 2.3 - Statistical comparisons of the euclidean distance to the Pareto front, between sexes for both clusters and between clusters for both sexes. Overview of the mean and standard deviation for each sex (F for females and M for males) and summary of the results obtained in each step of the statistical analysis. Mean and standard deviations are not presented for the last two rows, as the values are the same. There are sex-dependent differences in both clusters. In both sexes, neurons from cluster 2 are significantly more optimal than those from cluster 1. p-values in bold are statistically significant.

		Mean	Standard deviation	Shapiro-Wilk	Distribution	GLMM p-value
Comparing between sexes	**Cluster 1**	F: 0.227 µm M: 0.163 µm	F: 0.082 µm M: 0.097 µm	0.292	Normal	0.060
	Cluster 2	F: 0.097 µm M: 0.098 µm	F: 0.048 µm M: 0.061 µm	0.344	Normal	0.965
Comparing between clusters	**Females**	-	-	0.138	Normal	**1.35×10^{-8}**
	Males	-	-	0.021	Gamma	**0.024**

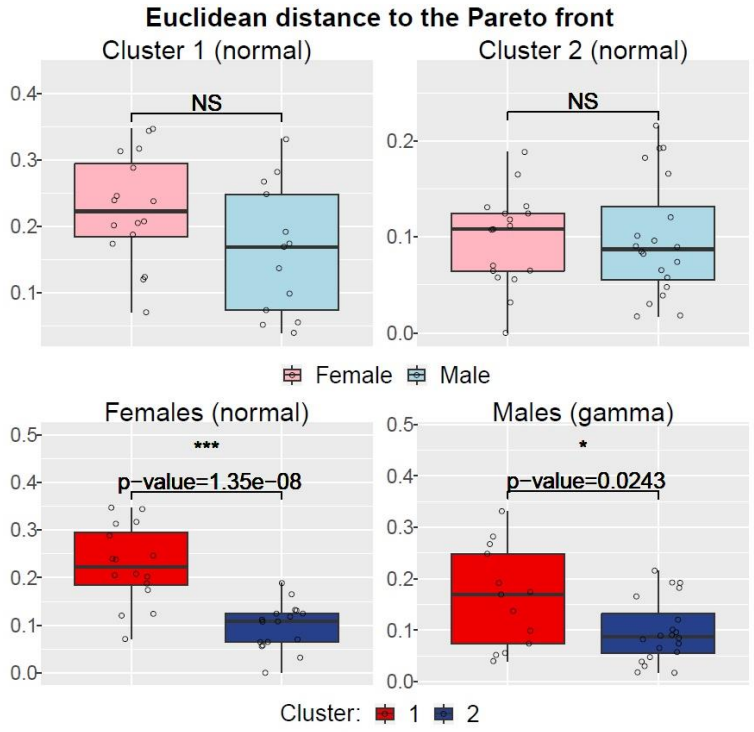

Figure 2.11 - Euclidean distance to the Pareto front shows no sex-dependent differences. The panels contain the boxplot and data points of each variable, the latter representing each neuron of the dataset. The title of each panel has the data and distribution used in the GLMM of each comparison. The significance level of the test is shown on top of each panel: NS is not significant, * is p-value<0.05, ** is p-value<0.05 and *** is p-value<0.001. If it passes the threshold of significance, the p-value is also shown. Both female and male neurons of cluster 2 are closer to optimality than neurons of cluster 1.

2.3.3. Measures of dendritic complexity

Sholl analysis revealed significant differences between sexes from radius *r*=55 µm to 105 µm when analysing the first cluster. Most of these differences have a p-value<0.005, except for *r* of 55 µm and 105 µm (p-value of 0.013 and 0.011, respectively) and the separation between the male and female SIPs is clear at first glance. This difference in complexity shows that from a distance to the soma of 55 µm, the male neurons have more dendrites **(Figure 2.12)**. These results are in line with the results presented in **Section 2.2.2**, where males had a significantly higher connectivity repertoire and cost **(Figure 2.8)**.

The AUCs are also significantly different (p-value 2.93×10^{-5}), the females with 692.5 µm^2 and the males with 1027.5 µm^2. This is in line with the results of **Chapter 1**, as we saw significant statistical differences for the majority of the metrics **(Figure 1.12)**. Of note, male neurons have longer quartiles than females, showing a larger variation in complexity estimation **(Figure 2.12)**.

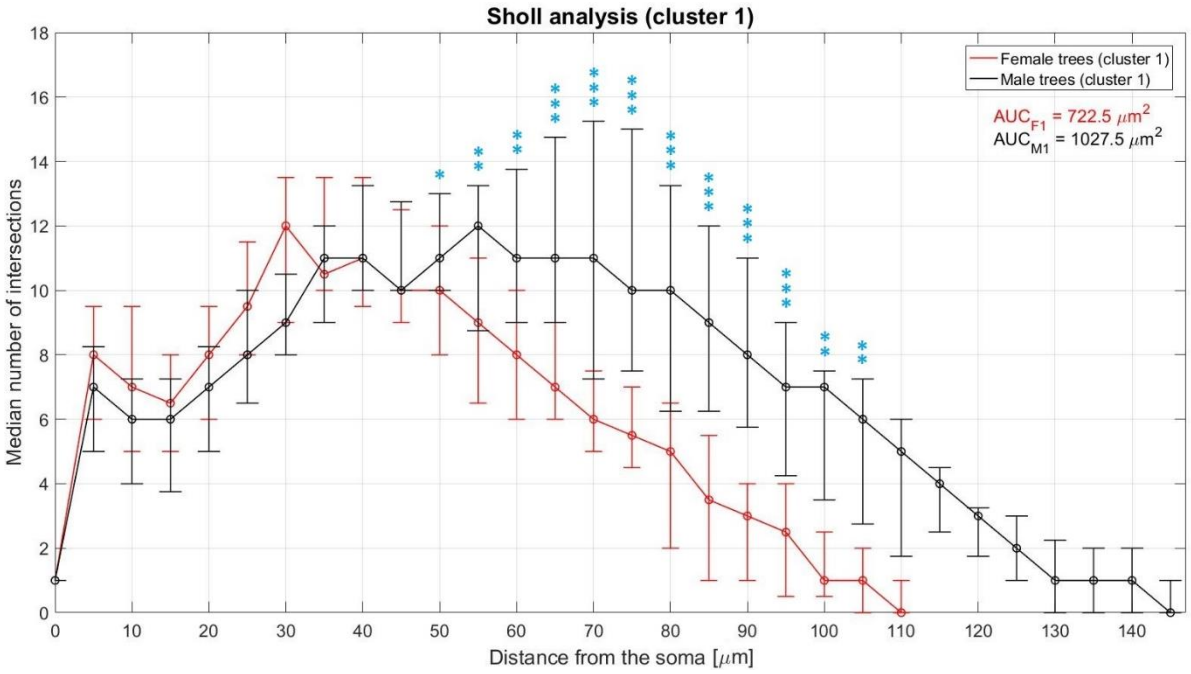

Figure 2.12 - Sholl interception profile of Cluster 1 for each sex. The median number of intersections with concentric spheres of increasing r are represented in function of the distance to the soma. Error bars are the first and third quartile. The significance level of each r is shown on the top: * is p-value<0.05, ** is p-value<0.01 and *** is p-value<0.001. There is a clear difference in complexity of female and male neurons, the latter having more dendrites longer than 55 µm. The AUCs are also significantly different (p-value<<0.001).

When considering solely the second cluster, Sholl analysis showed no significant differences at any *r*. The complexity of the neurons from this subset are the same regardless of sex, which also is observable in their AUCs (p-value 0.443): females with 382.5 μm^2 and males with 420 μm^2 **(Figure 2.13)**. This was expected, as for cluster 2 there were no significant differences in connectivity repertoire or cost **(Figure 2.8)**. Contrary to the first cluster **(Figure 2.12)**, females have a higher variation in complexity, since they have longer quartiles than males for larger *r* **(Figure 2.13)**.

We also calculated the correlation between the AUC and both the connectivity repertoire and cost. We obtained a high correlation for both, confirming our idea. The correlation with connectivity repertoire was 0.972, and with cost was 0.988.

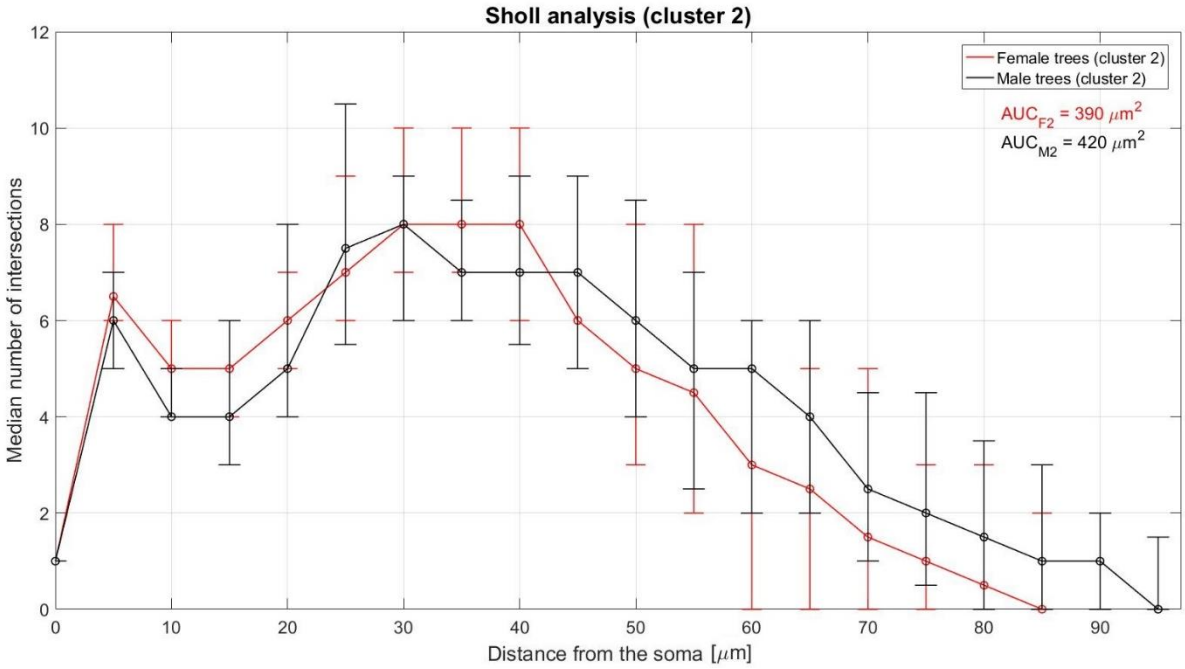

Figure 2.13 - Sholl interception profile of Cluster 2 for each sex. Labels are explained in **Figure 2.12**. There are no significant differences in complexity between male and female neurons, as well as on their AUCs, which are very similar.

With the fractal dimension *D*, we wanted to see if we could uncover more differences in complexity than what we saw with the Sholl analysis *(Jelinek et al., 2006)*. However, we were unable to distinguish between sexes, as there were no significant differences in either of the clusters (**Table 2.4** and **Figure 2.14**). This was unexpected for cluster 1, since we saw significant differences for the Sholl analysis **(Figure 2.12)**. The mean *D* was approximately 1.03 for females and 1.02 for males for both subsets, which is approximately the value dendritic branches take *(Marks & Burke, 2007)*. One of the female neurons from cluster 2 was an outlier, with $D \simeq 1.10$, and so we removed it from this analysis.

Table 2.4 - Statistical comparisons of fractal dimension D and centripetal bias k between sexes for both clusters. Overview of the mean and standard deviation for each sex (F for females and M for males) and summary of the results obtained in each step of the statistical analysis. There are no significant p-values in the GLMM. An outlier with $D \simeq 1.10$ was removed from the analysis of cluster 2.

	Cluster	**Mean**	**Standard deviation**	**Shapiro-Wilk (p-value)**	**Assumed distribution**	**GLMM p-value**
Fractal dimension *D*	1	F: 1.027 M: 1.024	F: 0.008 M: 0.007	0.0038	Log-normal	0.741
	2	F: 1.027 M: 1.024	F: 0.010 M: 0.007	0.255	Normal	0.161
Centripetal bias *k*	1	F: 6.99 M: 5.66	F: 3.38 M: 3.32	0.0030	Log-normal	0.346
	2	F: 6.70 M: 5.86	F: 3.41 M: 1.86	0.0023	Log-normal	0.689

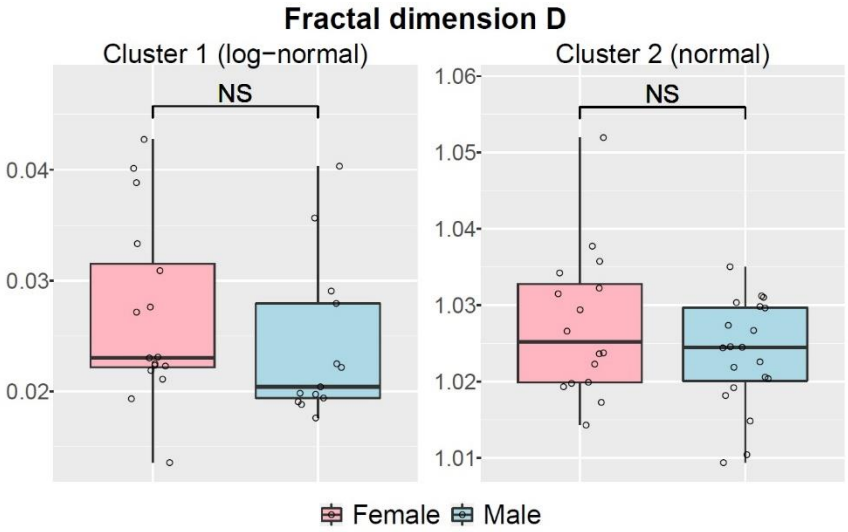

Figure 2.14 - Fractal dimension *D* shows no significant sex differences for both clusters. Overall *D* is the same in all subsets: 1.03 for females and 1.02 for males, with no differences between data of neither cluster.

Just as for fractal analysis **(Figure 2.14)**, when analysing the centripetal bias *k* we once more saw no sex differences in both of the subsets (**Table 2.4** and **Figure 2.15**). The mean *k* is of 6.99 and 6.70 for females and 5.66 and 5.86 for males (for clusters 1 and 2, respectively), meaning the neurons have some centripetal bias. Thus, the neurons from our dataset favoured a faster conduction of the signals over a smaller dendritic length. To note that female trees have more bias than males **(Table 2.4)**. The larger the bias, the smaller is the path length, and so one would expect a lower cable cost in females, which is what we previously saw **(Figure 2.8)**. This also has a relationship with Sholl analysis, since the dendritic branches would be overall smaller as well, which is why we have significant differences at radii r larger than 55 µm **(Figure 2.12)**. The larger the bias, the faster the conduction as well, so one would expect to see a relationship with signal integration efficiency. However, signal integration efficiency is not higher in females of cluster 1 **(Figure 2.8)**, being only significantly higher after normalizing **(Figure 2.9)**.

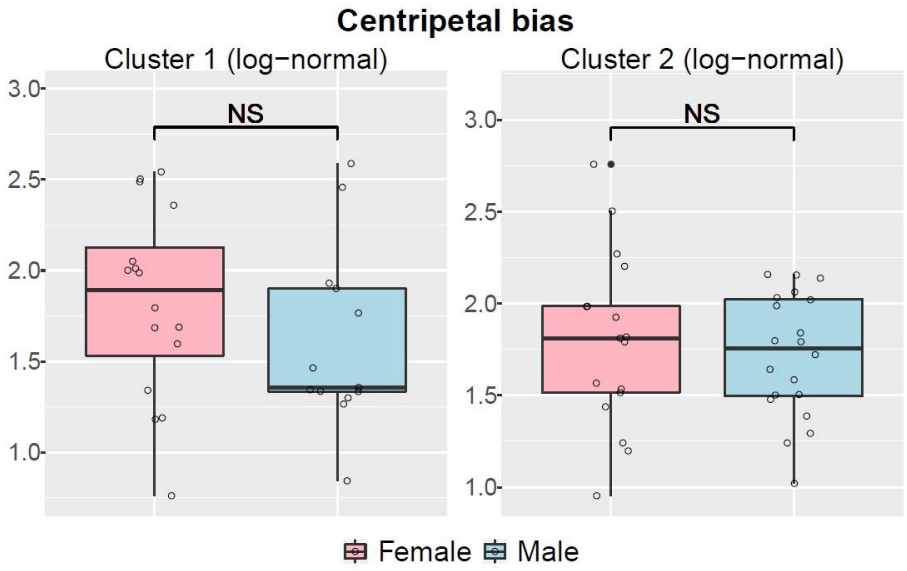

Figure 2.15 - Centripetal bias *k* shows no significant sex differences in both clusters. These values indicate the existence of bias, and thus that the neurons favoured a faster conduction speed.

2.4. Discussion and conclusions

In this chapter we set out to determine the relationship between neuronal morphology and function, and more particularly its implications in optimality. From the results of **Chapter 1** we expected to see significant differences in optimality between males and females of cluster 1, but not cluster 2.

Applying Cuntz's and Wen' power laws we could not identify sex-related differences in neither of the neuronal clusters identified in **Chapter 1**. This was unexpected given the significant differences in total length, number of branch points and tree radius in cluster 1 **(Figure 1.12)**. Results from Cuntz's power law were more consistent, with neurons from cluster 1 being considered as optimal, and neurons from cluster 2 only deviating slightly. It is interesting to highlight that, when Cuntz calculated the power law fits with datasets from NeuroMorpho.Org, it resulted in an estimated power of 0.72 only when considering all 74 datasets together. However, when fitting each dataset separately, a great number of them deviated from the optimal fit *(Cuntz et al., 2012, fig. S5)*. So even though the authors claim the general applicability of the power law to every cell type, one wonders to what extent the results are reliable for their data.

Results from Wen's power law were more unexpected, especially in cluster 1, as the values of the fit (0.24 and -0.01 for females and males, respectively) are not significantly different. The lack of significance is probably due to the standard errors and small sample size. The fact that neurons of cluster 2 are actually found to be optimal (estimated power of 0.44 and 0.43 for females and males, respectively), when cluster 1 is so far from it, was also unexpected. One possible explanation explanation would rely on the fact that this power law was derived from pyramidal cells of the neocortex, and not hippocampus. The morphology of pyramidal neurons varies across brain areas, and differences have also been shown in electrophysiological properties *(Spruston, 2008)*. Therefore, the same power law may not apply to hippocampal pyramidal neurons. Moreover, Wen's power law was derived using more than 2,000 2D trees, but only 10 3D. Even though they mention that the 3D neurons also follow the power law, the sample size was very small. Hence, it is possible this power law is not suited for 3D data, only being valid for 2D dendritic trees.

Our lab has previously worked with these power laws, and the variability in the estimated powers was assumed to be due to using a small dataset (6 neurons for each group). The results for Wen's power law were also unexpected, even though the dendritic trees used in this study were 2D. In it, a model of Down syndrome was the closest to optimality, as opposed to its control, with an estimated power of 0.33 and -0.02, respectively *(Manubens-Gil, 2018)*. The unreliability of the power laws was once more demonstrated with the present dataset. Furthermore, few information can be withdrawn from the power laws. One is able to classify the neurons as optimal or suboptimal, but it does not help in understanding the direct functional implications. Hence the use of the power laws needs to be complemented with other metrics of dendritic complexity and functionality, so a bridge between neuronal morphology, functional capability and optimality can be made.

Even though both of these power laws are extensively cited, we only found 2 studies that actually estimated Cuntz's power law, but no study that estimated Wen's. Interestingly, in these 2 studies the results deviated from the ⅔ power obtained by Cuntz. Iyer *et al.* compared dendritic arborization sensory neurons of *Drosophila*, assessing the power law for class I and class IV neurons (C-I and C-IV, respectively). C-IV neurons followed the law, only deviating slightly, with an estimated power of 0.73, but C-I neurons did not follow any relationship between total length and number of branch points *(Iyer et al., 2013)*. Zippo and Biella did not estimate the power law directly, but assessed the correlation between the two metrics. Using a random sample of 100 neurons from the

entire NeuroMorpho.Org, they only found a weak correlation between total length and number of branch points *(Zippo & Biella, 2015)*. Both studies used large sample sizes, so the issue is not a small sample as in both the current study and in the previous study in the lab *(Manubens-Gil, 2018)*. We thus advice caution when assessing optimality with the use of these power laws.

Given the unreliability of the power laws, we also assessed wiring optimality through a multi-objective approach, in which three measures need to be balanced out as a Pareto configuration. This means maximizing connectivity repertoire and signal integration efficiency while minimizing the cable cost. When comparing each Pareto measure, the results for each cluster were as expected, since for cluster 1 there are sex-dependent morphological differences, but not for cluster 2 **(Section 1.3.3)**. Male neurons are significantly more efficient and have a higher connectivity repertoire than female neurons of cluster 1, but at a significantly higher cost. Hence, we cannot directly extrapolate which sex is closer to being optimal. Even though signal integration efficiency and connectivity repertoire are lower in female neurons, given that the cost is also lower, female neurons of cluster 1 may actually be more optimal than male neurons. When normalizing both signal integration efficiency and connectivity repertoire by the cost, connectivity repertoire showed no significant differences between sex, and thus the differences found in normalized signal integration efficiency are highly important. Not only there are still significant sex-dependent differences in cluster 1, but female neurons are more efficient. Thus, when removing the influence of total length, it is shown that female neurons of cluster 1 generate action potentials faster than male neurons. This could indicate that the females are closer to being optimal than males.

However, even though we were able to unambiguously classify each individual neuron in terms of optimality through its euclidean distance to the Pareto front, the statistical analysis revealed no significant sex-dependent differences in optimality for either cluster. These results indicate that we cannot extract conclusions from comparing each Pareto measure individually, stressing out the need to obtain the Pareto front and calculate the euclidean distances.

What turned out to be more interesting was to compare the neurons from each cluster. Both male and female neurons of cluster 2 had significantly smaller euclidean distances, indicating they are more optimal than neurons of cluster 1. We had previously speculated that neurons from cluster 2 are evidence of dendritic pruning, which means their synaptic connections had been refined **(Chapter 1)**. In terms of optimality, this would mean that only the necessary and strongest connections remained, and so the neuron would be as optimal as possible. This could explain why neurons of cluster 2 are significantly more optimal than those of cluster 1.

An issue of our Pareto front is how it was derived from the values of synthetic dendritic trees. The ideal method would be to maximize and minimize the functions of each Pareto measure, as there would be no dependencies on experimental data. Because signal integration efficiency is generated through computational models, this method was not possible. Estimating the Pareto front from experimental points is a good workaround, but it also forces one to fit a surface to the points identified as being on this boundary. These points do not necessarily provide the full picture of the real Pareto front, and thus, the obtained surface could deviate from it. Furthermore, this method requires visually choosing the surface fit, and one's definition of "best fit" might be different. Here, we wanted a surface that fitted the points and was easy to understand and visualize. The surface we chose had a coefficient of determination (R^2) of 0.879 and root mean square error (RMSE) of 0.069, which shows it fits the points well. However, other surfaces also fit the data such as a polynomial of degree 3 for both x and y **(Figure SV.5)**. This other surface has a R^2=0.874 and RMSE=0.067, so it also fits the points as well as the surface we chose. It is more orthogonal to the XY plane, and consequently, the calculated euclidean distances are different. In fact, in cluster 1 female neurons would be significantly more optimal than males **(Figure SV.6)**, as we expected. Comparing the results of these two very distinct

surfaces shows the unreliability of the method, and the importance of determining the real Pareto front to accurately obtain the euclidean distances. Thus, it would be interesting to determine a function that obtains signal integration efficiency, so one can accurately classify the neurons in terms of optimality.

Because we had some unexpected results regarding neuron optimality, we expected to see it in the results of centripetal bias, since it is a more direct measure of optimality, as the existence of bias implies that the neuron favours a faster conduction time over a smaller cable cost. Sholl analysis and fractal dimension are, instead, direct measures of branch geometry and density, and not of functional capabilities.

Our results for the Sholl analysis are in line with previous results, where males are significantly more complex than females *(Keil et al., 2017)*. Females of cluster 1 reach the peak of number of intersections earlier than males, at a distance to the soma of 40 µm, as opposed to a distance of 55 µm. After reaching the peak, both sexes start to decrease the number of intersections at a similar rate. This means the overall sex-dependent difference in complexity is only at the distal part of the dendritic trees, and is a consequence of the earlier decrease in females. Thus, male neurons of cluster 1 either have more bifurcations at the distal part, or male dendrites originated in the proximal part are longer. This significant difference in cluster 1 was expected, as we saw sex-dependent differences for both total length and number of branch points in **Chapter 1**. However, it is important to stress that the difference in complexity is not solely because male trees are significantly larger than female ones; in fact, if we only analysed dendritic trees of approximately the same size, male neurons of cluster 1 would still be significantly more complex than females (not shown). As for the Sholl analysis in cluster 2, it revealed no significant differences, as expected. Both sexes reach the peak of number of intersections at the same distance of 30 µm, which is closer to the soma than neurons from cluster 1. Interestingly, in both clusters there is a local maxima in the SIP at a distance of 5 µm to the soma, meaning some of the branches that originate very close to the soma are smaller than 10 µm. Because Keil *et al.* performed Sholl analysis using a radius step of 10 µm, this variation is not visible in their results. Other than that, our results confirm the same significant differences they found *(Keil et al., 2017)*.

As we noted previously, Sholl analysis and fractal dimension are related, with the latter usually uncovering differences in complexity patterns that the former cannot *(Jelinek et al., 2006)*. Because we saw significant sex-dependent differences in the Sholl analysis of cluster 1, we also expected to see significant differences with fractal dimension. However, this was not the case, which means that even though the dendritic patterns are significantly different, neurons of both sexes fill their dendritic space equally. Neurons of cluster 2 also did not show significant differences. One of the issues of calculating fractal dimension is that there are many different methods, which generate different results. The comparability between studies is not direct, as even different software using the same method can calculate different values for *D*. However, the results are always consistent, so that making the same comparison with different methods should yield the same differences *(Fernández & Jelinek, 2001; Jelinek et al., 2006)*. In the case of the method we used, values for *D* are much lower than one would get with other methods such as box-counting. Marks and Burke said that with the method we used, $D \approx 1.05$ *(Marks & Burke, 2007)*, but our results are around 1.02. We found another study where they also used L-measure to obtain *D* for pyramidal neurons (neocortical layer 5), and their results were also 1.02 *(Blackman et al., 2014)*, which is in agreement with our values. We also looked for other studies which used the fractal dimension in neurons to compare between sexes, but were unable to find any. Nevertheless, we found sex comparison of fractal dimension in different applications. In terms of brain structure, Farahibozorg *et al.* compared global and hemispheric white matter fractal dimension, and found that males had significantly higher complexity than females, which reversed after adjusting for volume *(Farahibozorg et al., 2015)*. Considering the brain waves,

Ahmadi *et al.* analysed scalp electroencephalogram (EEG) signals and found a higher complexity in females *(Ahmadi et al., 2013)*.

Given the lack of sex-dependent differences in optimality, we also expected to see no differences in centripetal bias. This was the case for both clusters, suggesting that both sexes have similar bias when connecting the dendrites, favouring a faster conduction time. The value we obtained of centripetal bias is close to that stated in the original paper. Using hippocampal CA1 basal pyramidal neurons from male rats, they calculated a bias of 7.39, with a 95% confidence interval of [5.89, 8.88] *(Bird & Cuntz, 2019, table S1)*. Curiously, our obtained value for the female neurons is within the confidence interval, but not the value for the males **(Table SII.3)**. This is most likely due to the difference in species between rats and mice. Because the introduction of the root angle is quite recent *(Bird & Cuntz, 2019)*, there still lacks studies calculating the centripetal bias. It will be interesting to see if others will obtain similar results to us regarding the bias of basal pyramidal neurons, as well as if any sex-dependent differences will be reported.

Even though our multi-objective approach to optimality has limitations, it is still more informative than Cuntz's and Wen's power laws. Besides classifying the neurons in terms of optimality through the distance to the Pareto front, we also have insight into the neuron's functional capabilities. We have shown that sex-dependent differences in the individual Pareto measures do not necessarily imply differences in optimality, and are not enough to determine it. Assessing the Pareto front is relevant to understand optimality, but to accurately determine it, our method falls short. Results from centripetal bias follow the lack of sex-dependent differences in optimality, and those from Sholl analysis validated the results from **Chapter 1**. Fractal dimension contradicted these results, but fractal analysis comparing sexes in single neuron morphology is lacking. We thus encourage more studies of this kind.

General conclusions

In this dissertation we explored sexual dimorphism in CA1 basal pyramidal neurons from C57BL/6J mice. Our results uncovered differences in dendritic morphology, that had implications in the neuron's functional capabilities but not in their optimality. We conclude that:

1. Neurons cluster in two well defined groups, being size the main factor. All sex-related differences were found in the larger-sized neurons, which we interpret as more developed neurons. This suggests cell-non-autonomous differences account for sexual dimorphism.
2. This sexual dimorphism could be related to differences in hippocampal or total brain volume. Estimating them together with single-neuron morphology analysis would be of interest to uncover possible correlations.
3. Male neurons of larger size are significantly more complex than female ones, but fractal analysis showed no sex-dependent differences so that both sexes fill their dendritic space equally, regardless of neuron size. All neurons are also centripetally biased, but not in a sex-dependent manner, meaning both sexes favour a faster conduction time over a smaller cable length.
4. Cuntz's and Wen's power laws showed opposite results regarding optimality and our results suggest that they are unreliable and should be used with caution when determining optimality.
5. The sex-related differences in the morphological metrics impact the neuron's functional capabilities. Males have significantly higher signal integration efficiency and connectivity repertoire, but at a higher cable cost. After normalizing by total length, females have significantly higher signal integration efficiency.
6. In our approach to optimality, using different Pareto fronts, we cannot conclude if the differences we found in the morphological metrics impact the neuron's optimality.
7. Our approach to optimality revealed that smaller-sized neurons are actually more optimal than larger ones, regardless of sex.

Our findings support our initial hypothesis that male and female CA1 pyramidal neurons differ significantly in dendritic morphology and functional capabilities, but only for larger neurons. However, we were unable to support nor dismiss our hypothesis that optimality would also differ between males and females. This is left as future work, where we will try to obtain a function that calculates signal integration efficiency. Thus, we will be able to estimate the euclidean distances to the real Pareto front and validate (or not) the hypothesis.

References

Ahmadi, K., Ahmadlou, M., Rezazade, M., Azad-Marzabadi, E., & Sajedi, F. (2013). Brain activity of women is more fractal than men. *Neuroscience Letters*, *535*(1), 7–11. https://doi.org/10.1016/j.neulet.2012.12.043

Akaike, H. (1974). A New Look at the Statistical Model Identification. *IEEE Transactions on Automatic Control*, *19*(6), 716–723. https://doi.org/10.1109/TAC.1974.1100705

Ascoli, G. A. (2006). Mobilizing the base of neuroscience data: The case of neuronal morphologies. *Nature Reviews Neuroscience*, *7*(4), 318–324. https://doi.org/10.1038/nrn1885

Ascoli, G. A., Donohue, D. E., & Halavi, M. (2007). NeuroMorpho.Org: A central resource for neuronal morphologies. *Journal of Neuroscience*, *27*(35), 9247–9251. https://doi.org/10.1523/JNEUROSCI.2055-07.2007

Beery, A. K., & Zucker, I. (2011). Sex bias in neuroscience and biomedical research. *Neuroscience and Biobehavioral Reviews*, *35*(3), 565–572. https://doi.org/10.1016/j.neubiorev.2010.07.002

Beining, M., Mongiat, L. A., Schwarzacher, S. W., Cuntz, H., & Jedlicka, P. (2017). T2N as a new tool for robust electrophysiological modeling demonstrated for mature and adult-born dentate granule cells. *ELife*, *6:e26517*. https://doi.org/10.7554/eLife.26517.001

Bird, A. D., & Cuntz, H. (2019). Dissecting Sholl Analysis into Its Functional Components Cell Reports Resource Dissecting Sholl Analysis into Its Functional Components. *Cell Reports*, *27*, 3081–3096. https://doi.org/10.1016/j.celrep.2019.04.097

Blackman, A. V., Grabuschnig, S., Legenstein, R., & Sjöström, P. J. (2014). A comparison of manual neuronal reconstruction from biocytin histology or 2-photon imaging: morphometry and computer modeling. *Frontiers in Neuroanatomy*, *8:65*. https://doi.org/10.3389/fnana.2014.00065

Bolker, B., & others. (n.d.). GLMM FAQ: Why doesn't lme4 display denominator degrees of freedom/p values? What other options do I have? Retrieved January 26, 2019, from https://bit.ly/2tP0iCI

Bozdogan, H. (1987). Model selection and Akaike's Information Criterion (AIC): The general theory and its analytical extensions. *Psychometrika*, *52*(3), 345–370. https://doi.org/10.1007/BF02294361

Brown, K. M., Gillette, T. A., & Ascoli, G. A. (2008). Quantifying neuronal size: Summing up trees and splitting the branch difference. *Seminars in Cell and Developmental Biology*, *19*(6), 485–493. https://doi.org/10.1016/j.semcdb.2008.08.005

Calí, C., Wawrzyniak, M., Becker, C., Maco, B., Cantoni, M., Jorstad, A., … Knott, G. W. (2018). The effects of aging on neuropil structure in mouse somatosensory cortex-A 3D electron microscopy analysis of layer 1. *PLoS ONE*, *13*(7), e0198131. https://doi.org/10.1371/journal.pone.0198131

Cembrowski, M. S., & Spruston, N. (2019). Heterogeneity within classical cell types is the rule: lessons from hippocampal pyramidal neurons. *Nature Reviews Neuroscience*, Vol. 20, pp. 193–204. https://doi.org/10.1038/s41583-019-0125-5

Cuntz, H., Forstner, F., Borst, A., & Häusser, M. (2010). One Rule to Grow Them All: A General Theory of Neuronal Branching and Its Practical Application. *PLoS Computational Biology*, *6*(8), e1000877. https://doi.org/10.1371/journal.pcbi.1000877

Cuntz, H., Forstner, F., Borst, A., & Häusser, M. (2011). The TREES toolbox-probing the basis of axonal and dendritic branching. *Neuroinformatics*, *9*(1), 91–96. https://doi.org/10.1007/s12021-010-9093-7

Cuntz, H., Mathy, A., & Häusser, M. (2012). A scaling law derived from optimal dendritic wiring. *Proceedings of the National Academy of Sciences of the United States of America*, *109*(27), 11014–11018. https://doi.org/10.1073/pnas.1200430109

Damodaran, A. (2008). Probabilist Approaches: Scenario Analysis, Decision Trees, and Simulations. In *Strategic Risk Taking: A Framework For Risk Management* (pp. 145–200). New Jersey: Pearson Prentice Hall.

Danielson, N. B., Zaremba, J. D., Kaifosh, P., Bowler, J., Ladow, M., & Losonczy, A. (2016). Sublayer-Specific Coding Dynamics during Spatial Navigation and Learning in Hippocampal

Area CA1. *Neuron*, *91*(3), 652–665. https://doi.org/10.1016/j.neuron.2016.06.020
Duarte-Guterman, P., Yagi, S., Chow, C., & Galea, L. A. M. (2015). Hippocampal learning, memory, and neurogenesis: Effects of sex and estrogens across the lifespan in adults. *Hormones and Behavior*, *74*, 37–52. https://doi.org/10.1016/j.yhbeh.2015.05.024
Egloff, L., Lenz, C., Studerus, E., Harrisberger, F., Smieskova, R., Schmidt, A., *et al* (2018). Sexually dimorphic subcortical brain volumes in emerging psychosis. *Schizophrenia Research*, *199*, 257–265. https://doi.org/10.1016/j.schres.2018.03.034
Farahibozorg, S., Hashemi-Golpayegani, S. M., & Ashburner, J. (2015). Age- and Sex-Related Variations in the Brain White Matter Fractal Dimension Throughout Adulthood: An MRI Study. *Clinical Neuroradiology*, *25*(1), 19–32. https://doi.org/10.1007/s00062-013-0273-3
Fernández, E., & Jelinek, H. F. (2001). Use of fractal theory in neuroscience: Methods, advantages, and potential problems. *Methods*, *24*(4), 309–321. https://doi.org/10.1006/meth.2001.1201
Flurkey, K., Currer, J. M., & Harrison, D. E. (2007). Chapter 20 - Mouse Models in Aging Research. In J. G. Fox, M. T. Davisson, F. W. Quimby, S. W. Barthold, C. E. Newcomer, & A. L. Smith (Eds.), *American College of Laboratory Animal Medicine*, *The Mouse in Biomedical Research* (2nd ed., Vol. 3, pp. 637–672). https://doi.org/10.1016/B978-012369454-6/50074-1
Franceschetti, S., Sancini, G., Panzica, F., Radici, C., & Avanzini, G. (1998). Postnatal differentiation of firing properties and morphological characteristics in layer V pyramidal neurons of the sensorimotor cortex. *Neuroscience*, *83*(4), 1013–1024. https://doi.org/10.1016/S0306-4522(97)00463-6
Gibbons, J. D., & Chakraborti, S. (2003). Tests of Goodness of Fit. In *Nonparametric Statistical Inference Fourth Edition, Revised and Expanded* (pp. 103–155). New York: Marcel Dekker, Inc.
Gould, E., Westlind-Danielsson, A., Frankfurt, M., & Mcewen, B. S. (1990). Sex Differences and Thyroid Hormone Sensitivity of Hippocampal Pyramidal Cells. *The Journal of Neuroscience*, *10*(3), 996–1003.
Gutin, A. M., Grosberg, A. Y., & Shakhnovich, E. I. (1993). Polymers with Annealed and Quenched Branchings Belong to Different Universality Classes. *Macromolecules*, *26*(6), 1293–1295. https://doi.org/10.1021/ma00058a016
Hajszan, T., MacLusky, N. J., Johansen, J. A., Jordan, C. L., & Leranth, C. (2007). Effects of androgens and estradiol on spine synapse formation in the prefrontal cortex of normal and testicular feminization mutant male rats. *Endocrinology*, *148*(5), 1963–1967. https://doi.org/10.1210/en.2006-1626
Hintze, J. L., & Nelson, R. D. (1998). Violin Plots: A Box Plot-Density Trace Synergism. *The American Statistician*, *52*(2), 181–184. https://doi.org/10.2307/2685478
Iyer, E. P. R., Iyer, S. C., Sullivan, L., Wang, D., Meduri, R., Graybeal, L. L., & Cox, D. N. (2013). Functional Genomic Analyses of Two Morphologically Distinct Classes of Drosophila Sensory Neurons: Post-Mitotic Roles of Transcription Factors in Dendritic Patterning. *PLoS ONE*, *8*(8), e72434. https://doi.org/10.1371/journal.pone.0072434
Jawaid, S., Kidd, G. J., Wang, J., Swetlik, C., Dutta, R., & Trapp, B. D. (2018). Alterations in CA1 hippocampal synapses in a mouse model of fragile X syndrome. *Glia*, *66*(4), 789–800. https://doi.org/10.1002/glia.23284
Jelinek, H. F., Elston, N., & Zietsch, B. (2006). Fractal Analysis: Pitfalls and Revelations in Neuroscience. In G. A. Losa, D. Merlini, T. F. Nonnenmacher, & E. R. Weibel (Eds.), *Fractals in Biology and Medicine. Mathematics and Biosciences in Interaction* (pp. 85–94). https://doi.org/10.1007/3-7643-7412-8_8
Kaufman, L., & Rousseeuw, P. J. (1990). *Finding Groups in Data: An Introduction to Cluster Analysis*. In *Wiley Series in Probability and Statistics*. https://doi.org/10.1002/9780470316801
Keil, K. P., Sethi, S., Wilson, M. D., Chen, H., & Lein, P. J. (2017). In vivo and in vitro sex differences in the dendritic morphology of developing murine hippocampal and cortical neurons. *Scientific Reports*, *7*(1), 1–15. https://doi.org/10.1038/s41598-017-08459-z
Konur, S., Rabinowitz, D., Fenstermaker, V. L., & Yuste, R. (2003). Systematic regulation of spine sizes and densities in pyramidal neurons. *Journal of Neurobiology*, *56*(2), 95–112. https://doi.org/10.1002/neu.10229
Koshibu, K., Ahrens, E. T., & Levitt, P. (2005). Postpubertal sex differentiation of forebrain structures

and functions depend on transforming growth factor-α. *Journal of Neuroscience*, *25*(15), 3870–3880. https://doi.org/10.1523/JNEUROSCI.0175-05.2005

Koshibu, K., Levitt, P., & Ahrens, E. T. (2004). Sex-specific, postpuberty changes in mouse brain structures revealed by three-dimensional magnetic resonance microscopy. *NeuroImage*, *22*(4), 1636–1645. https://doi.org/10.1016/j.neuroimage.2004.03.051

Koss, W. A., Belden, C. E., Hristov, A. D., & Juraska, J. M. (2014). Dendritic remodeling in the adolescent medial prefrontal cortex and the basolateral amygdala of male and female rats. *Synapse*, *68*(2), 61–72. https://doi.org/10.1002/syn.21716

Koss, W. A., & Frick, K. M. (2017). Sex differences in hippocampal function. *Journal of Neuroscience Research*, *95*(1–2), 539–562. https://doi.org/10.1002/jnr.23864

Kulkarni, V. A., & Firestein, B. L. (2012). The dendritic tree and brain disorders. *Molecular and Cellular Neuroscience*, *50*(1), 10–20. https://doi.org/10.1016/j.mcn.2012.03.005

Lein, P. J., Yang, D., Bachstetter, A. D., Tilson, H. A., Harry, G. J., Mervis, R. F., & Kodavanti, P. R. S. (2007). Ontogenetic Alterations in Molecular and Structural Correlates of Dendritic Growth after Developmental Exposure to Polychlorinated Biphenyls. *Environmental Health Perspectives*, *115*(4), 556–563. https://doi.org/10.1289/ehp.9773

Lenz, K. M., Nugent, B. M., & McCarthy, M. M. (2012). Sexual differentiation of the rodent brain: Dogma and beyond. *Frontiers in Neuroscience*, *6:26*. https://doi.org/10.3389/fnins.2012.00026

London, M., & Häusser, M. (2005). Dendritic Computation. *Annual Review of Neuroscience*, *28*(1), 503–532. https://doi.org/10.1146/annurev.neuro.28.061604.135703

Ma, S. (2014). find_pareto_frontier - MATLAB Central File Exchange. Retrieved August 26, 2020, from https://www.mathworks.com/matlabcentral/fileexchange/45885-find_pareto_frontier

Mackay, D. J. C. (2003). *Information Theory, Inference, and Learning Algorithms*. Retrieved from http://www.inference.phy.cam.ac.uk/mackay/itila/

Madeira, M. D., Sousa, N., Lima-Andrade, M. T., Calheiros, F., Cadete-Leite, A., & Paula-Barbosa, M. M. (1992). Selective vulnerability of the hippocampal pyramidal neurons to hypothyroidism in male and female rats. *Journal of Comparative Neurology*, *322*(4), 501–518. https://doi.org/10.1002/cne.903220405

Manubens-Gil, L. (2018). *Computational and modeling approaches to multi-scale anatomical description of neuronal circuitry* (Universitat Pompeu Fabra, Barcelona, Spain). Retrieved from http://www.tdx.cat/handle/10803/664511

Marks, W. B., & Burke, R. E. (2007). Simulation of motoneuron morphology in three dimensions. I. Building individual dendritic trees. *The Journal of Comparative Neurology*, *503*(5), 685–700. https://doi.org/10.1002/cne.21418

McEwen, B. S. (2010). Stress, sex, and neural adaptation to a changing environment: Mechanisms of neuronal remodeling. *Annals of the New York Academy of Sciences*, *1204*(SUPPL.1), 38–59. https://doi.org/10.1111/j.1749-6632.2010.05568.x

McLaughlin, K. J., Baran, S. E., & Conrad, C. D. (2009). Chronic stress- and sex-specific neuromorphological and functional changes in limbic structures. *Molecular Neurobiology*, *40*(2), 166–182. https://doi.org/10.1007/s12035-009-8079-7

Meyer, C. E., Kurth, F., Lepore, S., Gao, J. L., Johnsonbaugh, H., Oberoi, M. R., … MacKenzie-Graham, A. (2017). In vivo magnetic resonance images reveal neuroanatomical sex differences through the application of voxel-based morphometry in C57BL/6 mice. *NeuroImage*, *163*, 197–205. https://doi.org/10.1016/j.neuroimage.2017.09.027

Mizuseki, K., Diba, K., Pastalkova, E., & Buzsáki, G. (2011). Hippocampal CA1 pyramidal cells form functionally distinct sublayers. *Nature Neuroscience*, *14*(9), 1174–1183. https://doi.org/10.1038/nn.2894

Orlandi, J. G., Soriano, J., Alvarez-Lacalle, E., Teller, S., & Casademunt, J. (2013). Noise focusing and the emergence of coherent activity in neuronal cultures. *Nature Physics*, *9*(9), 582–590. https://doi.org/10.1038/nphys2686

Pareto, V. (1963). *The Mind and Society: A Treatise on General Sociology* (Vol. 3). New York: Dover Publications.

Persson, J., Spreng, R. N., Turner, G., Herlitz, A., Morell, A., Stening, E., … Söderlund, H. (2014). Sex differences in volume and structural covariance of the anterior and posterior hippocampus. *NeuroImage*, *99*, 215–225. https://doi.org/10.1016/j.neuroimage.2014.05.038

Phoenix, C. H., Goy, R. W., Gerall, A. A., & Young, W. C. (1959). Organizing action of prenatally administered testosterone propionate on the tissues mediating mating behavior in the female guinea pig. *Endocrinology*, *65*, 369–382. https://doi.org/10.1210/endo-65-3-369

Qiu, L. R., Fernandes, D. J., Szulc-Lerch, K. U., Dazai, J., Nieman, B. J., Turnbull, D. H., … Lerch, J. P. (2018). Mouse MRI shows brain areas relatively larger in males emerge before those larger in females. *Nature Communications*, *9*(1), 1–15. https://doi.org/10.1038/s41467-018-04921-2

Ramón, F., Moore, J. W., Joyner, R. W., & Westerfield, M. (1976). Squid giant axons. A model for the neuron soma? *Biophysical Journal*, *16*, 953–963. https://doi.org/10.1016/S0006-3495(76)85745-1

Ramón y Cajal, S. (1995). *Histology of the Nervous System of Man and Vertebrates* (Vol. 1). New York: Oxford University Press.

Ritz, C., & Streibig, J. C. (2008). *Nonlinear Regression with R*. https://doi.org/10.1007/978-0-387-09616-2

Rousseeuw, P. J. (1987). Silhouettes: A graphical aid to the interpretation and validation of cluster analysis. *Journal of Computational and Applied Mathematics*, *20*(C), 53–65. https://doi.org/10.1016/0377-0427(87)90125-7

Sasaki, T., Matsuki, N., & Ikegaya, Y. (2012). Effects of axonal topology on the somatic modulation of synaptic outputs. *Journal of Neuroscience*, *32*(8), 2868–2876. https://doi.org/10.1523/JNEUROSCI.5365-11.2012

Schröter, M., Paulsen, O., & Bullmore, E. T. (2017). Micro-connectomics: Probing the organization of neuronal networks at the cellular scale. *Nature Reviews Neuroscience*, *18*(3), 131–146. https://doi.org/10.1038/nrn.2016.182

Scorcioni, R., Polavaram, S., & Ascoli, G. A. (2008). L-Measure: A web-accessible tool for the analysis, comparison and search of digital reconstructions of neuronal morphologies. *Nature Protocols*, *3*(5), 866–876. https://doi.org/10.1038/nprot.2008.51

Shapiro, S. S., & Wilk, M. B. (1965). An Analysis of Variance Test for Normality (Complete Samples). *Biometrika*, *52*(3/4), 591–611. https://doi.org/10.2307/2333709

Sholl, D. A. (1953). Dendritic organization in the neurons of the visual and motor cortices of the cat. *Journal of Anatomy*, *87*(4), 387–406.

Spring, S., Lerch, J. P., & Henkelman, R. M. (2007). Sexual dimorphism revealed in the structure of the mouse brain using three-dimensional magnetic resonance imaging. *NeuroImage*, *35*(4), 1424–1433. https://doi.org/10.1016/j.neuroimage.2007.02.023

Spruston, N. (2008). Pyramidal neurons: Dendritic structure and synaptic integration. *Nature Reviews Neuroscience*, *9*(3), 206–221. https://doi.org/10.1038/nrn2286

Sussman, D., Leung, R. C., Chakravarty, M. M., Lerch, J. P., & Taylor, M. J. (2016). The developing human brain: age-related changes in cortical, subcortical, and cerebellar anatomy. *Brain and Behavior*, *6*(4), 1–15. https://doi.org/10.1002/brb3.457

Tan, A., Ma, W., Vira, A., Marwha, D., & Eliot, L. (2016). The human hippocampus is not sexually-dimorphic: Meta-analysis of structural MRI volumes. *NeuroImage*, *124*, 350–366. https://doi.org/10.1016/j.neuroimage.2015.08.050

Tsai, H. W., Grant, P. A., & Rissman, E. F. (2009). Sex differences in histone modifications in the neonatal mouse brain. *Epigenetics*, *4*(1), 47–53. https://doi.org/10.4161/epi.4.1.7288

Voges, N., Schüz, A., Aertsen, A., & Rotter, S. (2010). A modeler's view on the spatial structure of intrinsic horizontal connectivity in the neocortex. *Progress in Neurobiology*, *92*(3), 277–292. https://doi.org/10.1016/j.pneurobio.2010.05.001

Wang, W., Le, A. A., Hou, B., Lauterborn, J. C., Cox, C. D., Levin, E. R., … Gall, C. M. (2018). Memory-related synaptic plasticity is sexually dimorphic in rodent hippocampus. *Journal of Neuroscience*, *38*(37), 7935–7951. https://doi.org/10.1523/JNEUROSCI.0801-18.2018

Webster, R., & Oliver, M. A. (2007). *Geostatistics for Environmental Scientists* (2nd ed.). West Sussex: John Wiley & Sons, Ltd.

Wen, Q., & Chklovskii, D. B. (2008). A Cost–Benefit Analysis of Neuronal Morphology. *Journal of Neurophysiology*, *99*(5), 2320–2328. https://doi.org/10.1152/jn.00280.2007

Wen, Q., Stepanyants, A., Elston, G. N., Grosberg, A. Y., & Chklovskii, D. B. (2009). Maximization of the connectivity repertoire as a statistical principle governing the shapes of dendritic arbors. *Proceedings of the National Academy of Sciences of the United States of America*, *106*(30),

12536–12541. https://doi.org/10.1073/pnas.0901530106
Wilson, M. D., Sethi, S., Lein, P. J., & Keil, K. P. (2017). Valid statistical approaches for analyzing sholl data: Mixed effects versus simple linear models. *Journal of Neuroscience Methods*, *279*, 33–43. https://doi.org/10.1016/j.jneumeth.2017.01.003
Woitowich, N. C., Beery, A. K., & Woodruff, T. K. (2020). A 10-year follow-up study of sex inclusion in the biological sciences. *ELife*, *9*, 1–8. https://doi.org/10.7554/eLife.56344
Wold, S., Esbensen, K., & Geladi, P. (1987). Principal component analysis. *Chemometrics and Intelligent Laboratory Systems*, *2*(1–3), 37–52. https://doi.org/10.1016/0169-7439(87)80084-9
Woolley, C. S. (2007). Acute Effects of Estrogen on Neuronal Physiology. *Annual Review of Pharmacology and Toxicology*, *47*(1), 657–680. https://doi.org/10.1146/annurev.pharmtox.47.120505.105219
Yagi, S., & Galea, L. A. M. (2019). Sex differences in hippocampal cognition and neurogenesis. *Neuropsychopharmacology*, *44*(1), 200–213. https://doi.org/10.1038/s41386-018-0208-4
Zippo, A. G., & Biella, G. E. M. (2015). Quantifying the Number of Discriminable Coincident Dendritic Input Patterns through Dendritic Tree Morphology. *Scientific Reports*, *5*(1), 11543. https://doi.org/10.1038/srep11543

Supplementary Information

All code generated in this dissertation can be found in the online repository Bitbucket (https://bitbucket.org/NatsMrqs/master-thesis/src/master/), alongside a .txt file which explains how each file should be used. To access this repository, log in with the email *fc45870@alunos.fc.ul.pt* and password *mthesis_NM45870*. All analysis performed with R was with version 3.0.5; most of the analysis with MATLAB was with version 2016a, except for obtaining signal integration efficiency, which used version 2018a.

I. Dataset selection criteria

In this dissertation we used data from NeuroMorpho.Org *(Ascoli, 2006; Ascoli et al., 2007)*. This is an online repository of curated digitally reconstructed neurons. Alongside each neuron is the respective published article and available metadata. This database contains different types of neurons (pyramidal, Purkinje, interneuron, etc.), species (human, mouse, rat, fly, etc.) and brain regions (hippocampus, neocortex, optic nerve, etc.) from over 500 laboratories around the world, comprising more than one hundred thousand samples.

To select the datasets to work with, we searched the metadata available in the database (option "search by metadata"). This allows to filter the inventory at the same time by multiple criteria, such as species, experimental condition, brain region and age. To have two comparable groups, all metadata needs to be the same, except for the variable of interest. We performed multiple searches with the following combination of specifications: availability of data from a control experiment; species: mouse, rat or human; brain region: hippocampus, from CA1 or CA3 layer; cell type: pyramidal cell; gender: male or female.

The first exclusion criterion was datasets with less than 5 neurons and not providing the age of the subjects. With these conditions, 22 sets of neurons were obtained (version 7.6). We visually explored sets with similar metadata (e.g. CA1 reconstruction of male rats of different ages), and selected those with at least 15 neurons per group, avoiding very small datasets. This resulted in 12 datasets that allowed 4 possible comparisons: sex, species, region or age **(Table SI.1)**. We looked closely at them to select the one with the best quality.

We first considered performing an age-dependent comparison of dendritic morphologies. For this comparison, data from 7 different rat studies were available. However, we discarded this possibility because not all animals were of the same strain, which would affect our results. We also regarded the possibility of comparing different species. However, one important constraint was that animals of the same age from different species may be at different neurodevelopmental stages. This would introduce another source of variability in our study, so we also discarded this comparison. The other possible comparison was among different regions of the hippocampus (CA1 and CA3). However for one of the regions, the data pertained to 2 different studies, which used different reconstruction methods which may also lead to variations **(Table SI.1)**. Finally, we selected a dataset in which all neurons were from the same study, and hence no technical constraints. This allowed us to compare sex-dependent differences in pyramidal cells. The selected sample was composed of 66 neurons, 33 of each sex (variable of interest) reconstructed from the CA1 hippocampal region of 10 C57BL/6J mice. The neurons come only from 5 male and 5 female mice, meaning we have multiple neurons from the same animal *(Wilson et al., 2017)*.

Table SI.1 - Summary of the 4 considered comparisons from NeuroMorpho.Org, and reasons for discarding. The last comparison (sex) was the chosen one.

Type of comparison	Groups	Number of neurons	Strain	Name of the dataset	Reason for discarding
Age: CA1 male rats	11-19 days	10	Wistar	Escaplez	Different strains
		12	Wistar	Groen	
	21-28 days	20	Wistar	Storm	
	1-2 months	30	Sprague-Dawley	Johnston	
	2 months	10	Fischer 344	Turner	
	2-3 months	19	Wistar	Kole	
	8-10 months	18	Sprague-Dawley	Chen	
Species: CA1 males (3-4 months)	Mouse	30	ICR	Oguro-Ando	Different developmental stage
	Hamster	36	Siberian Hamster	Ikeno	
Region: male rats (11-19 days)	CA1	10	Wistar	Escaplez	Group of CA1 neurons has data from 2 different studies
		12	Wistar	Groen	
	CA3	24	Wistar	Jonas	
Sex: CA1 mice (33 days)	Female	33	C57BL/6J	Lein	Not discarded
	Male	33	C57BL/6J	Lein	

II. Analysis on whole data

The statistical analysis of **Chapter 1** and all analysis of **Chapter 2** were also applied to the whole data, i.e., without separating the neurons by cluster. Here we will only present the results, as the methods can be found in the main text, except if we have done something different. In that case, the methods will be clearly explained.

When performing the statistical analysis on the neuronal metrics, Shapiro-Wilk tests revealed only 2 of the metrics were not normal, total length and volume (p-values of 0.002 and <0.001, respectively). Total length assumes a log-normal distribution. As for the volume, we used volume/1000 to be able to fit the Gamma distribution, which turned out to be the best fit. Maximum path length and straightness passed the Shapiro-Wilk test but with very small p-values (0.070 and 0.071 respectively). For this reason, we calculated their skewness: straightness is considered normal (-0.29) but not maximum path length (0.55), which fits a gamma distribution **(Table SII.1)**.

Table SII.1 - Statistical comparisons between sexes. Overview of the mean and standard deviation for each sex (F for females and M for males) and summary of the results obtained in each step of the statistical analysis. If there is a dash, it means the test was not performed. There are no significant p-values in the GLMM.

Name	Mean	Standard deviation	Shapiro-Wilk (p-value)	Skewness	Assumed distribution	GLMM p-value
Total length [µm]	F: 759.70 M: 905.19	F: 245.12 M: 421.86	0.002	-	Log-normal	0.373
Max. path length [µm]	F: 121.84 M: 137.80	F: 34.40 M: 41.77	0.070	0.55	Gamma	0.358
Mean branch length [µm]	F: 27.59 M: 26.80	F: 5.63 M: 6.91	0.307	-	Normal	0.745
Soma radius [µm]	F: 9.51 M: 9.18	F: 1.46 M: 1.44	0.285	-	Normal	0.510
Tree radius [µm]	F: 50.98 M: 55.49	F: 10.66 M: 13.95	0.593	-	Normal	0.262
Volume [µm^3]	F: 117308.7 M: 142088.3	F: 76490.4 M: 108863.8	<0.001	-	Gamma (Volume/1000)	0.531
Number of branch points	F: 16.58 M: 18.91	F: 4.39 M: 6.01	-	-	Negative binomial	0.087
Mean branch order	F: 5.59 M: 5.86	F: 1.08 M: 0.94	0.215	-	Normal	0.285
Straightness	F: 0.86 M: 0.85	F: 0.05 M: 0.05	0.071	-0.29	Normal	0.453

After defining the distribution of each metric, we applied the GLMMs. We found no sex-related differences in any of the studied metrics **(Figure SII.1)**. The metric with the smallest p-value was the number of branch points, with a p-value of 0.087, with the remaining all having p-values>0.25. These results are in line with the means and standard deviations of the metrics, which overall are very similar for both sexes **(Table SII.1)**. A closer look at the results shows the data points seem to be binomially distributed, which supports the need to perform the cluster analysis **(Figure SII.1)**. The obtained results on the whole dataset are thus not significant because two subgroups are being considered. Because we saw no significant differences in all the metrics, we expected to see no differences in the remaining analysis.

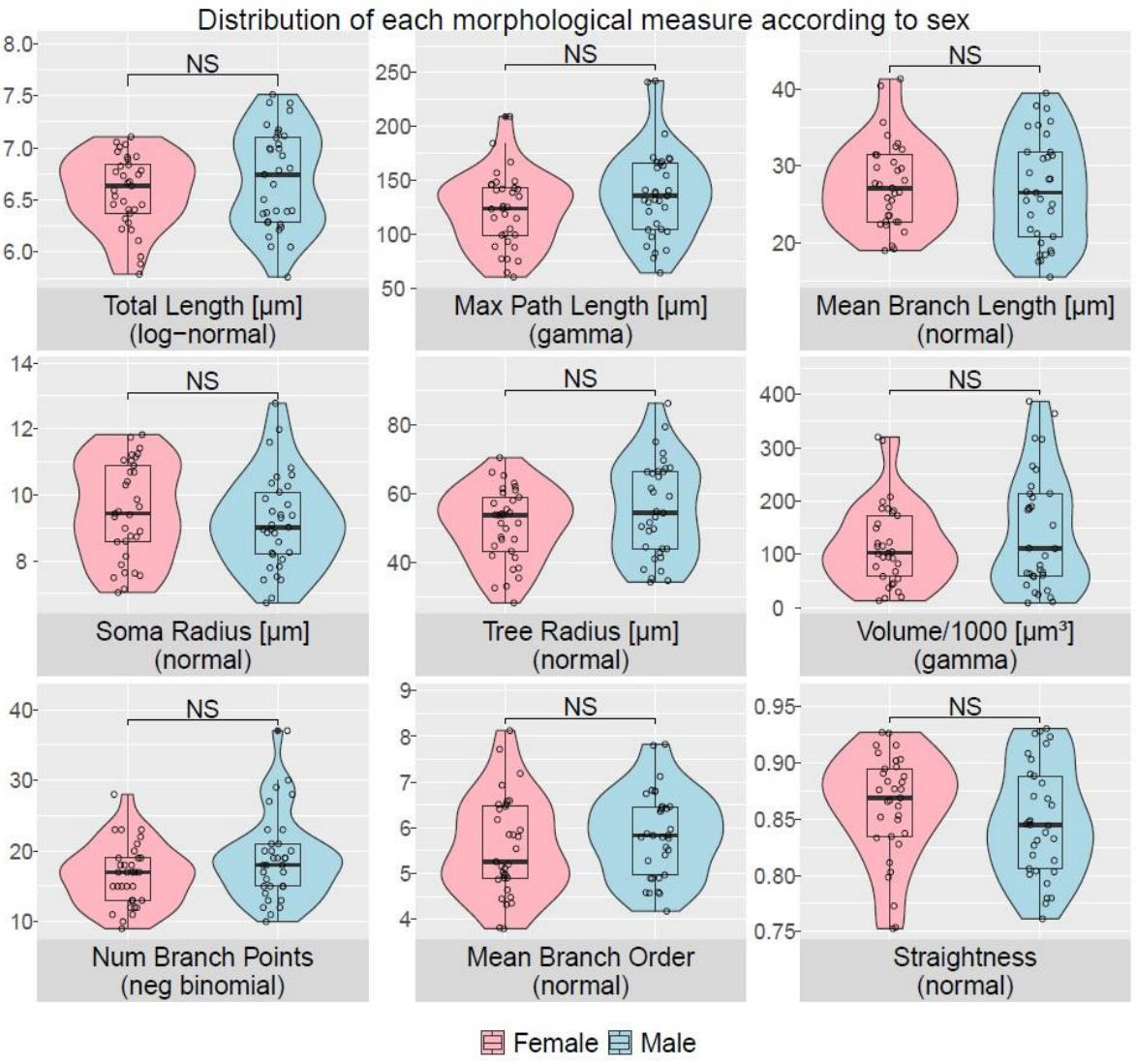

Figure SII.1 - Variation of the data by sex and statistical difference for each neuromorphological metric. Each panel has violin, boxplot and data points of each variable, the latter representing each neuron of the dataset. The label of the panels has the name, unit and distribution used in the GLMM of the corresponding metric. The significance level of the test is shown on top of each panel: NS is not significant, * is p-value<0.05, ** is p-value<0.05 and *** is p-value<0.001. If it passes the threshold of significance, the p-value is also shown. There are no significant metrics when we consider the whole dataset.

When assessing the power laws, once again results were different between Cuntz's and Wen's power laws. With Cuntz's power law, female neurons come closer to optimality (0.76±0.05), with males having an estimated power of 0.90±0.04, much further from the expected value of 0.67 **(Figure SII.2)**. Considering Wen's power law, the estimated values for power follow the 0.43 optimal value (males 0.43±0.05 and females 0.48±0.08) ***(Figure SII.3)***.

We performed an ANOVA between the models with and without accounting for sex, to see if the estimated power laws had significant sex-dependent differences. There are no significant differences for Wen's power law, but for Cuntz's there are (p-value 0.787 and 0.047, respectively). Because we are estimating two parameters in the model, *a* and *b* **(Eq. 2.1)**, we need to understand if both or just one of them is significantly different. We can assess this through ANOVA, by comparing the model where both parameters depend on sex with a model where one of the parameters is fixed. If p-value≤0.05, the non-fixed parameter depends on sex *(Ritz & Streibig, 2008, Chapter 8)*. In this case we are more interested in finding differences in parameter *b*, since it is the exponent of the power law and what determines optimality, while *a* is just a multiplying factor **(Eq. 2.1)**. The ANOVA was significant for *a* but not for *b* (p-values 0.029 and 0.122, respectively). Thus, the significant difference with Cuntz's power law is only in the multiplying factor, meaning there is no significant difference in optimality between sexes.

As we mentioned in the discussion **(Section 2.4)**, Cuntz obtained an estimated power of 0.72 only when fitting 74 datasets together; when fitting each dataset separately, many deviated from the optimal fit *(Cuntz et al., 2012, fig. S5)*. For this reason, we decided to assess if we could obtain an optimal fit when considering the data together, i.e., without separating by sex. This was not the case, as the estimated power law was of 0.85±0.03. This further shows how Cuntz's power law is not reliable for our data.

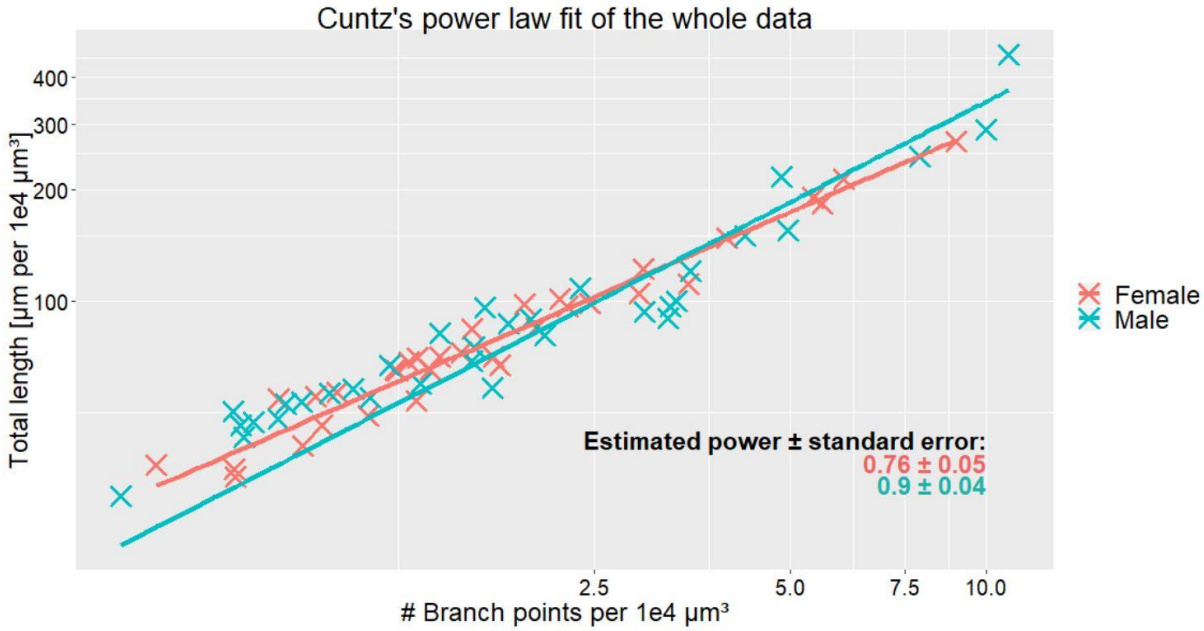

Figure SII.2 - Estimation of Cuntz's power law for each sex. Both the number of branch points and total length are normalized by the volume of the neuronal tree, and represented in logarithm scale. Each cross is a neuron, with the lines being the power law fit for each sex. Female neurons have a power relationship of 0.76±0.05, the closest to Cuntz's obtained value for optimality of 0.67. Males show a strong deviation, with an estimated power of 0.90±0.04.

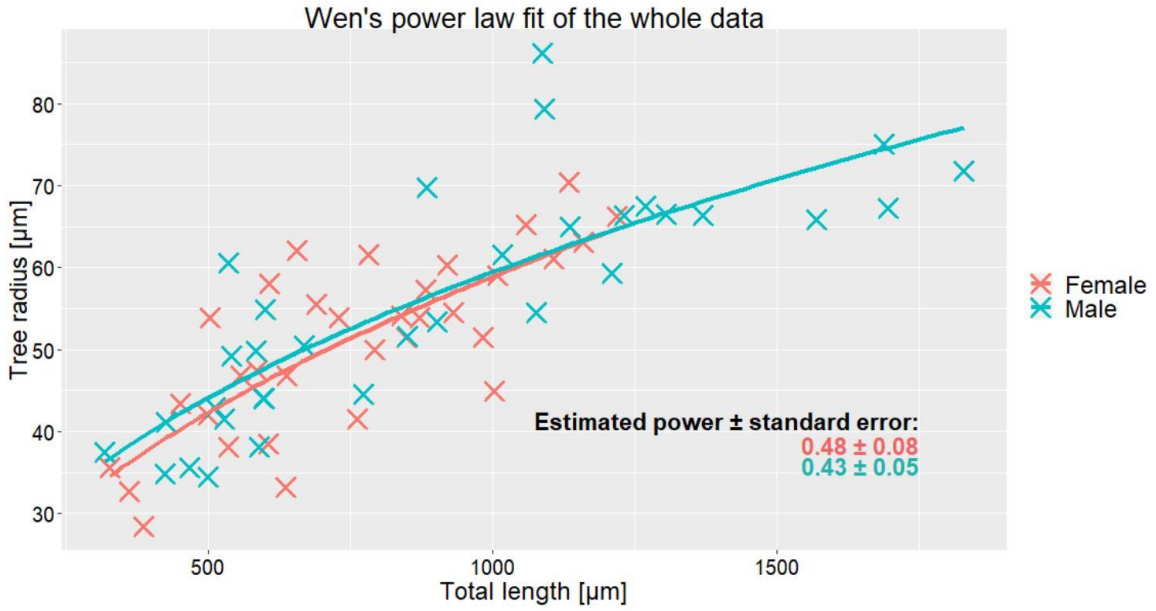

Figure SII.3 - Estimation of Wen's power law for each sex. Labels are explained in **Figure SII.2**. Male neurons are optimal (0.43±0.05), and the female trees only deviate slightly, still being considered optimal (0.48±0.08).

When assessing the Pareto measures, Shapiro-Wilk revealed that connectivity repertoire and cost were not normal (p-value 0.002 for both). Both measures follow a log-normal distribution. The GLMM showed no significant sex-dependent differences (**Table SII.2** and **Figure SII.4**), which was expected since we saw no neuromorphological differences either **(Figure SII.1)**. This means that if we analyse all neurons together, we see no differences in optimality. We also compared the connectivity repertoire and signal integration efficiency after normalizing by cost. The latter did not pass the Shapiro-Wilk test (p-value 0.030), fitting a gamma distribution. As expected, there were no significant differences in the GLMMs of both Pareto measures (**Figure SII.2** and **Figure SII.5**).

We did not compare the euclidean distances to the Pareto front because they would not provide new information. We already saw there were no differences in optimality between males and females (**Figure SII.4** and **Figure SII.5**), hence we would have the same result with the euclidean distances.

Table SII.2 - Statistical comparisons of the Pareto measures between sexes. Overview of the mean and standard deviation for each sex (F for females and M for males) and summary of the results obtained in each step of the GLMM. There are no significant p-values in the GLMM.

	Mean	**Standard deviation**	**Shapiro-Wilk (p-value)**	**Assumed distribution**	**GLMM p-value**
Connectivity repertoire	F: 3460.84 M: 4393.23	F: 1186.78 M: 2173.18	0.002	Log-normal	0.258
Signal integration efficiency [ms^{-1}]	F: 0.466 M: 0.516	F: 0.105 M: 0.128	0.435	Normal	0.263
Cost [µm]	F: 759.70 M: 905.19	F: 245.12 M: 421.86	0.002	Log-normal	0.373
Normalized connectivity repertoire [per µm]	F: 4.540 M: 4.786	F: 0.471 M: 0.491	0.362	Normal	0.095
Normalized signal integration efficiency [ms^{-1} per µm]	F: 6.51×10^{-4} M: 6.48×10^{-4}	F: 1.65×10^{-4} M: 2.27×10^{-4}	0.030	Gamma	0.674

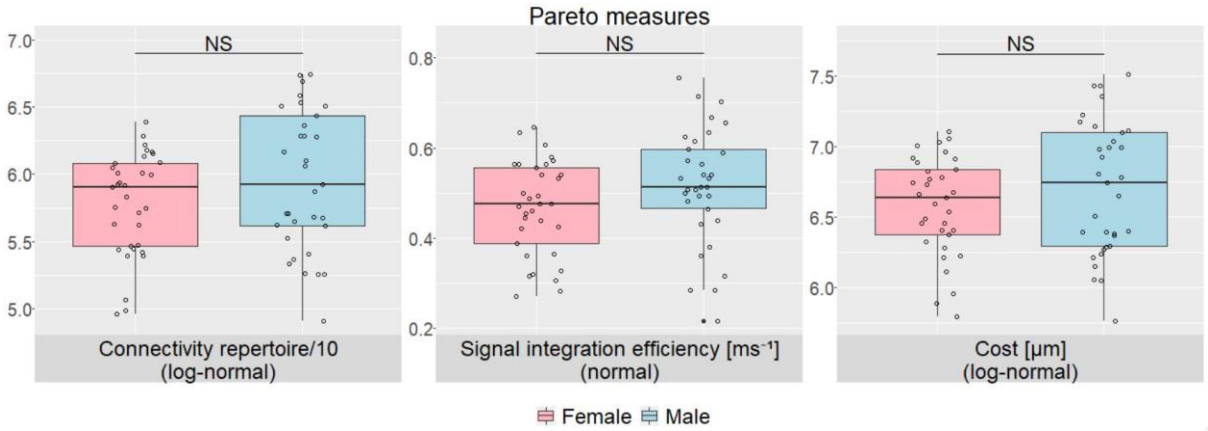

Figure SII.4 - Statistical analysis of the 3 Pareto measures in the whole data. There were no significant differences, which means males and females have no differences in optimality. Labels are explained in **Figure SII.1**.

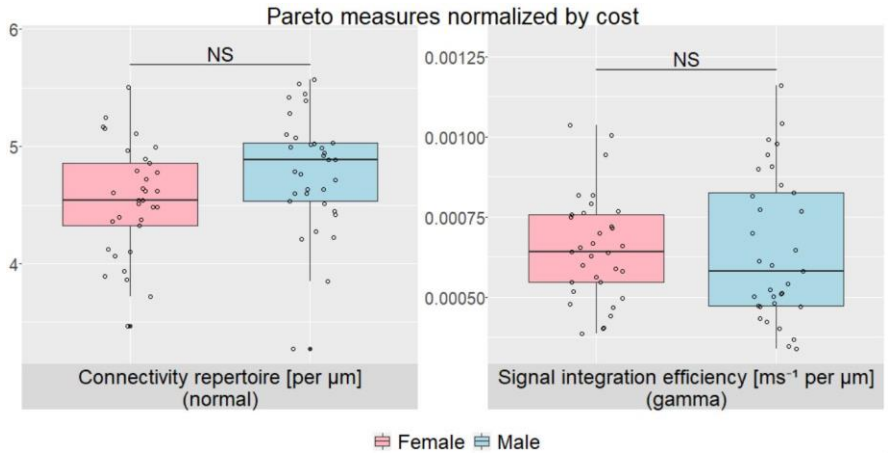

Figure SII.5 - Statistical analysis of the Pareto measures normalized by total length in the whole data. There are no significant differences. Labels are explained in **Figure SII.1**.

When performing Sholl analysis of the whole dataset, we expected to see some differences for longer distances to the soma. This is because the statistical analysis is performed at each *r*, and for cluster 2 **(Figure 2.13)** the maximum *r* analysed is smaller than that of cluster 1 **(Figure 2.12)**. Thus, the differences we saw on cluster 1 for larger values of *r* should also be distinguishable here. We found significant differences between sexes only for distances to the soma of 80, 90 and 95 µm (p-values 0.031, 0.022 and 0.047, respectively). Surprisingly, distance of 85 µm does not reach significance, but is very close (p-value of 0.055). The last *r* compared in cluster 2 is *r*=80 µm **(Figure 2.13)**, which is why they do not mask the significant differences here, as it happened in all the previous analysis (**Figure SII.1**, **Figure SII.4** and **Figure SII.5**). It is clear the male neurons have longer dendrites, as they only have a median of zero at *r*=115 µm **(Figure SII.6)**.

The AUCs are not significantly different (p-value 0.333): the females have an AUC of 557.5 μm^2 and the males of 582.5 μm^2. This makes sense as we see significant differences for only a few *r* **(Figure SII.6)**.

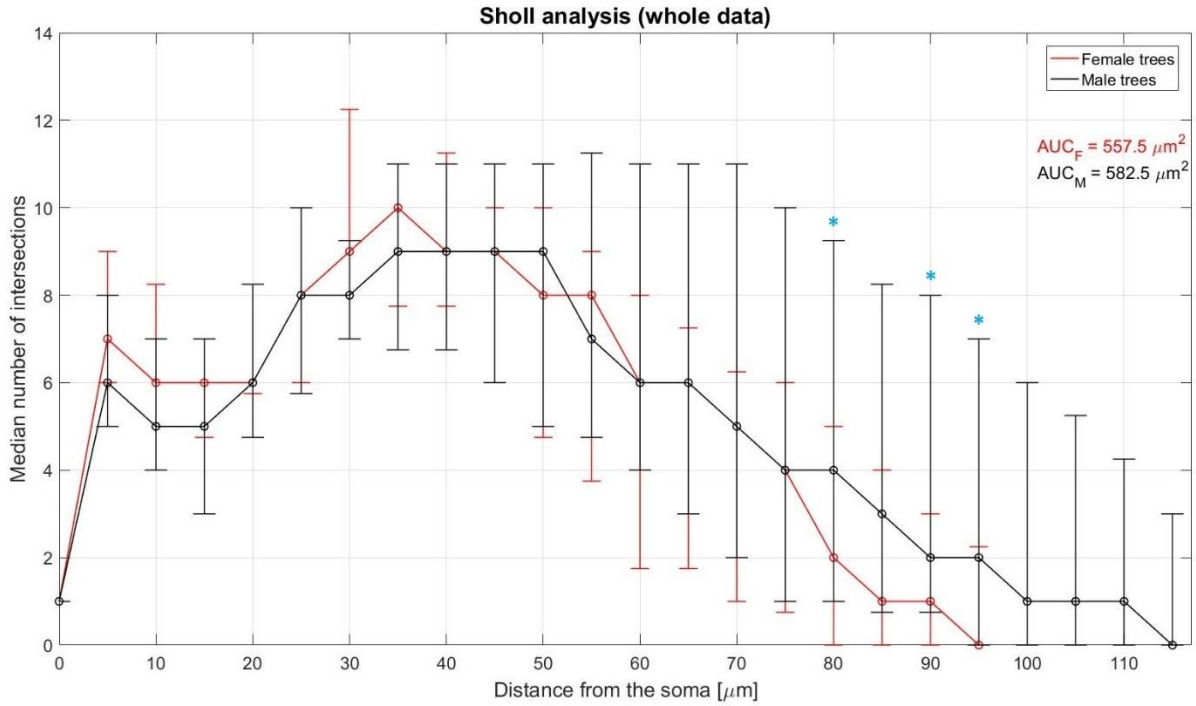

Figure SII.6 - Sholl interception profile of the whole data for each sex. The median number of intersections with concentric spheres of increasing r are represented in function of the distance to the soma. Error bars are the first and third quartile. The significance level of each r is shown on the top: * is p-value<0.05, ** is p-value<0.01 and *** is p-value<0.001. There are few r with significant differences, mainly because female trees have shorter dendrites. The AUC is not significantly different.

Since there were no significant differences for fractal dimension *D* or centripetal bias in both clusters (**Table 2.4**, **Figure 2.14** and **Figure 2.15**), we were expecting similar results for the whole data. Both metrics did not pass the Shapiro-Wilk test, with p-values<0.001, and followed a log-normal distribution. As expected, we saw no significant sex-dependent differences (**Table SII.3** and **Figure SII.7**).

Table SII.3 - Statistical comparisons of fractal dimension D and centripetal bias k between sexes. Overview of the mean and standard deviation for each sex (F for females and M for males) and summary of the results obtained in each step of the statistical analysis. There are no significant p-values in the GLMM. We removed one neuron from the analysis of fractal dimension, since it was an outlier with $D \simeq 1.10$.

	Mean	**Standard deviation**	**Shapiro-Wilk (p-value)**	**Assumed distribution**	**GLMM p-value**
Fractal dimension *D*	F: 1.027 M: 1.024	F: 0.009 M: 0.007	0.026	Log-normal	0.267
Centripetal bias *k*	F: 6.84 M: 5.78	F: 3.35 M: 2.49	<0.001	Log-normal	0.323

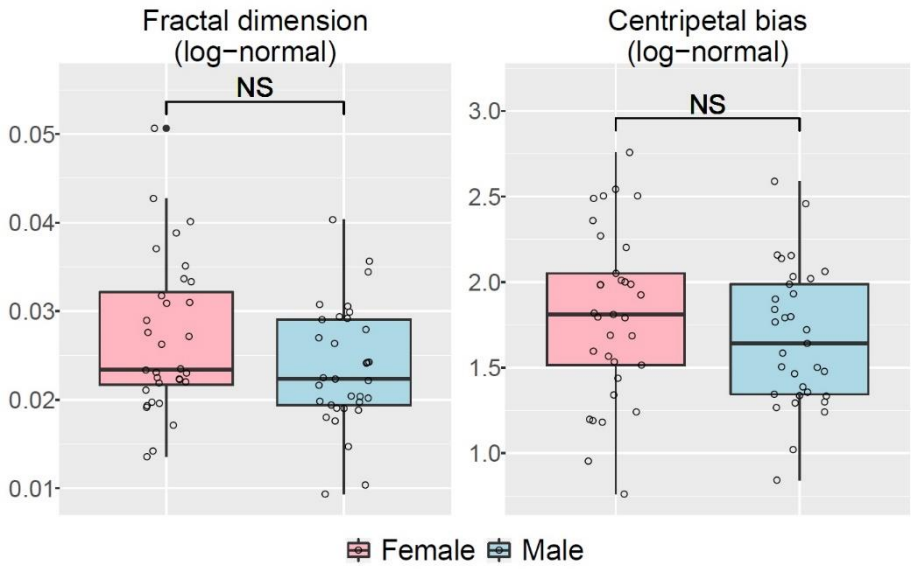

Figure SII.7 - Fractal dimension D and centripetal bias k show no significant differences between sexes in the whole data. D has the typical values for dendritic branches, and k implies the existence of bias, which means the neurons favour a faster conduction speed.

By looking at all results together, we can conclude that sex-dependent differences cannot be uncovered unless the neurons are separated by their size. Sholl analysis was the only exception, and just because the statistical analysis of the SIP is performed at each *r* **(Figure SII.6)**. This stresses the need of carefully selecting a dataset to work with, and providing all necessary information about sample selection and respective metadata.

III. Silhouette Coefficient

To classify the obtained clusters, we can compute the silhouette coefficient (SC) for *k=2*, with *k* the number of clusters *(Rousseeuw, 1987)*. The SC calculates the ratio between the intra and inter cluster distances. The first is how close the point is to its cluster, and the second how distant it is to its neighbour cluster. If the SC is between 0 and 0.25, the clustering is not necessarily due to some structure to the data; between 0.25 and 0.5 there is some structure; between 0.5 and 1 it is a good cluster. We can also calculate SC values for each data point, determining if they were classified in the correct cluster. A negative SC means a misclassified neuron and a positive SC a correctly classified. When the SC is close to zero, then the neuron lies between clusters. Considering this last type of SC, in the analysis (b) **(Section 1.2.2)** when the SC to any data point was negative, we manually changed it to the other cluster to improve the overall classification.

When clustering the whole data, the average SC of the analysis with just 2 clusters is of 0.29, indicating there is some structure to the data. As for the SC of each neuron, four are considered misclassified. Neuron #42 (male, SC=-0.135) is in cluster 1 but should be in cluster 2, and neurons #7, #27 and #33 are the opposite (all females, SCs of -0.051, -0.070 and -0.081, respectively). Lastly, the SC of each cluster is 0.25 for cluster 1 (26 neurons) and 0.31 for cluster 2 (40 neurons), both over the threshold of 0.25 **(Figure SIII.1)**.

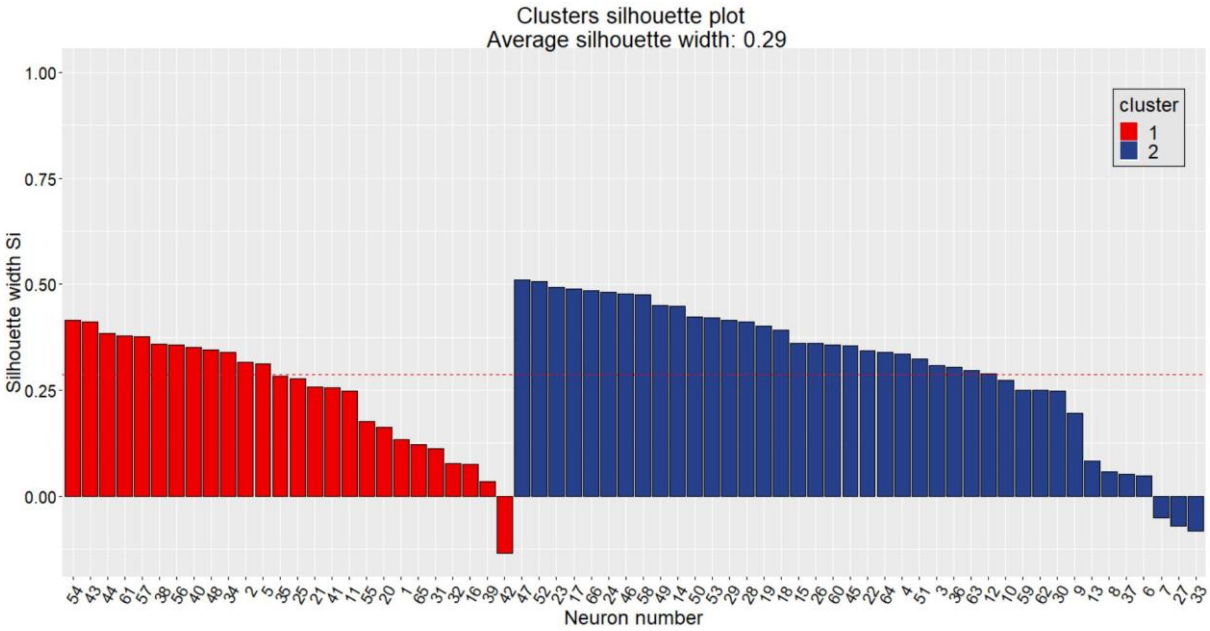

Figure SIII.1 - Silhouette plot of the hierarchical clustering analysis on the whole dataset. Each bar is a neuron and respective SC, coloured by which cluster they are in. Cluster 1 has 26 trees and a SC of 0.25, with one neuron being misclassified (#32, SC=-0.135). Cluster 2 has the remaining 40 trees with a SC of 0.31, with four misclassified neuron (#7, #27 and #33, SCs of -0.051, -0.070 and -0.081, respectively). The average SC is of 0.29 (red horizontal dashed line), indicating there is some structure to the data.

When clustering each sex separately, the results differ between them. For the males the average SC is 0.37, and of each cluster is 0.35 for the first (13 neurons) and 0.38 for the second (20 neurons). All values are over the threshold of 0.25, and there are no neurons considered as misclassified **(Figure SIII.2)**. As for the females, the initial average SC is 0.22, and of each cluster is 0.24 for the first (13 neurons) and 0.21 for the second (20 neurons). Neither of the clusters pass the threshold of 0.25, which might happen due to the misclassification of 3 neurons. They are neurons #6 (SC=-0.029), #27 (SC=-0.143) and #7 (SC=-0.171) **(Figure SIII.3)**.

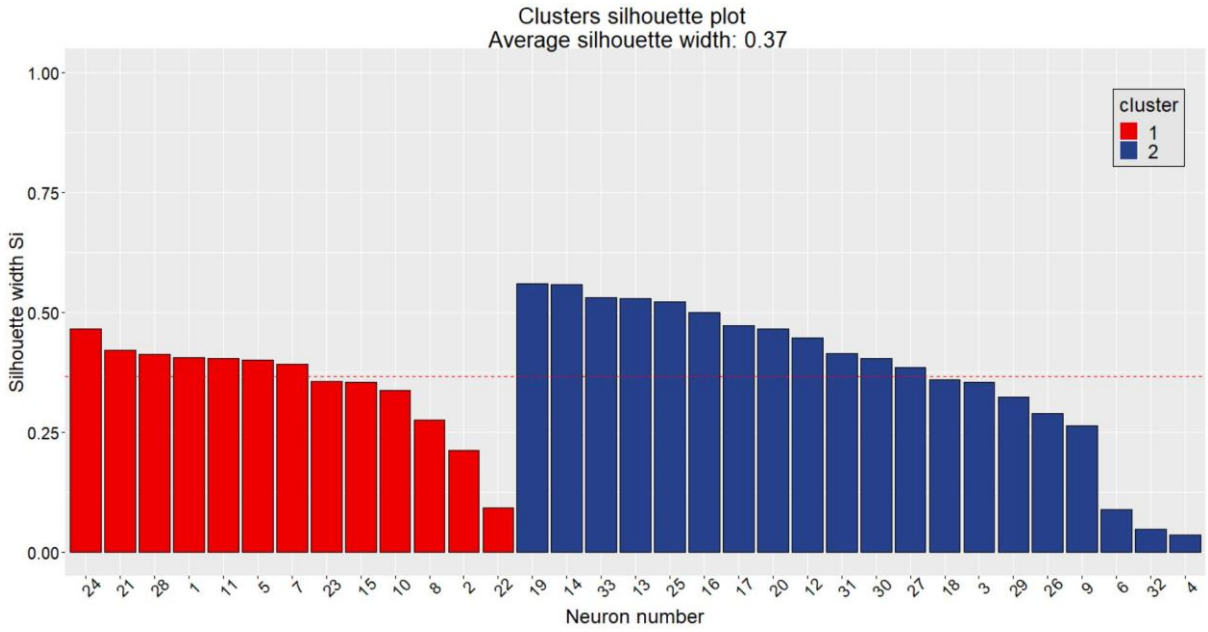

Figure SIII.2 - Silhouette plot of the hierarchical clustering analysis on the male trees. Cluster 1 has 13 trees and a SC of 0.35 and cluster 2 has the remaining 20 trees with a SC of 0.38. There are no misclassified neurons. Average SC is of 0.37, indicating there is some structure to the data.

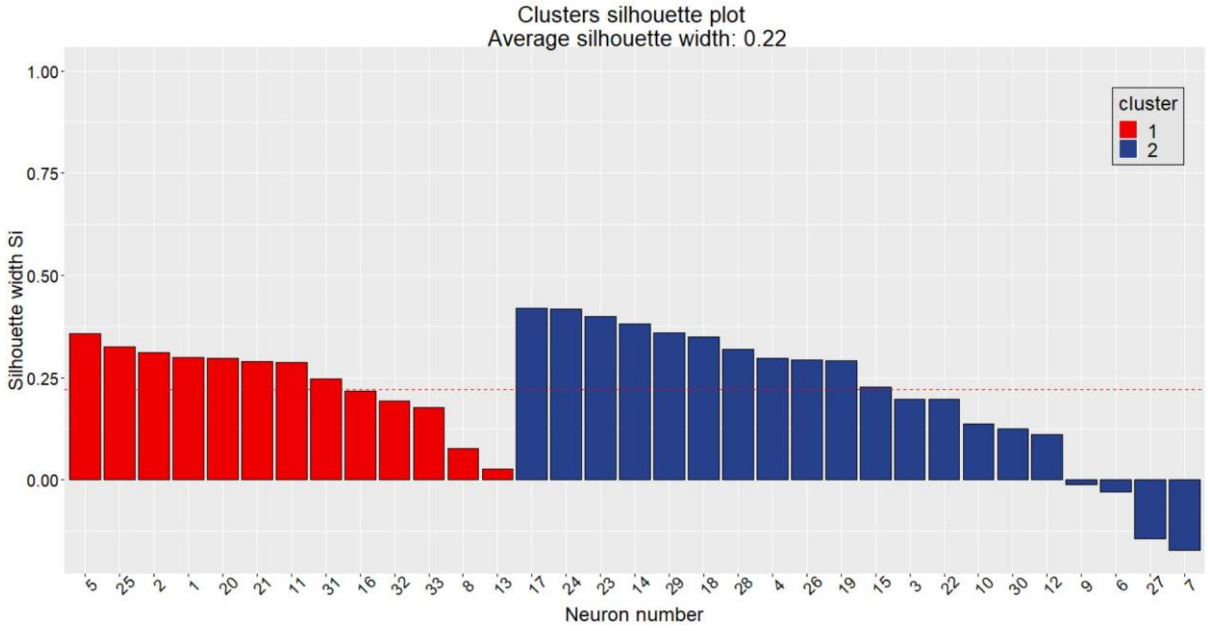

Figure SIII.3 - Silhouette plot of the hierarchical clustering analysis on the female trees. Cluster 1 has 13 trees and a SC of 0.24, and cluster 2 has the remaining 20 trees with a SC of 0.21, with three neurons being misclassified (#6, #27 and #7, with SCs of -0.029, -0.143 and -0.171, respectively). Average SC is of 0.22, which is below the threshold of 0.25.

It is possible to manually change neurons from one cluster to the other. Doing this for misclassified neurons not only improves the clustering itself, but also the SCs. For this reason, neurons #6, #7 and #27 of the female analysis were reclassified from cluster 2 to cluster 1. After recalculating the SCs, this final cluster now has an average SC of 0.28. The first cluster has 16 neurons and a SC of 0.23, while the second has 17 neurons and a SC of 0.32 **(Figure SIII.4)**. Neuron #13 is now considered as misclassified. This could be why the SC of cluster 1 is just below the 0.25 threshold. We decided not to move this neuron to the second cluster, as it would be a biased improvement.

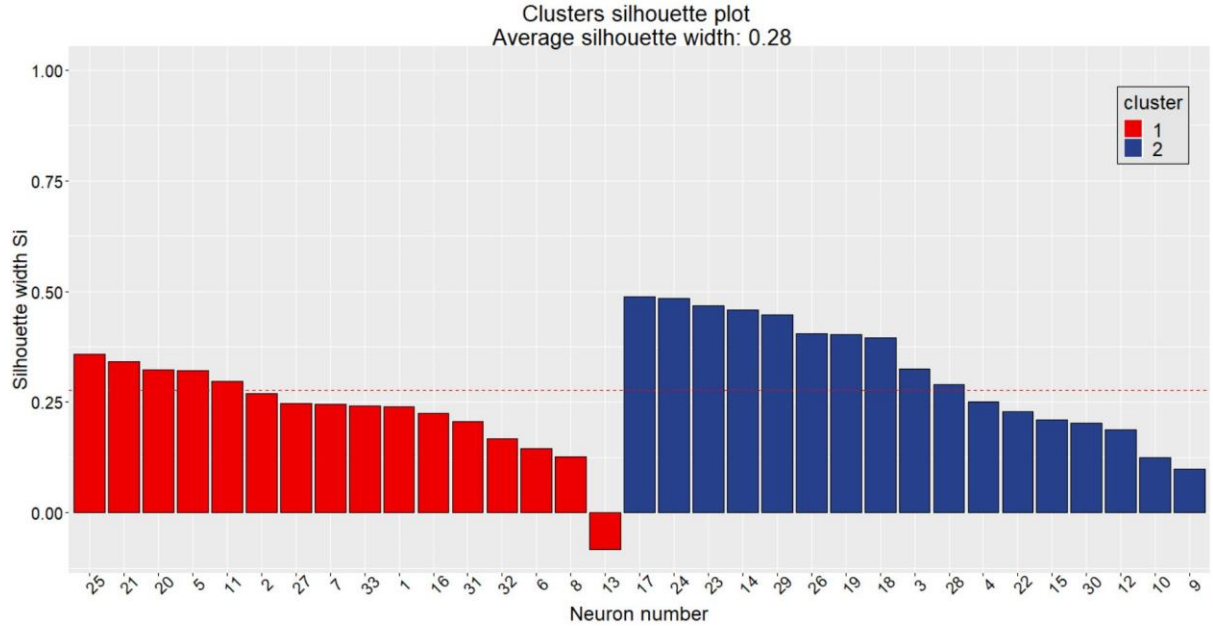

Figure SIII.4 - New silhouette plot of the hierarchical cluster applied to the female trees, after changing the 3 neurons from cluster 2 to cluster 1. These neurons had negative SC (neurons #6, #7 and #27). With these changes, cluster 1 now has 16 trees and a SC of 0.23 and cluster 2 has the remaining 17 trees with a SC of 0.32. Average SC is of 0.28, which now passes the threshold of 0.25, indicating there is indeed some structure to the data.

Given that an average SC between 0.26 and 0.50 is still very low, we also calculated the SC with the metric of highest separation between clusters. This meant using the intra and inter cluster distances of only one metric, instead of the combination of all 9. The metric that best separated the two clusters of the male trees was volume. The average SC is 0.63, of the first cluster is 0.56 and of the second one is 0.68. All values are over 0.50, and only neuron #32 is misclassified in the second cluster **(Figure SIII.5)**. In the case of the females, the metric used was total length, with an average SC is of 0.52. The SC of each cluster is 0.49 for the first and 0.54 for the second, with neurons #13 and #9 misclassified in the cluster 1 and 2 respectively **(Figure SIII.6)**.

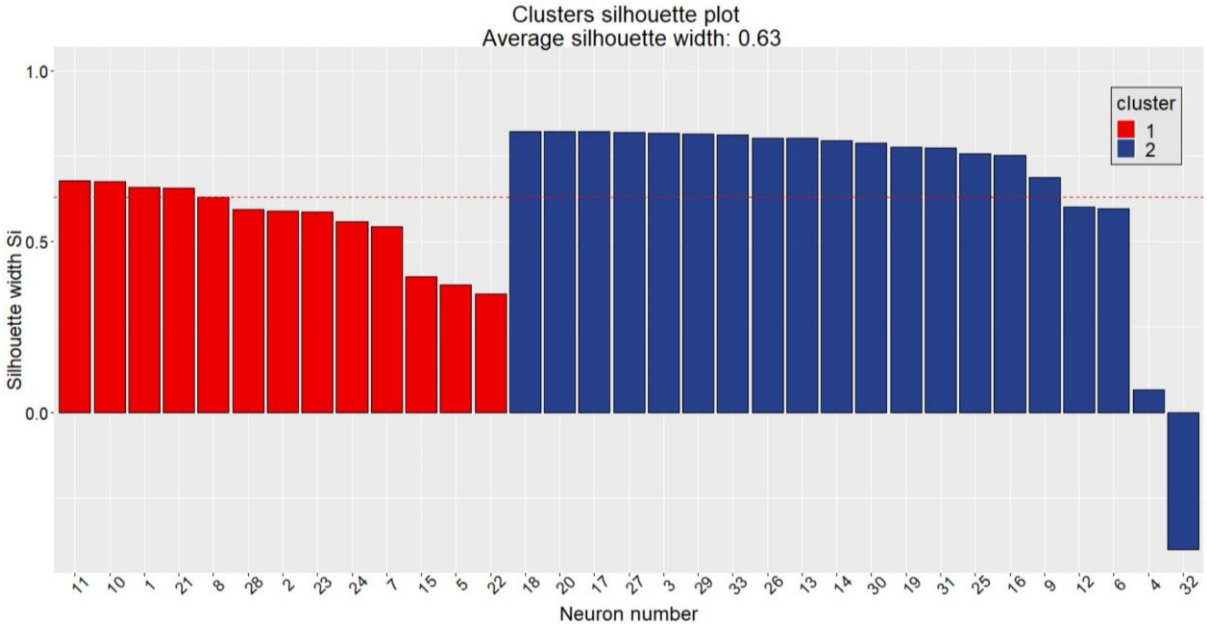

Figure SIII.5 - Silhouette plot of the hierarchical clustering analysis on the male trees, considering only the volume of the neurons. Cluster 1 has a SC of 0.56 and cluster 2 has a SC of 0.68, with neuron #32 misclassified. Average SC is of 0.63, which is above 0.50.

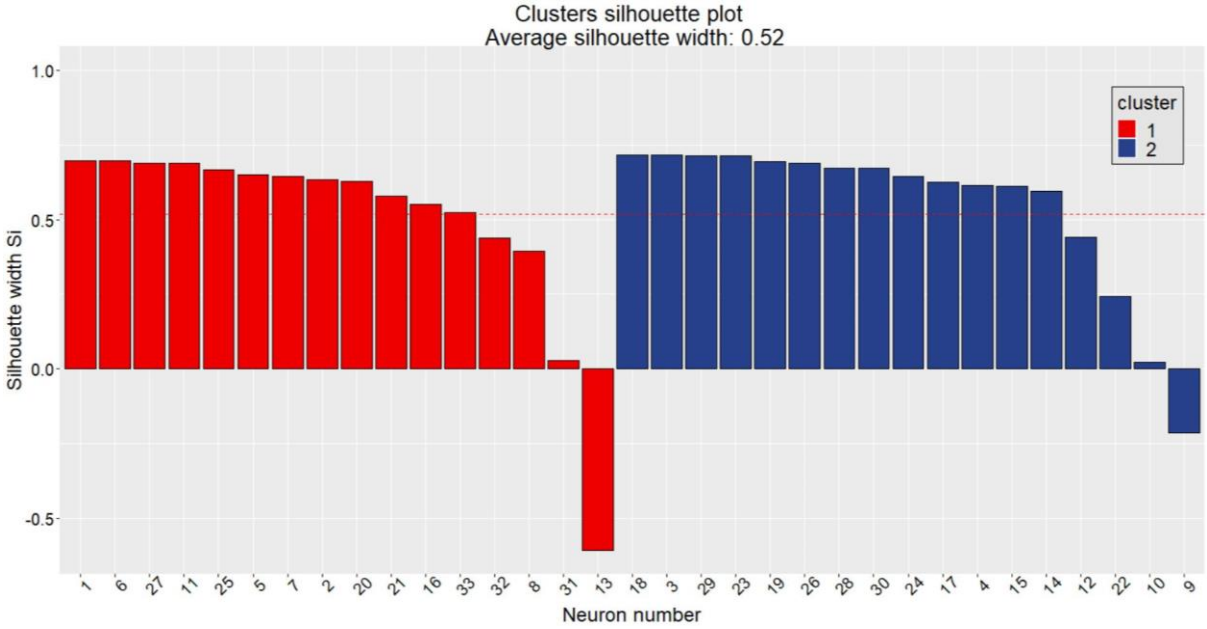

Figure SIII.6 - Silhouette plot of the hierarchical clustering analysis on the female trees, considering only the total length of the neurons. Cluster 1 has a SC of 0.49, with neuron #13 misclassified, and cluster 2 has a SC of 0.54, with neuron #9 misclassified. Average SC is of 0.52, which is above 0.50.

IV. Principal Component Analysis

We performed a scaled Principal Component Analysis (PCA) *(Wold et al., 1987)* using R's function *prcomp*, to see if we could identify which metrics best separated the male from the female trees. By plotting the results with the use of *ggbiplot* package (version 0.55), not only one can identify the neuromorphological metrics that explain most of the variance in the data, but also to what degree the Principal Components (PC) explain the possible differences between the groups. This was performed for the whole dataset, as well as per cluster.

By applying a scaled PCA in the whole data we were hoping to see some separation due to sex that we were unable to find when performing the statistical analysis (**Table SII.1** and **Figure SII.1**). This separation would be along the lines of PC1 and PC2, since those are the ones who explain a total of 71.1% of the variance in the data, but this was not the case **(Figure SIV.1)**. PC1 explains 54.4% of the variance and is mainly contributed by metrics related to the size of the trees: total length, volume, tree radius, and maximum path length. PC2 has an explained variance of 16.7% and is mainly contributed by metrics related to the branches: mean branch order, mean branch length and number of branch points. As one can note, the larger contributions of one PC are usually the smallest of another, which is why just PC1 and PC2 already explain more than 70% of the variance in the data. Straightness and soma radius are the only metrics which never contribute more than 11%, meaning they do not reflect the data's variance.

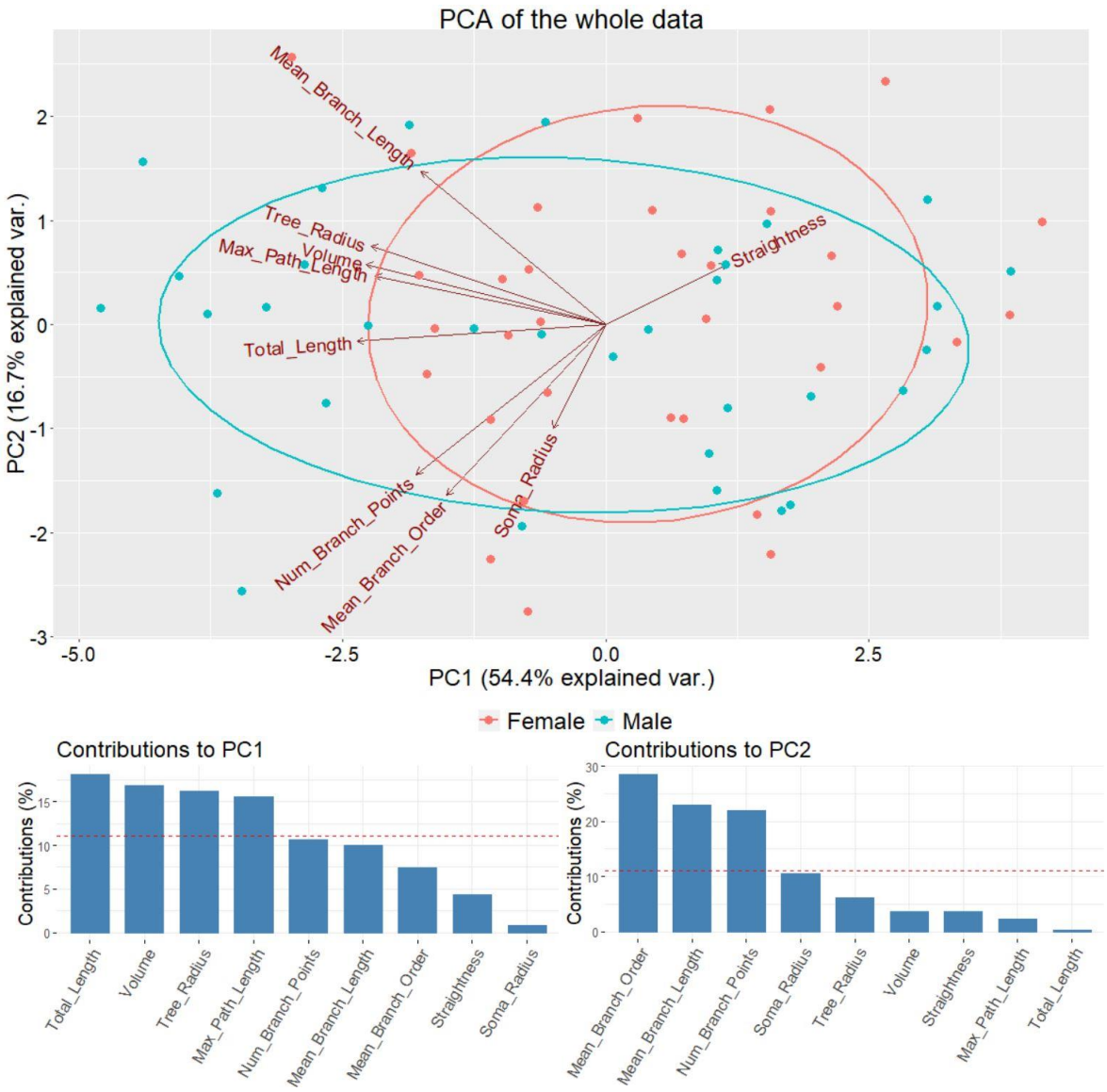

Figure SIV.1 - Scaled PCA on the whole dataset. Top: PCA of the variables. Each arrow represents the direction of that variable in the PCA space, as well as its contribution - the longer the arrow, the more it is well represented by PC1 and PC2. Each dot is one of the neurons, coloured by sex, and for each group we have in solid lines the normal data ellipses of 68% confidence. **Bottom**: Bar plots showing the contribution, in percentage, of each metric to the PC in question. The red dashed lines are the expected average contributions of the metrics, assuming they would contribute equally - 100/(number of metrics), which in our case is 100/9≃11%. PC1 is a composite of metrics related mostly to the size of the tree, while PC2 is a composite of metrics related to the branches.

We wondered if the reason why there was no separation in the PCA visualization between the sexes could be due to the neurons from specific animals being outliers among the rest, leading to a "shift" in the group's ellipse in the direction to an overlap of the groups. To test this, we plotted once again the PCA space, but instead of colouring by sex, we coloured according to the animal ID **(Figure SIV.2)**. This time we only plotted the ellipses, because otherwise the results would be difficult to read and interpret. Male mice are coloured in shades of blue and green, while the females vary from yellow through red and purple. By the size and location of the ellipses it is possible to understand how the data from each subject is well spread across the PCA space, meaning this effect does not happen. These results make sense with what we saw for the CV **(Table 1.3)**.

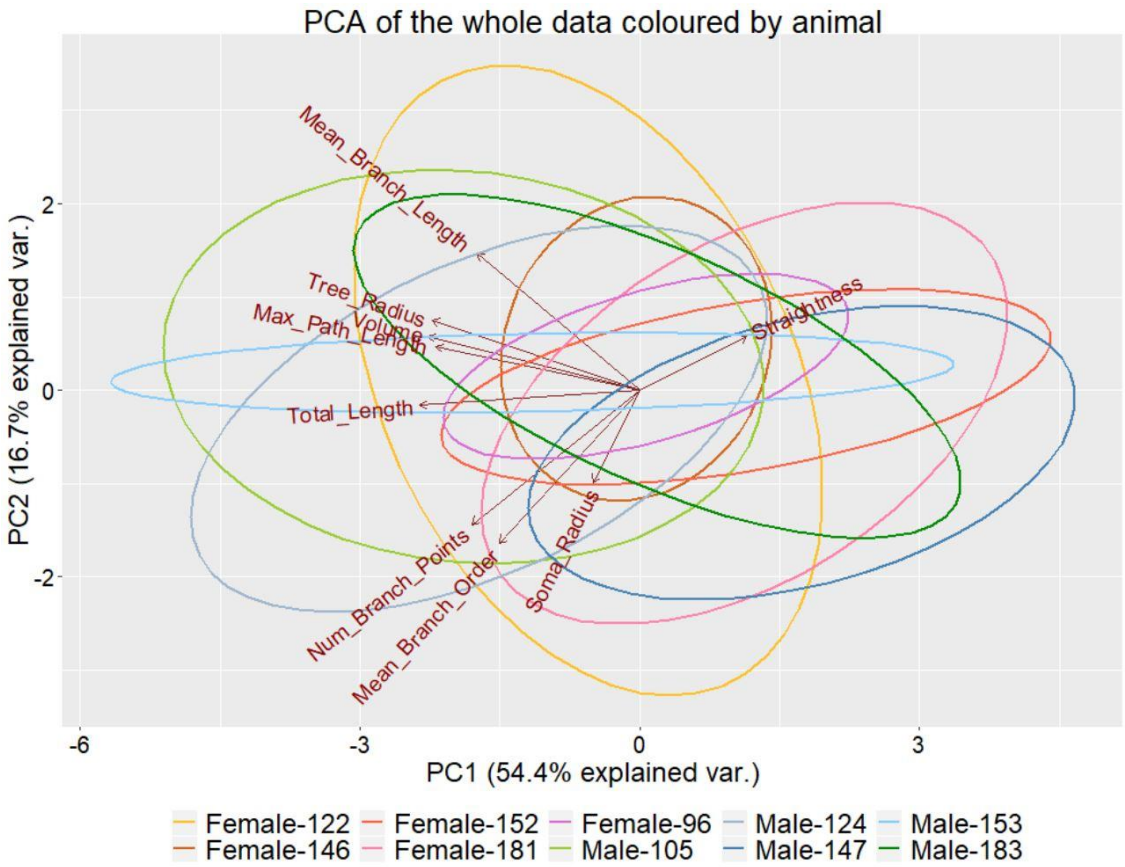

Figure SIV.2 - Scaled PCA of the metrics coloured by animal ID. This id has no meaning of categorization. To aid the underlying visualization of sex comparison, the female mice take the colours yellow, orange/brown, red, pink and purple, and the males have shades of blue and green (light and dark) and grey. Remaining plot specifications are explained in **Figure SIV.1**.

Having defined our 2 different clusters, we proceeded to apply PCAs to each of them. As expected, the PCA for cluster 1 shows a separation of the sexes defined by PC1, which explains 35.1% of the variation in the data and is mainly contributed by metrics of size: volume, tree radius, maximum path length, mean branch length and total length **(Figure SIV.3)**. PC2 explains 24.2% of the variance, and is contributed mostly by number of branch points, as well as mean branch order and total length. PC1 and PC2 somehow resemble its counterparts of the PCA on the whole data, since the contributions are of the same categories and straightness and soma radius once again explain less than 11% of both PCs **(Figure SIV.4)**. These results confirm the significant differences found in the statistical analysis of cluster 1 (**Table 1.4** and **Figure 1.12**).

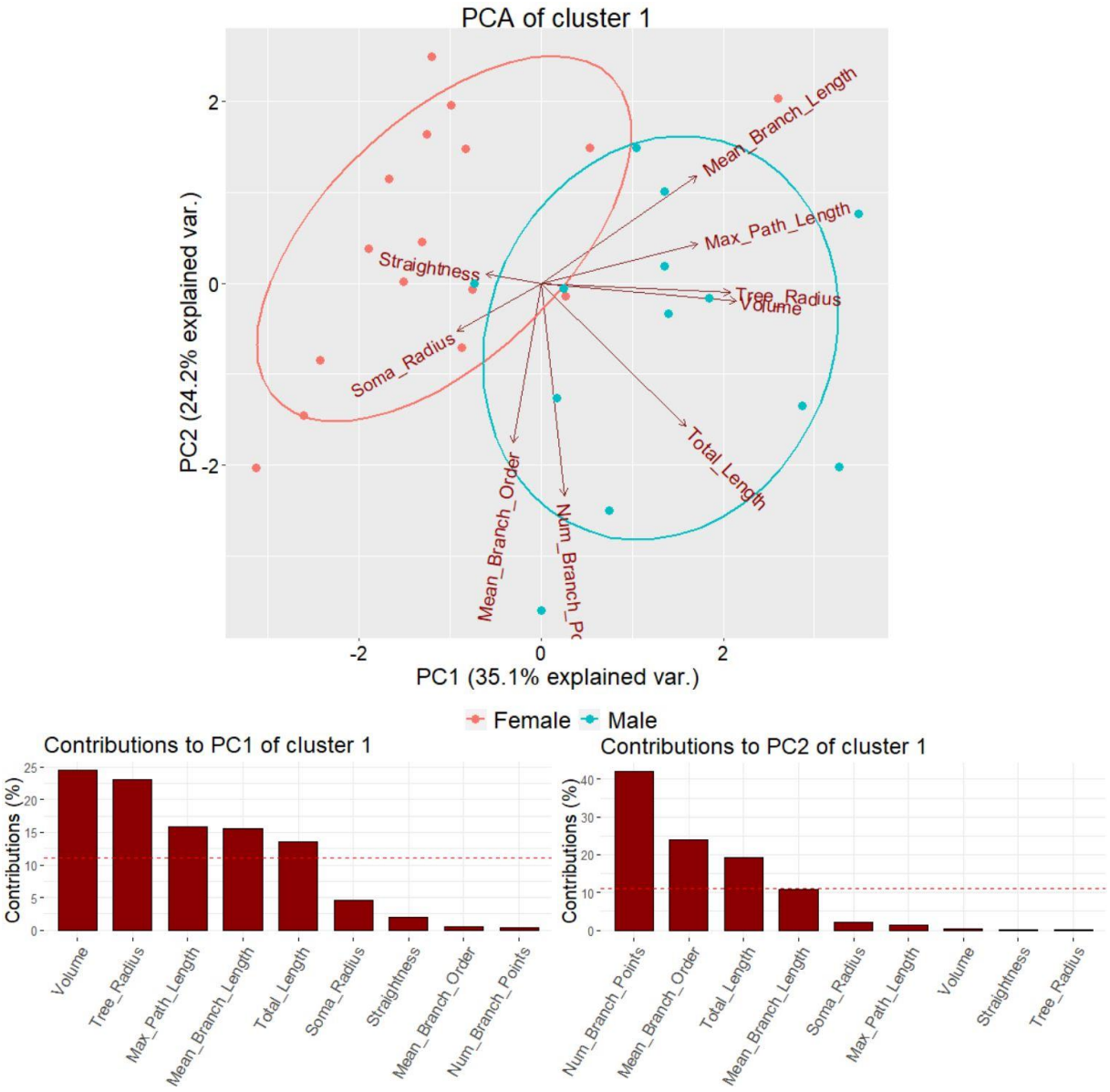

Figure SIV.3 - Scaled PCA of the metrics for cluster 1. Top: PCA space for cluster 1. **Bottom**: Contributions, in percentage, of each metric to the PC in question. PC1 is a composite of metrics related mostly to the size of the tree, while PC2 is a composite of metrics related to the branches. Females and males are separated due to PC1. Remaining plot specifications are explained in **Figure SIV.1**.

As for the PCA of the second cluster, once again we see no separation due to sex along the lines of PC1 and PC2 **(Figure SIV.4)**, just as it happened for the whole data **(Figure SIV.1)**. PC1 and PC2 still follow the "rule" about the contributions: the first, explaining 43.5% of the variance, is mostly defined by metrics of size (total length, volume, maximum path length and tree radius), and the second, with an explained variance of 24.9%, is contributed by metrics regarding the branches (mean branch length and order, number of branch points and tree radius). These results confirm the lack of significant differences in the statistical analysis of cluster 2 (**Table 1.4** and **Figure 1.13**).

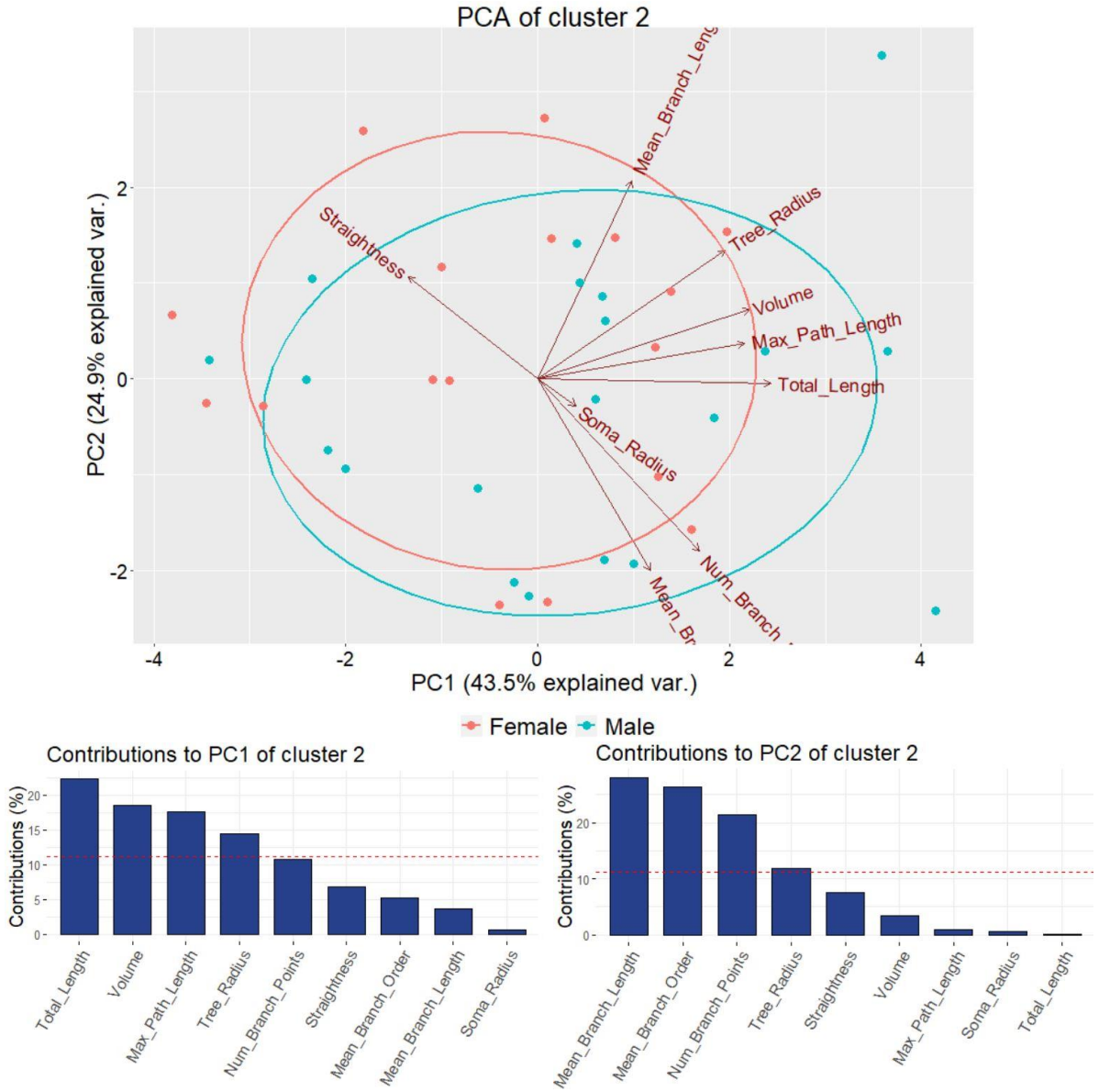

Figure SIV.4 - Scaled PCA of the variables for cluster 2. Top: PCA space of cluster 2. **Bottom**: Contributions, in percentage, of each metric to the PC in question. PC1 is a composite of metrics related mostly to the size of the tree, while PC2 is a composite of metrics related to the branches. Remaining plot specifications are in **Figure SIV.1**.

V. Multi-objective optimality

Number of spines

Instead of using a constant number for the spine density, which is usually taken as 2 spines/µm, we wanted to have the number of spines in function of the dendritic distance to the soma. For this reason, we searched for studies where they measured the spine density or related measures at different distances. We looked preferably for studies in mice CA1 neurons since this is the same as our data. We came across Konur *et al*., 2003, which matches all these requirements. Using intervals of 50 or 40 µm, they found some variability in the interspine distance in apical and basal dendrites, respectively. Given that the trees from our dataset only have basal dendrites, only those values were used. They provide both the mean and standard deviation for each interval, to which we fitted polynomial functions of different degrees.

The registered mean values of interspine distance for each interval of path distance to the soma were: (0.84±0.82) µm for [0, 40] µm, (0.63±0.61) µm for [40, 80] µm, (0.65±0.61) µm for [80, 120] µm, (0.87±0.64) µm for [120, 160] µm *(Konur et al., 2003)*. To be able to plot a graph of interspine distance for each path length, we set each observed mean values to their upper bound of the interval it corresponds to (e.g. (0.84±0.82) µm at 40 µm). To apply the polynomial fit we assumed that at path distance 0 µm the interspine distance would be 0 µm, to force the function to pass through the origin. The value for path distance 20 µm was also extrapolated as (0.42±0.41) µm, which is half of the value at 40 µm, so the polynomial fits would respect this linear relationship between observations.

Having a total of 6 observations, we proceeded to use MATLAB's *polyfit* function with increasing polynomial degree, from 2 to 5 (the maximum possible, given the small number of observations). We plotted both the fit, means and standard deviations, to see if the estimated fit would behave similarly and stay between the standard deviation **(Figure SV.1)**. We explored all plots with the polynomial degrees to choose the best one, while at the same time avoiding overfitting. This led to the conclusion of using a degree of 4 to map the behaviour of the interspine distance in function of the path distance to the soma **(Figure SV.1)**. After extracting the coefficients, the function for interspine distance s_{dist} was:

$$s_{dist}(i) = -1.3 \times 10^{-9} l(i)^4 + 9.6 \times 10^{-7} l(i)^3 - 2.3 \times 10^{-4} l(i)^2 + 0.0204 l(i) + 0.0085 \qquad (\mathbf{SV.1})$$

The distance is calculated for each compartment *i* of the tree, and so we have a value at each path length *l*(*i*). Given that the standard deviation of the measured s_{dist} is very close to it, we need to take it into account *(Konur et al., 2003)*. For this reason, after calculating $s_{dist}(i)$ we added a randomized number for each compartment *i* which was in the range of the standard deviation. Unless this addition resulted in a negative value, then it substituted the previously calculated $s_{dist}(i)$ for said compartment. It is important to note that **Eq. SV.**1 is valid until a distance *l*(*i*) of 160 µm; when the tree had a compartment *i* with $l(i)$>160 µm, then we assumed the $s_{dist}(i)$ was 0.87, the same as the last value of the study *(Konur et al., 2003)*.

Having the value of the interspine distance for each compartment *i* of the tree, we obtained its number of spines $s(i)$. By summing the number of spines of each compartment *i*, one can determine the number of spines for the whole tree:

$$s = \sum_i s(i) = \sum_i \frac{l(i)}{s_{dist}(i)} \qquad (\mathbf{SV.2})$$

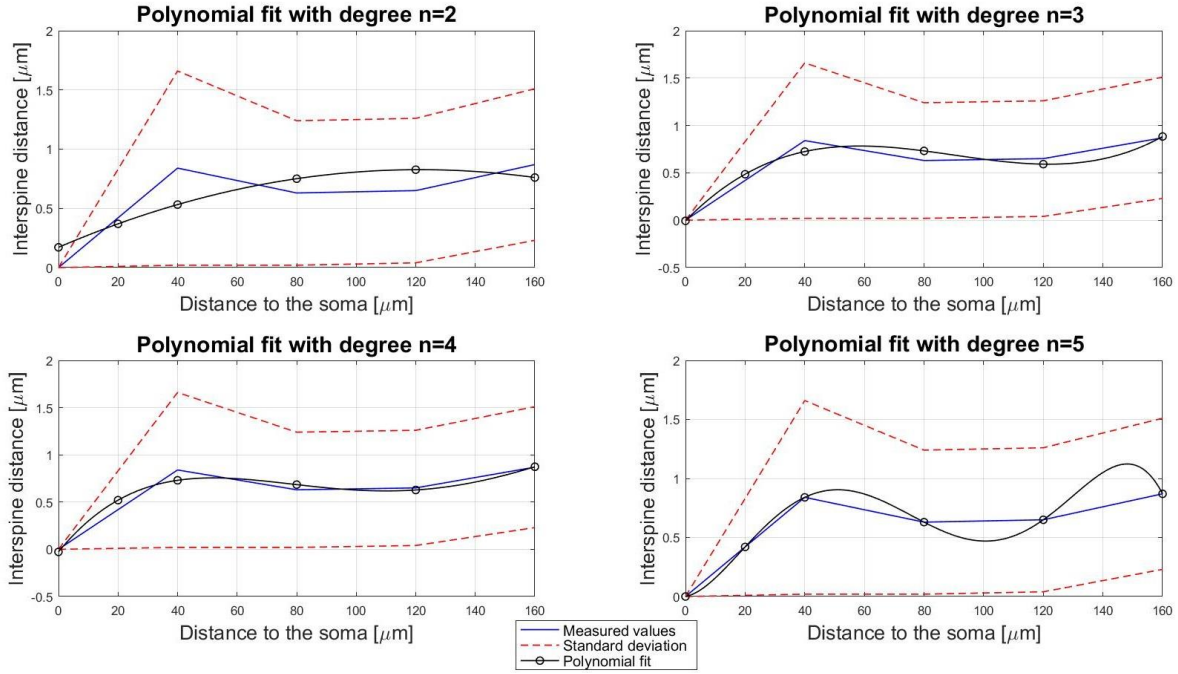

Figure SV.1 - Interspine distance in function of the distance to the soma, with polynomial fits of different degrees. The polynomial of degree 2 does not represent the variation correctly. With degree 5 even though all observations are perfectly met, the polynomial has more variability between points than desired. Polynomials of degree 3 and 4 have a negative value when the distance to the soma is zero, but they still represent better the observations and behaviour we have. Comparing both, the polynomial with degree 4 is the best suited.

Connectivity repertoire

To obtain an equation for the connectivity repertoire *S* that we could implement in MATLAB, we started from equation S32 from the supplementary information of Wen *et al.*, 2009:

$$S \simeq \log\binom{s_l L \rho_a}{N} - \frac{s_l L}{R^2} N + \frac{L}{a}\left(1 + \log\left(1 - \frac{R}{l}\right)\right) - \frac{l^2}{La} \qquad (\mathbf{SV.3})$$

With each variable representing the following: s_l the spine reach length, in µm; L the total length, in µm; ρ_a the axon length per unit of volume, in µm/µm^3; N the number of connections per dendritic arbor; R the tree radius, in µm; a the persistence length, in µm; l the average path length from the soma to the branch tip, in µm.

The value of the persistence length a is already provided as being approximately 4 µm, and of the spine reach length s_l as 2 µm; N is shown to be approximate to L *(Wen et al., 2009)*. To account for the spine density s_d, which we calculate from the total number of spines **(Eq. SV.2)**, we introduced it by approximating $N \sim s_d L$ *(Gutin et al., 1993)*. The axon length per unit of volume ρ_a is the only variable not provided, so we searched and came across the measured value of 8.15±0.19 µm of axons per µm^3 for 4 months old mice *(Calí et al., 2018)*. The only thing left to simplify was the first term of **Eq. SV.3**, the logarithm of a combinatorial. We used Stirling's approximation to the logarithm of a factorial function:

$$\log n! \simeq n \log n - n + \mathcal{O} \log n \qquad (\mathbf{SV.4})$$

The last term of **Eq. SV.4** can be removed, assuming it is negligible by the other terms. We can apply this relationship to the logarithm of a combinatorial *(Mackay, 2003)*:

$$\log\binom{M}{r} = \log\frac{M!}{r!\,(M-r)!} = \log M! - \log(r!\,(M-r)!) \simeq$$
$$\simeq M\log M - M - r\log r + r - (M-r)\log(M-r) + (M-r) =$$
$$= M\log M - r\log r - (M-r)\log(M-r) \qquad (\mathbf{SV.5})$$

If we consider the binary entropy function:

$$\mathcal{H}(x) = x\log\frac{1}{x} + (1-x)\log\frac{1}{1-x} \qquad (\mathbf{SV.6})$$

By introducing the terms $r\log M - r\log M$ to **Eq. SV.5**, we can restructure the equation and lastly simplify with **Eq. SV.6**:

$$M\log M - r\log r - (M-r)\log(M-r) + r\log M - r\log M =$$

$$= r\log M - r\log r + (M-r)\log M - (M-r)\log(M-r) =$$

$$= r\log\frac{M}{r} + (M-r)\log\frac{M}{M-r} =$$

$$= M\left[\frac{r}{M}\log\frac{1}{\frac{r}{M}} + \left(1-\frac{r}{M}\right)\log\frac{1}{1-\frac{r}{M}}\right] =$$

$$= M\mathcal{H}\left(\frac{r}{M}\right) \qquad (\mathbf{SV.7})$$

By applying the relationship in **Eq. SV.**7 to **Eq. SV.3**, comes that $M = s_l L\rho_a$ and $r = N \simeq s_d L$. Simplifying to $\frac{r}{M} = W$, our final equation for connectivity repertoire *S* is given by:

$$S = M\mathcal{H}(W) + \frac{L}{a}\left(1 + \log\left(1-\frac{R}{l}\right)\right) - \frac{l^2}{La} - s_l s_d\frac{L^2}{R^2} \qquad (\mathbf{SV.8})$$

Signal integration efficiency

Since we generated the signal integration efficiency through multi-compartmental models, we wanted to understand more about its behaviour in relation to other neuromorphological metrics. We were specifically interested to see if there was any relationship with total length, given we have a high dependency on our dataset, and it was the metric with the most significance sex difference **(Section 1.3.3)**. To this end, we generated synthetic dendritic trees and explored the impact of neuron architecture in signal integration efficiency. These synthetic trees were obtained using the TREES Toolbox's function *clone_tree*, as we previously explained in **Section 2.2.2.** . For each set of parameters, 3 clones of each sex were generated, making a total of 750 clones for analysis (375 males and 375 females), which we then modelled to obtain the signal integration efficiency.

To look for a relationship between signal integration efficiency and total length, we put together not only the data from the clones, but also from the original dataset, to make sure they were in accordance. There is a clear log-like relationship, where with a longer total length, the more efficient is the neuron, until reaching a plateau; after this, there is no improvement in efficiency with an increase in length. Male and female neurons used in the study are also in agreement with this relationship **(Figure SV.2)**.

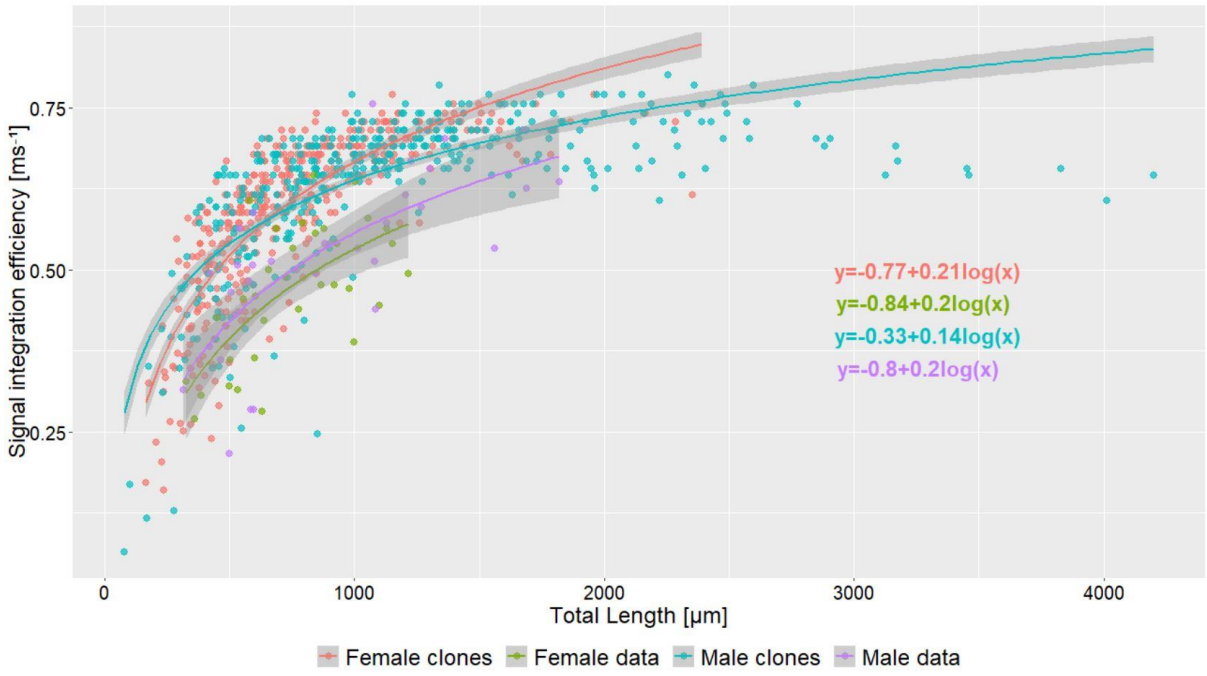

Figure SV.2 - Evidence of log-like relationship between total length and signal integration efficiency in both clones and original dataset. Each dot is a neuron and the lines represent the log fit of each group, with respective equations on the right. Shaded areas represent the 95% confidence level interval for the fits.

We wondered if this log-like profile was because more inputs were given with the increase in length. This is because, as mentioned before **(Section 2.2.2)**, all neurons had 8% of their spines being activated. With a longer total length comes a higher density of spines, and so 8% translates into more spines being activated than in a smaller neuron. Hence, longer neurons are receiving more input signals, which could explain why they generated an action potential faster, and thus were more efficient. It also makes sense to have a plateau, since neurons are known to reach a point of saturation where, no matter how many more inputs are given, the cell response will be the same.

To determine if this was the case, we assessed the total number of spines of each dendritic tree (see above) and took 8% of that value, which is the number of inputs to the cell. Dividing it by the number of nodes of the tree and multiplying by 100, one gets the percentage of received inputs for said tree. Both the percentage of received inputs and signal integration efficiency are related to total length. Thus, to be able to assess if the increase in efficiency is due to an increase in percentage, signal integration efficiency needs to be normalized by total length. Hence, the dependency is removed, and any conclusion found is not due to the influence of total length. No relationship whatsoever was found between the percentage of activated spines and signal integration efficiency normalized by total length **(Figure SV.3)**. Therefore, it is clear this link between total length and signal integration efficiency is present, and the log-like relationship is not due to more spines being activated.

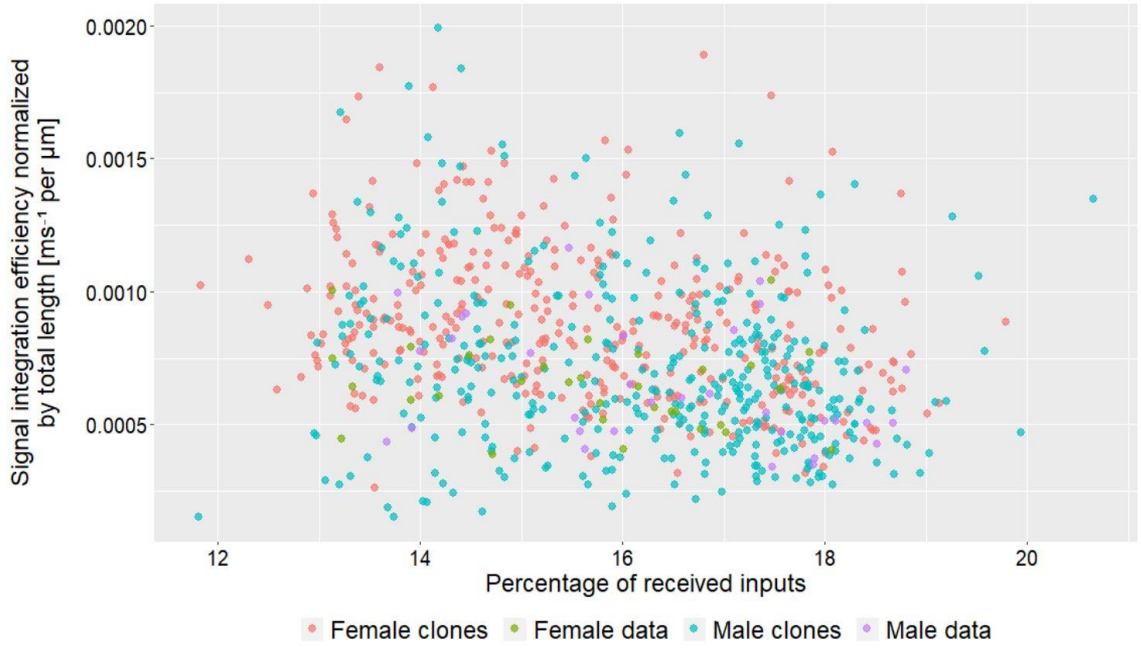

Figure SV.3 - Normalized signal integration efficiency has no relationship with the percentage of received inputs. This denies the possibility that the log-like relationship between total length and signal integration efficiency was because of the percentage of received inputs. Each dot represents a neuron, coloured by sex and dataset.

We also assessed if there was any relationship between signal integration efficiency and the number of branch points. This is because this metric was also significantly different between sexes **(Section 1.3.3)**, and is not directly related to dendritic size. Contrary to total length, we found no relationship between number of branch points and efficiency **(Figure SV.4)**.

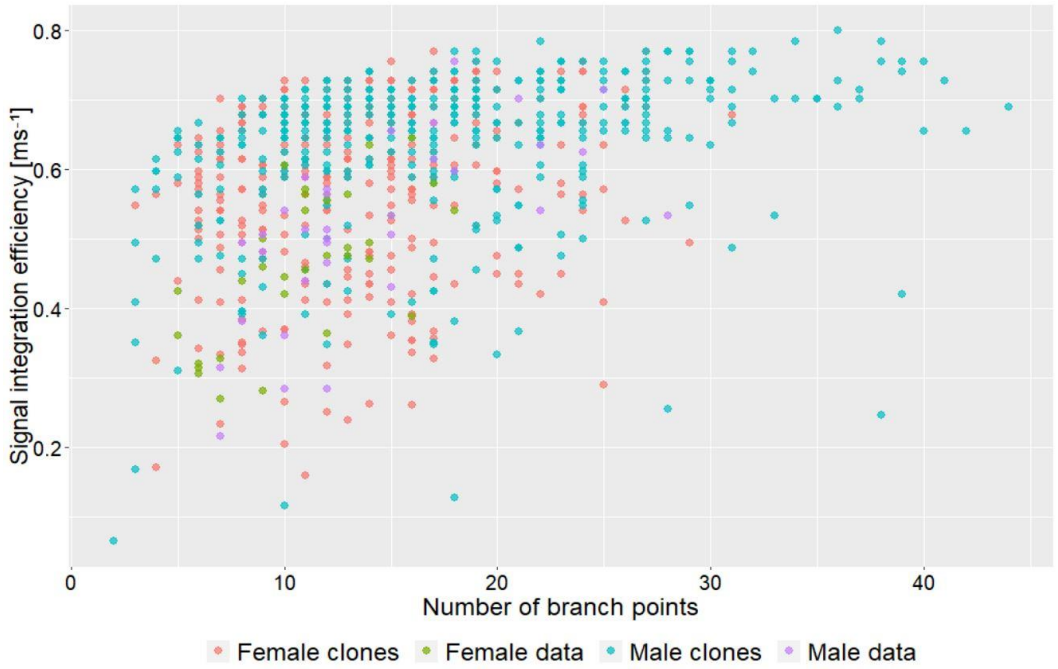

Figure SV.4 - Signal integration efficiency has no relationship with the number of branch points. Each dot represents a neuron, coloured by sex and dataset.

Pareto front

When assessing the Pareto front from the values of synthetic trees, we used MATLAB's Curve Fitting App. One of the issues with this method is how different surfaces can fit the points well, even if they have completely different behaviours. Our data points are one example of this issue, as a surface with f(x,y) with degree 3 for both x and y fits them as well as the surface we chose to work with. These two surfaces are almost opposites, as the latter behaves orthogonally to the z-axis **(Figure 2.10)**, whereas the former behaves orthogonally to the XY plane **(Figure SV.5)**. Consequently, the euclidean distances estimated with each of them are also different. With this other surface, distances are much smaller (all below 0.10) and, in fact, they are significantly different in cluster 1 **(Figure SV.6)**. Females of cluster 1 are significantly more optimal than males, a result we expected from analysing signal integration efficiency normalized by cost **(Figure 2.9)**. However, this significant difference was not present in our considered surface (**Table 2.3** and **Figure 2.11**). This discrepancy in results showcases the unreliability of the method, and stresses the importance of obtaining the Pareto front by minimizing and maximizing functions, and not by fitting surfaces.

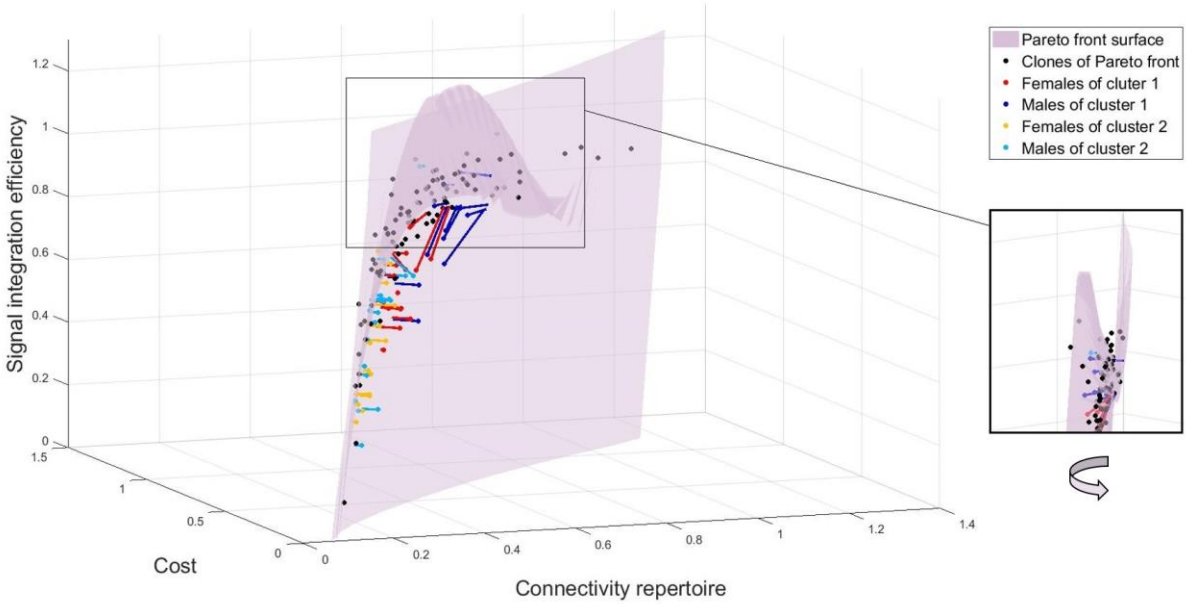

Figure SV.5 - Euclidean distance of each neuron to a different Pareto front in the 3D space. The surface is determined by a polynomial function f(x,y) of degree 3 for both variables, obtained with the Curve Fitting App. Each coloured point represents a neuron, with the respective colour classifying it by sex and cluster. The lines represent the minimum euclidean distance between them and the surface. Connectivity repertoire, cost and signal integration efficiency were normalized to [0.1, 1.1], and so are adimensional. Neurons that are to the right and left of the surface are suboptimal, and the ones that are on the surface are optimal. **Inlet:** Close-up of the local peak of the surface, from a different angle (rotated in the direction of the arrow), to ease in visualization and 3D perception of the surface.

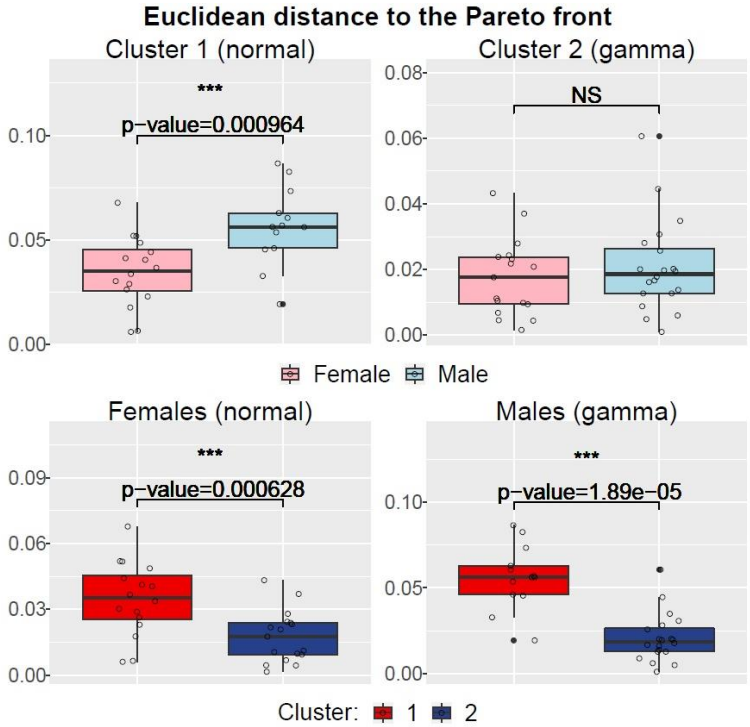

Figure SV.6 - Euclidean distances to a different Pareto front uncover sex-dependent differences in cluster 1. Females of cluster 1 are significantly more optimal than males. Both female and male neurons of cluster 2 are also closer to optimality than neurons of cluster 1. Panels contain the boxplot and data points of each data subset. The title of the panels have the name of the subset and distribution used in the GLMM. The significance level of the test is shown on top of each panel: NS is not significant, * is p-value<0.05, ** is p-value<0.05 and *** is p-value<0.001. If it passes the threshold of significance, the p-value is also shown.